Incipience of Two-phase Flow from a Stratified Gas-liquid Region in Multiple Discharging Branches: Experimental Investigation Including PIV Measurements

Robert Constantinos Bowden

A Thesis

in

The Department

of

Mechanical and Industrial Engineering

Presented in Partial Fulfillment of the Requirements

For the Degree of Master of Applied Science at

Concordia University

Montreal, Quebec, Canada

January 2006

Your file Votre référence
ISBN: 0-494-14298-7
Our file Notre référence
ISBN: 0-494-14298-7

ABSTRACT

Incipience of Two-phase Flow from a Stratified Gas-liquid Region in Multiple Discharging Branches: Experimental Investigation Including PIV Measurements

Robert Constantinos Bowden

The importance of predicting the incipience of two-phase flow from a stratified gas-liquid region in discharging braches has strong implications in industries where safe operation is of primary concern. This is particularly true in the nuclear reactor industry, where two-phase flow in the reactor cooling channels occurs due to a loss-of-coolant accident (LOCA). The incipience of two-phase flow can be characterized by the location of the gas-liquid interface relative to the discharging branch. If the gas-liquid interface is above the discharging branch, gas can entrain into the branch liquid flow by either vortex formation or vortex-free gas pull through. If the gas-liquid interface is below the discharging branch, liquid can entrain into the branch gas flow.

A semi-circular test section geometry, with three discharging branches, was used to simulate a typical CANDU header-feeder. The experimental investigation consisted of a two part study. In the first, the onset of liquid entrainment was investigated in multiple discharge scenarios. In the second, the liquid velocity flow field was investigated at the onset of gas entrainment in a single discharging bottom branch.

The experimental investigation of the onset of liquid entrainment (OLE) was reported with single, dual and triple discharge scenarios. The critical height, H, at which liquid entrainment occurs in the primary branch was presented as a function of the branch flow Froude number, Fr. To record the critical height at the onset of liquid entrainment two methods were used, the increasing liquid level (ILL), and decreasing liquid level (DLL) techniques. The results showed that under multiple discharge scenarios a secondary branch may either assist, or prevent liquid entrainment in the primary branch. The location of the secondary branch, and its Froude number, determine the impact it has on the onset of liquid entrainment in the primary branch.

The liquid velocity field at the onset of gas entrainment (OGE) in a single discharging bottom branch was investigated using a particle image velocimetry (PIV) technique. The flow field was divided into four separate, non-simultaneous, two-dimensional planes. The liquid velocity fields in each of the four planes were recorded using the particle image velocimetry technique. New information regarding the liquid flow structure was presented. It showed a strong tendency of the flow to be dominated by the radial velocity, towards the branch center, in the horizontal plane results. Contours of the tangential velocity, from the horizontal plane results, were presented and showed a strong dependence in regions near the solid wall.

Acknowledgements

This work would not have been possible without the unwavering support of my parents, family, friends, and in particular, my darling Tamlyn.

My sincerest thanks and appreciation to my supervisor, Dr. Ibrahim Hassan, for helping me grow as an individual and a professional.

To my friends and colleagues in the micro-scale heat transfer group, your insightfulness and encouragement throughout this endeavor are appreciated with heartfelt gratitude. In addition, the dedication of Tariq Ahmad in the development of the test facility must be recognized with utmost appreciation.

Table of Contents

List of Tables

List of Figures

Nomenclature

d	Branch diameter (m)
Bo	Bond number, $Bo = \frac{d}{\sqrt{\sigma / g\Delta\rho}}$
Fr	Froude number with a circular branch, $\mathrm{Fr} = \frac{4\dot{m}}{\pi\sqrt{(gd^5\rho\Delta\rho)}}$
H	Critical height at onset of liquid or gas entrainment, measured from the center of the primary branch to the air-water interface, (m)
L	Center-to-center vertical distance between branches, (m)
$\dot{m}$	Mass flow rate of fluid entering branch, $\dot{m} = \rho A v$ (kg/s)
m_1, m_2	Constant coefficients
N_Γ	Circulation number, $N_\Gamma = \frac{V_t d}{2V_r H}$
N_μ	Viscosity number, $N_\mu = \mu\left(\frac{g\Delta\rho}{\rho^2\sigma^3}\right)^{0.25}$
P	Absolute pressure, (Pa)
R	Ratio of liquid cross-flow velocity to branch velocity, $R = \frac{\rho_L v_{LC}}{\rho_L v}$
Re	Reynolds number, $\mathrm{Re} = \frac{\rho v d}{\mu}$
s	Distance from the branch center to the tip of the deflected interface, (m)
T	Absolute temperature, (K)
v	Average velocity of fluid at the branch inlet, (m/s)
V	Velocity vector component (m/s)

Greek Letters

$\Delta\rho$	Difference between densities of heavier and lighter fluids, (kg/m^3)
ρ	Density of continuous fluid at the branch inlet, (kg/m^3)
σ	Surface tension, (N/m)

Subscripts

0	Stagnation property
1	Primary branch where onset of liquid entrainment occurs
2, 3	Secondary branches for dual and triple discharge
A, B, C	Branches located at 0°, 45°, 90° from horizontal axis
b	General notation to indicate any branch
h	Horizontal separating distance
L	Liquid phase
LC	Liquid cross-flow
x,y,z,r,t	Coordinate directions, in x, y, z, radial [r] or tangential [t] directions

Constants

C_p	Specific heat at constant pressure, (J/kg-K)
C_v	Specific heat at constant volume, (J/kg-K)
k	Ratio of specific heats, $k = C_P/C_V$
g	Gravitational acceleration, (m/s^2)
R′	Gas constant for air, (J/kg-K)

Acronyms

CANDU	Canada Deuterium and Uranium
DLL	Decreasing Liquid Level
ILL	Increasing Liquid Level
LOCA	Loss-Of-Coolant Accident
OGE	Onset of Gas Entrainment
OLE	Onset of Liquid Entrainment
PIV	Particle Image Velocimetry

Chapter I

Introduction

Of paramount importance in the design of industrial coolant distribution systems operating at high pressures and temperatures, is safety. The CANDU (CANada Deuterium and Uranium) nuclear reactor incorporates a coolant distribution system whereby coolant flows from a large reservoir, the header, through a network of pipes, called feeders, to the cooling channels of the reactor. Under normal circumstances the fluid flowing in the channels in the direction of the reactor core is a liquid. A break in the header-feeder can cause a loss-of-coolant accident (LOCA), whereby, the coolant rapidly escapes the header thus reducing the amount of coolant being distributed to the reactor. In this instance, the coolant vaporizes, creating a two-phase environment.

In another instance of a LOCA scenario, it is possible that the pump that re-circulates the coolant back into the header experiences a partial, or total, loss of power thus reducing the flow of liquid towards the header. In this case, the level of coolant in the header will decrease and a two-phase region will result. As the liquid level in the header decreases, the possibility of a two-phase mixture occurring in the feeder branches increases. The incipience of two-phase flow, with the interface above the inlet of the feeder branch, is termed the onset of gas entrainment. This represents the instance when the cooling effectiveness will begin to reduce in that particular branch. As the height of liquid in the header decreases further, the flow in the feeder branch experiences a transition from a

two-phase mixture to a single phase gas, at which the onset of liquid entrainment occurs. It is at this point that cooling effectiveness in the particular feeder branch is at a minimum. The LOCA scenario can therefore be characterized as the transition from a single phase liquid flow to a two-phase gas-liquid flow, and finally a single phase gas flow in the cooling channels. The presence of two-phase flow results in a reduction of the cooling capacity of the fluid due to the reduction of the heat transfer characteristics of the two-phase mixture. The magnitude of a LOCA can be catastrophic, and has been well documented to have caused either a partial or full meltdown of the nuclear reactor core. As a result, predicting the phenomena during a LOCA has received significant attention.

The current experimental investigation is intended to present results pertaining to the critical height at the onset of liquid entrainment (OLE) in a simulated CANDU header-feeder system, using air and water as the two fluid phases. A typical header has a circular cross-section and measures approximately 6 meters in length, with an internal diameter between 0.356 and 0.406 meters, and closed on both ends. Flow enters the top of the header through a number of orifices called turrets, and exits through a network of feeder banks. Each feeder bank contains five 50.8 mm openings located at radial positions of 0°, 45°, 90°, 135° and 180° from the horizontal axis, as shown in Figure 1.1. In addition, a second experimental investigation will describe the liquid velocity flow field occurring during the onset of gas entrainment (OGE) in a single bottom branch.

A parametric study to demonstrate the effect of multiple discharging branches on the incipience of liquid entrainment in the primary branch is presented. Throughout the text, the branch at which entrainment occurs, be it OLE or OGE, is referred to as the primary branch and additional branches are referred to as secondary branches. The results of the OLE experiments demonstrate that the critical liquid height, H, at which liquid entrainment occurs can be influenced differently depending on the location and strength of the secondary branches. The effects of surface wetness on OLE are demonstrated by using two methods to record the critical height, being the increasing liquid level (ILL) and decreasing liquid level (DLL) techniques.

A novel feature of this study is the liquid velocity field measurements, at the onset of gas entrainment, using a state-of-the-art particle image velocimetry (PIV) system. Gas entrainment presents a complex three-dimensional flow field, and the PIV system was able to capture the phenomena in multiple two-dimensional planes. By predicting the velocity field of the complex flow, at the onset of gas entrainment, theoretical models can be verified.

This study is not limited to nuclear reactor cooling systems, and generally speaking can be applied to pressure vessels with discharging branches from a stratified two-phase region. The correct prediction of the phenomena that occur during the transition from a single phase liquid to two-phase gas-liquid to single phase gas, as in a LOCA scenario, will ultimately establish a benchmark for designers when creating the next generation coolant distribution systems.

A literature review of previous studies relevant to the LOCA scenario will be presented. The experimental methodology is presented, including a description of the test facility, test sections, experimental procedures, test matrices, measurement uncertainty and technical challenges. A discussion of the results obtained from the onset of liquid entrainment experiments is presented. Following this, a discussion of the liquid velocity fields obtained using the PIV system, at the onset of gas entrainment, is presented. A summary of the conclusions formed from both the OLE and OGE experimental results are presented, followed by a discussion of the future directions.

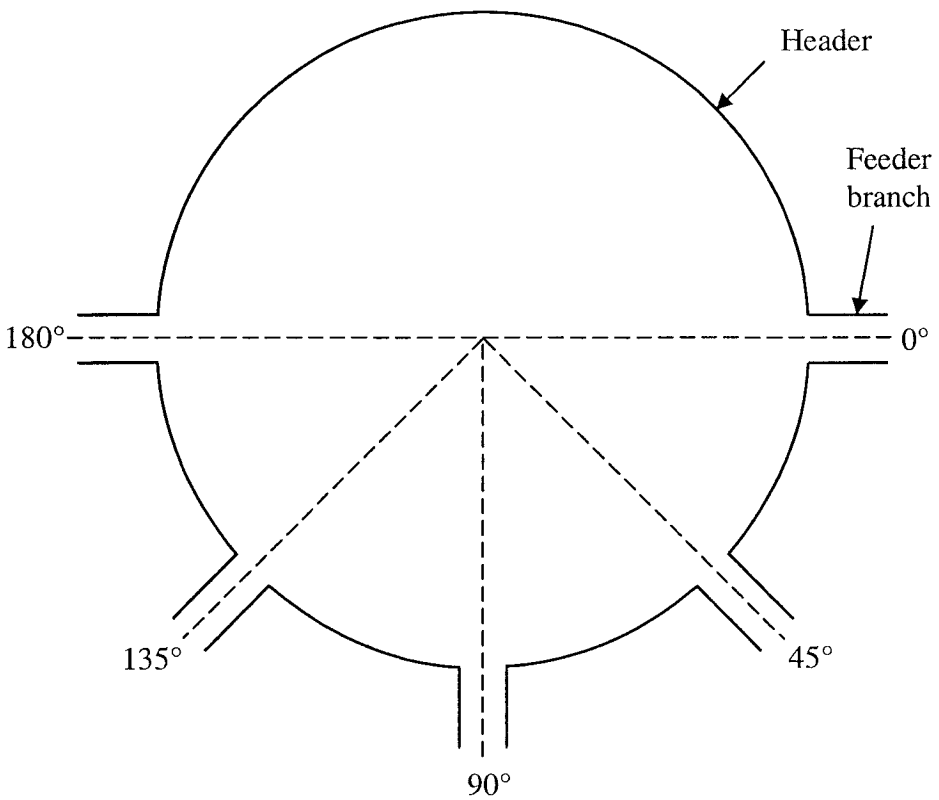

Figure 1.1.Typical cross section of a CANDU header-feeder bank.

Chapter II

Literature Review

2.1 Introduction

Presented here will be a brief review of research dealing with LOCA, in particular with both single and multiple discharging branches on the side of large pressure vessels. This review will incorporate a comprehensive set of experimental works dealing with the onset of liquid and gas entrainment phenomena.

2.2 Foundations of LOCA Modeling

Zuber (1980)'s report for the United States Nuclear Regulatory Commission titled "Problems in Modeling of Small Break LOCA" presented the ground work for future studies in LOCA. The focus of the study dealt with the onset of both liquid (OLE) and gas entrainments (OGE) in a small discharging side branch. When the branch is located above the gas-liquid interface, liquid could be entrained into the branch (OLE). On the other hand, when the branch is located below the gas-liquid interface, gas could entrain into the branch due either to vortex formation, or by vortex-free gas pull through (OGE). Zuber (1980) found correlations for both OLE and OGE in prior literature and were of the form,

$$\frac{H}{d} = m_1 (Fr)^{m_2}, \qquad 2.1$$

where

$$Fr = \frac{v_b}{\sqrt{gd\frac{\Delta\rho}{\rho}}}. \qquad 2.2$$

The correlation presented in Equation 2.1 describes the critical height, H, as the distance from the gas-liquid interface to the center of the branch, as a function of the Froude number, Fr, and two constants m_1 and m_2. The Froude number is shown to be dependant on the discharge velocity of the continuous phase at the inlet of the branch, v_b, as well as the gravitational acceleration, g, branch diameter, d, and density of the continuous fluid, ρ. The remaining term, $\Delta\rho$, is the difference between the heavier and lighter fluid phases. The constants m_1 and m_2 are dependant on the type of entrainment (OLE or OGE) and the physical geometry. Zuber (1980)'s review presented the work of several authors who demonstrated reasonable validity of their correlations with different values of m_1 and m_2, but stipulated the need for more complete models relevant to LOCA.

2.2.1 Onset of Liquid Entrainment

An analytical model for the onset of liquid entrainment through a side branch and was derived by Craya (1949) and verified experimentally by Gariel (1949). Their work dealt with two immiscible fluids at atmospheric pressure. Zuber (1980) argued their validity, in that they demonstrated reasonable scaling and velocity field considerations. Craya (1949)'s model used Bernoulli's equation along the interface of the two fluids, and potential theory to describe the motion of the lighter fluid. The branch was

approximated as a point sink, and both viscous and surface tension effects were neglected. The analytical model yielded values of m_1 and m_2 to be 0.625 and 0.400. The analytical model demonstrated reasonable accuracy with Gariel (1949)'s experimental results.

2.2.2 Vortex-free Onset of Gas Entrainment

The onset of gas entrainment due to vortex-free pull through was presented by Lubin and Hurwizt (1967) with experimental data and analysis. Their experimental investigation comprised of a fluid draining through an orifice located at the bottom of a tank. The purpose of their investigation was to provide a correlation for the liquid height at which a dip formed at the interface during draining. This formation of the dip was said to define the onset of vortex-free gas entrainment. Their analysis yielded two correlations dependant on the height of fluid relative to the orifice inlet as,

$$\left(\frac{H}{d}\right) = 0.574(Fr)^{0.667}\,;\ \left(\frac{H}{d}\right) < 1, \qquad 2.3$$

and

$$\left(\frac{H}{d}\right) = 0.624(Fr)^{0.400}\,;\ \left(\frac{H}{d}\right) > 1. \qquad 2.4$$

2.2.3 Vortex Induced Onset of Gas Entrainment

In the case of OGE due to vortex formation, Daggett and Keulegan (1974) correlated their experimental results for gas entrainment in a bottom orifice. In addition, their experimental study provided the development of the velocity profile in the depth of the fluid as a function of the distance from the orifice for both radial and tangential components. Their parametric study included the effects of surface tension and viscosity by using mixtures of different fluids. The experimental results yielded correlations of the critical height for vortex formation as,

$$\left(\frac{H}{d}\right) = 17.5\times10^{-3} N_{\Gamma}\,\mathrm{Re};\quad \mathrm{Re} < 5\times10^{4}, \tag{2.5}$$

and

$$\left(\frac{H}{d}\right) = 75 N_{\Gamma};\quad \mathrm{Re} \geq 5\times10^{4}. \tag{2.6}$$

Where the Reynolds number, Re, circulation number, N_{Γ}, are defined as

$$\mathrm{Re} = \frac{\rho v d}{\mu}, \tag{2.7}$$

And

$$N_{\Gamma} = \frac{V_t d}{2 V_r H}. \tag{2.8}$$

The initial tangential velocity, V_t, initial radial velocity, V_r, and initial height of fluid in the tank, H are defined. In addition, using the radial velocity components that were measured experimentally, and the continuity equation in cylindrical coordinates, an estimate of the vertical velocity component (z-direction) was determined. The estimate assumed the flow was incompressible and that velocity was a function of the radial distance from the center of the orifice. The results of this analysis demonstrated that a significant vertical velocity component was present at a distance far from the inlet to the orifice.

The outcome of Zuber (1980)'s report was the need for further studies regarding the two-phase phenomena pertinent to LOCA in nuclear reactor cooling systems. As a result, several studies were conducted to broaden the scope of knowledge concerning the complex phenomena. Presented here will be the works dedicated to this effort, in terms of the onset of both gas and liquid entrainment from side or bottom branches. To begin, a discussion of the onset of gas and liquid entrainments from a stratified two-phase region in single discharging side and bottom branches will be presented. Following this, the work relating to the onset of gas and liquid entrainments in multiple discharge scenarios will be presented.

2.3 Single Discharge

Reimann and Khan (1984) performed two-phase experiments in a horizontal cylindrical pipe with a downward oriented branch, using air and water at an operating pressure of 0.5 MPa. Their work dealt with the onset of gas entrainment in the downward branch with stratified flow in the pipe. The horizontal pipe had an overall length of 6 m with an inside diameter of 206 mm. The downward branches consisted of 6, 12 and 20 mm inside diameter bores with a length of 75 mm. Their work presented three scenarios of cross flow, and demonstrated the dependence of onset due to either vortex-induced or vortex free flow. In the instance of a symmetrical inflow of both air and water, their observations indicated that the onset of gas entrainment was due to vortex-free gas pull through and correlated well with the form of Equation 2.1. This correlation resulted in similar values of m_1 and m_2 as found by Lubin and Hurwitz (1967). In the instance of non-symmetric inflow, their results indicated that the onset of gas entrainment was strongly influenced by the vortex formation, but fit the same correlation as Equation 2.1 with m_1 and m_2 equal to 1.9 and 0.4 respectively. Their work presented insightful flow visualization by capturing images of the gas entrainment phenomena.

Smoglie and Reimann (1986) performed similar two-phase experiments for both bottom and side oriented branches from a horizontal cylinder using air and water. They presented results for both the onset of gas and liquid entrainment during single discharge cases at an operating pressure of 0.5 MPa with stratified flow and using the same test facility as Reimann and Khan (1984). Their correlations for both the bottom and side branches demonstrated agreement with the form of Equation 2.1 with a value of 0.4 for

m_2 for both the onsets of gas and liquid entrainments. The value of m_1 for the onset of gas entrainment for the side branch was found to be 0.681, and for liquid entrainment to be 0.626. For OGE in the bottom branch the authors found m_1 for vortex flow as 1.816, and 0.625 for vortex-free flow.

Schrock et al. (1986) presented experimental results for the critical height at the onset of gas and liquid entrainments, at side and bottom branches discharging from a stratified two-phase region. The experimental test facility consisted of a 102 mm I.D. horizontal pipe with branches of 4, 6 and 10mm located at the side and bottom of the tube. They used both steam-water and air-water as the two fluids at an operating pressure ranging up to 1.07 MPa. It was found that the experimental results for the onset of gas entrainment, for either the side or bottom branch, did not correlate well with the form of Equation 2.1. As a result, the effects of viscosity and surface tension were accounted for and a correlation for the side branch was found to be,

$$FrBo^2 N_\mu^{-0.5} = 19.4\left(\frac{H}{\sqrt{\sigma/g\Delta\rho}}\right)^{2.2}, \qquad 2.9$$

and for a bottom branch,

$$FrBo^2 N_\mu^{-0.5} = 40.6\left(\frac{H}{\sqrt{\sigma/g\Delta\rho}}\right)^{2.1}. \qquad 2.10$$

The effects of surface tension,σ, are accounted for in the Bond number, Bo, defined as

$$Bo = \frac{d}{\sqrt{\sigma / g\Delta\rho}}. \qquad 2.11$$

The effects of viscosity, μ, were accounted for with the dimensionless viscosity number, N_μ, defined as

$$N_\mu = \mu\left(\frac{g\Delta\rho}{\rho^2\sigma^3}\right)^{0.25}. \qquad 2.12$$

In terms of the critical height at the onset of liquid entrainment, the side branch results were found to be independent of viscosity and surface tension effects, and of the same form as Equation 2.1 with $m_1 = 0.624$ and $m_2 = 0.400$.

Yonomoto and Tasaka (1988) presented theoretical and experimental results for gas entrainment in side and bottom branches and also for liquid entrainment in a side branch from a stratified two-phase region. Their theoretical analysis provided a correlation between the liquid height and the two-phase quality during entrainment and was derived with several assumptions. They assumed that flow directions were toward the branch inlet with uniform velocity in both phases, and was a function of the distance from the branch. Pressure losses due to interactions of both phases and effects of flow contraction at the branch inlet were neglected. Lastly, they assumed that the two phases could be

considered to flow separately with negligible viscosity, compressibility effects, and phase change effects, while the branch inlet could be regarded as a point sink on an infinite flat plane. Their experimental facility consisted of a horizontal square duct with 190 mm side length with sharp-edged orifices of either 10 or 20 mm simulating the branch and an operating pressure of 0.7 MPa. They derived their theoretical model into the form of Equation 2.1 and correlated their experimental results. This resulted in values of m_1 and m_2 for OGE in the bottom branch of 0.909 and 0.400, and for the side branch of 0.681 and 0.400 respectively. The onset of liquid entrainment in the side branch yielded values of m_1 and m_2 of 0.559 and 0.400. The liquid entrainment results demonstrated good agreement with their theoretical model, but the gas entrainment model did not. The reason for the disagreement was explained based on the earlier assumptions that were made regarding the stability of the flow, and that the presence of a vortex and cross-flow was omitted from the model. Notably, they mentioned that the presence of intermittent entrainment could be neglected and represented a single phase flow in the branch.

Micaelli and Memponteil (1989) presented experimental results for the onset of gas entrainment in side and bottom branches, as well as, the onset of liquid entrainment in a side branch from a stratified steam-water region. Their experimental facility included a 135 mm I.D main pipe with 12 and 20 mm I.D branches at the side and bottom. The operating pressure ranged between 2 and 7 MPa. One of the objectives of the study was to extend the range of flow conditions presented by previous authors. Their experimental results for the onset of liquid entrainment correlated well with the form of Equation 2.1, with values of m_1 and m_2 similar to that of Smoglie and Reimann (1986). With regard to

the onset of gas entrainment in the bottom branch, the authors cited results for vortex-free gas pull-through, stating that they represent the most probable case of gas entrainment. Their results indicated that for low cross flow velocities in the main pipe, their results correlated well with Equation 2.1. Values of m_1 and m_2 were found similar to that of Smoglie and Reimann (1986), however, at higher cross flow velocities a significant difference was observed. The authors stated that the gas core could be broken by the transverse flow, and so the stability of the gas pull through is dictated by a balance of the horizontal and vertical inertial forces and characterized by a ratio, R, of liquid cross flow velocity, v_{LC}, to the velocity in of the flow in the branch, v, as

$$R = \frac{\rho_L v_{LC}}{\rho_L v}. \qquad 2.13$$

Using this ratio they developed an equation relating the critical height for the onset of gas entrainment in a bottom branch as,

$$\frac{H}{d} = 0.907\left[1 - R^{0.4}\right]Fr^{0.4}. \qquad 2.14$$

Soliman and Sims (1992) presented a theoretical analysis for the onset of liquid entrainment in a side branch from a stratified two-phase region. Their analysis provided an improvement of the previous correlation by Craya (1949) for the critical height at the onset of liquid entrainment. Their analysis demonstrated that the previous model had

limitations at very low Froude numbers, and did not approach the correct physical limits. The authors suggested that at very low Froude numbers a more appropriate limit was H/d = 0.5, which represents the gas-liquid interface located at the bottom of the branch inlet. By applying potential theory the authors derived a relation for the critical height as,

$$\frac{H}{d} = \frac{s}{d} + \frac{1}{2}\left(\frac{Fr}{\pi}\right)^2 \left[\ln\left(\frac{\frac{s}{d} - \frac{1}{2}}{\frac{s}{d} + \frac{1}{2}} \right) \right]^2 \qquad 2.15$$

and

$$\ln\left(\frac{\frac{s}{d} + \frac{1}{2}}{\frac{s}{d} - \frac{1}{2}} \right) = \frac{\left(\frac{s}{d}\right)^2 - \frac{1}{4}}{\left(\frac{Fr}{\pi}\right)^2}. \qquad 2.16$$

The additional parameter, s, defines the distance from the center of the branch to the tip of the deflected liquid interface. Solving these two equations, the critical height, H/d, approached the more appropriate limit of 0.5. At higher Froude numbers the model approached that of Craya (1949) with a 1% deviation at Fr = 30.9, 16.6% deviation at Fr = 1, and 106% deviation at Fr = 0.1. The authors compared their model with experimental data and demonstrated very good agreement for the range of Froude number investigated.

Hassan et al. (1994) presented an experimental study of the onset of gas and liquid entrainments, from a stratified two-phase region, in a single discharging side branch. The diameter of the branch used in the investigation was 6.35 mm. Additionally, their study presented experimental data regarding the two-phase quality and mass flow rate as the fluid goes through the transition from single phase liquid to single phase gas, as the liquid level is decreased. They performed their experiments using air and water at an operating pressure of between 316 and 517 kPa and using two methods to record the onset of liquid entrainment. Their first method used a decreasing liquid level technique which was conducive to the actual process occurring during a LOCA, due to the reduction in liquid height. The second method was to record the onset of liquid entrainment with an increasing liquid level, where the surface above the gas-liquid interface was dried prior to each case. The difference between the two methods indicated that the increasing liquid level resulted in slightly lower values of critical height at the onset of liquid entrainment. Their experimental results for the onset of gas entrainment demonstrated a significant difference with the correlations of previous researchers. The closest correlations were found to be with that of Micaelli and Memponteil (1989) and Parrott et al. (1991). The onset of liquid entrainment results demonstrated relatively good agreement with the correlations of previous researchers, although it is noted that their results tend to deviate at lower Froude numbers.

2.4 Multiple Discharges

Kowalski and Krishnan (1987) presented an experimental study on the flow phenomena occurring during steady, two-phase, steam-water injection in a typical full scale CANDU header-feeder. The test section consisted of a 4.15 m long pipe with 0.325 m internal diameter steel pipe acting as the header, with two vertical turrets at the north and south ends. Along the length of the header were six banks of equally spaced 50.8 mm diameter feeder branches located at 0°, 45°, 90°, 135° and 180° as shown in Figure 1.1. The operating pressure ranged from 1 to 5 MPa. They concluded that during steam injection through the turrets flow stratification in the header occurs, whereby a two-phase steam-water region is created. They compared their results for the critical height at the onset of gas and liquid entrainments with the correlations offered by Smoglie and Reimann (1986) and demonstrated very poor agreement. Their reasoning for the poor agreement was that the previous authors presented correlations with liquid cross flow velocities.

Parrott et al. (1991) experimentally investigated the onset of gas entrainment during dual discharge from a stratified air-water region. Their study was motivated by Kowalski and Krishnan (1987)'s study, and aimed to further the understanding of the gas entrainment phenomenon in multiple discharge scenarios. Their test section consisted of two 6.35 mm diameter branches located on a flat wall and separated by a vertical distance. Their experiments were carried out at an operating pressure of 510 kPa. In their investigation, the air-water interface was always above the top branch, indicating that the initial fluid phase in both branches was water. Their results for single discharge cases correlated well with the form of Equation 2.1, neglecting viscous and surface tension effects, with m_1

and m_2 of 0.425 and 0.529 for $H/d \leq 1.15$, and for $H/d > 1.15$ m_1 and m_2 were 0.508 and 0.435. The authors pointed out that their correlations demonstrated good agreement with the results presented by previous researchers, although, their investigation was carried out without cross flow, and with a flat wall rather than a curved one. The authors indicated that three regions are evident under the dual discharge scenario and depend greatly on the individual branch flow rates and separating distance. The vertical separating distances used in their investigation were 9.52 mm, 12.70 mm, 19.05, 25.40 mm and 38.10 mm. In the first region gas entrainment occurs in the branch closest to the gas-liquid interface; in the second gas entrainment occurs only in the bottom branch, and in the last simultaneous entrainment occurs in both branches. The influence of decreasing the separating distance between the two branches was seen to increase the critical height of gas entrainment.

Armstrong et al. (1992) investigated the onset of liquid entrainment during dual discharge from a stratified two-phase region both experimentally and theoretically. The test facility and test section was the same as used by Parrott et al. (1991) with an operating pressure of 310 kPa. The vertical separating distances used in their investigation were 9.52 mm, 12.70 mm, 19.05 mm and 25.40 mm. In their investigation, the air-water interface was always below the bottom branch, indicating that the initial fluid phase in both branches was air. The authors noted that in every experimental case, the onset of liquid entrainment was observed to occur only in the branch closest to the air-water interface. In the instance of single discharge, their results correlated well with the form of Equation 2.1 with m_1 and m_2 equal to 0.625 and 0.4 and in good agreement with Craya (1949). The dual discharge results indicated the effect of increasing the secondary branch flow rate is to increase the critical height at which liquid entrainment occurs. Secondly, the

authors point out that increasing the vertical separating distance between both branches results in a decrease in the critical height of liquid entrainment. The authors also presented a new theoretical analysis which modeled both branches as point sinks, neglecting both viscous and surface tension effects. The result of their analysis was a relationship between the Froude number of each branch, and the critical height for liquid entrainment. Comparisons of their theoretical model and experimental results demonstrated good agreement, with no more than 10% deviation.

Hassan et al. (1996a) experimentally investigated the onset of gas and liquid entrainments, from a stratified air-water region, in two branches located on the same horizontal plane. Their test section consisted of two 6.35 mm branches located on a flat wall separated by a horizontal distance. The authors selected horizontal separating distances, L_h, of 9.52 mm, 12.70 mm, 19.05 mm and 50.8 mm. The operating pressure ranged between 316 and 517 kPa. Their results for the onset of gas and liquid entrainment indicated that both branches will exhibit nearly identical values for the critical height, given similar flow rates in both branches. Their results for the onset of gas entrainment indicated that increasing the horizontal separating distance, keeping both branch flow rates constant, yields a decrease in the critical height. Limiting cases are also demonstrated in that as the separating distance increases, the results will approach that of a single discharge scenario. The other limiting case occurs when the separating distance approaches zero, and reduces to the case of a single discharging branch with double the flow rate. Similar conclusions were also demonstrated for the onset of liquid

entrainment experiments. The authors correlated their experimental results for the critical height for both the onset of gas and liquid entrainments as,

$$\frac{H_{OGE}}{d} = 0.57[A \cdot Fr_{OGE}]^{0.4} \qquad 2.17$$

and

$$\frac{H_{OLE}}{d} = 0.87[B \cdot Fr_{OLE}]^{0.31}, \qquad 2.18$$

where

$$A = 1 + \exp\left[\frac{-0.613(L_h / d)^{1.5}}{Fr_{OGE}^{0.4}}\right] \qquad 2.19$$

and

$$B = 1 + \exp\left[\frac{-2.06(L_h / d)^{2.54}}{Fr_{OLE}^{1.2}}\right]. \qquad 2.20$$

Hassan et al. (1996b) continued in the same manner with an experimental investigation using two branches located in the same vertical plane separated by a vertical distance L. Their results demonstrated the onset of gas and liquid entrainments as the air-water interface descended from above the top branch, to below the bottom branch, with both branches active. Their observations indicated that as the distance between the branches increased the interaction between the branches decreased. This resulted in a reduction in

the critical height for gas entrainment in the top branch with an increase in the critical height for the bottom branch. Similar conclusions were noted by the authors regarding the onset of liquid entrainment results. Of notable interest, the authors also investigated the two-phase quality and mass flow rates in the branches as the air-water interface descended from above the top branch to below the bottom branch. This demonstrated the effect of the location of the air-water interface relative to the branch where onset occurs. In fact, their observations indicated that depending on the location of the air-water interface relative to the branch where onset occurs, the secondary branch may assist or hinder entrainment. The authors presented correlations for the critical heights of both the onset of gas and liquid entrainments in the top, subscript A, and bottom, subscript B, branches neglecting viscous and surface tension effects as,

$$\frac{H_{OGE,A}}{d} = 0.57\left[A_1 \cdot Fr_{OGE}\right]^{0.4}, \tag{2.21}$$

$$\frac{H_{OGE,B}}{d} = 0.57\left[Fr_{OGE}\right]^{A_2}, \tag{2.22}$$

$$\frac{H_{OLE,A}}{d} = 0.87\left[Fr_{OLE}\right]^{A_3}, \tag{2.23}$$

and

$$\frac{H_{OLE,B}}{d} = 0.87\left[A_4 \cdot Fr_{OLE}\right]^{0.31}, \tag{2.24}$$

where

$$A_1 = 1 + \exp\left[\frac{-1.96(L/d)^{1.2}}{Fr_{OGE}^{0.32}}\right], \tag{2.25}$$

$$A_2 = 0.4 - 0.223\exp\left[\frac{-0.415(L/d)^{1.5}}{Fr_{OGE}^{0.20}}\right], \tag{2.26}$$

$$A_3 = 0.31 - 0.13\exp\left[\frac{-0.209(L/d)^{1.5}}{Fr_{OLE}^{0.20}}\right], \tag{2.27}$$

and

$$A_4 = 1 + \exp\left[\frac{-0.277(L/d)^{1.2}}{Fr_{OLE}^{0.32}}\right]. \tag{2.28}$$

Hassan et al. (1997) further investigated the two-phase quality and mass flow rate occurring in single, dual and triple discharges from a stratified air-water region. The test section they used was scaled from a typical CANDU header-feeder bank arrangement. In their case the authors used a 50.8 mm diameter semi-circular cross section to model the header with three branches located at 0°, 45° and 90° from the horizontal. Reasoning for the design of the test section was given due to the ease of measuring the liquid height relative to the branches, good flow visualization and the exposure of the branches to the stratified region was similar to the actual scenario as previously presented by Kowalski and Krishnan (1987). Consequently, it turned out that their semi-circular design was a good approximation of the circular cross section geometry with five branches, as in an

actual header-feeder. They discovered that the flow quality from the bottom 90° branch was virtually independent of whether flow was present in the other two branches within the tested range. They therefore concluded that it was unlikely for the missing two branches to have an impact on the flow in bottom branch. Additionally, they stated that the missing branches were sufficiently far from the 0° and 45° side branches as to not impact their flow either. By comparing their previous results for flat vertical wall with single and dual discharges the authors were able to demonstrate the effect of wall curvature on the two-phase quality and mass flow rate. The information available from their study regarding the onset of gas and liquid entrainment was somewhat limited due to their focus being with the two-phase quality and mass flow rate.

Hassan et al. (1999) followed their experimental investigations with a theoretical analysis of the onset of liquid entrainment in two discharging branches located on the side of an inclined wall. Their model neglected viscous and surface tension effects and assumed that inertia and gravity forces were dominant. Their finite branch model demonstrated an improvement to Armstrong et al. (1992)'s point sink model in predicting the critical height at the onset of liquid entrainment. This was due to its ability to predict the correct physical limit at very low Froude numbers, that is H/d = 0.5. At moderate to high Froude numbers, both the point sink and finite branch models predict almost identical values for the critical height. The authors compared their theoretical model with experimental data for a flat vertical wall with two discharging side branches, from a stratified air-water region, with excellent agreement. This was particularly true at the lower Froude range, where the physical limit was correctly predicted.

Maier et al. (2001a) provided a theoretical investigation of the onset of liquid entrainment during dual discharge, from a stratified gas-liquid region, with branches located on a flat wall and with centerlines falling on an inclined plane. Their analysis predicts the critical height for liquid entrainment to occur, and neglects viscous and surface tension effects, while assuming that gravity and inertia forces are dominant. Their analysis follows a similar finite branch analysis as demonstrated by Hassan et al. (1999) and demonstrates the ability to correctly predict the physical limits, as the Froude number approaches 0, at H/d = 0.5. Maier et al. (2001b) further investigated experimentally the onset of gas and liquid entrainments during dual discharge, from a stratified air-water region, with branch centerlines falling on an inclined plane. The test section was a flat wall with four 6.35 mm branches located with center-to-center separating distances of 12.7 mm and 50.8 mm. To achieve the inclined axis, along which both branches were located, the authors could rotate the entire test section to yield the desired angle between 0° and 90°. They used an operating pressure range between 510 kPa and 310 kPa for the gas and liquid entrainment experiments respectively. Their results demonstrated the effect of separating distance, relative inclination of the branch centerlines, and branch Froude number on the critical height of both gas and liquid entrainments. The authors also compared their experimental results with the finite branch model they developed earlier with excellent agreement.

Ahmad and Hassan (2005) established an experimental test facility at Concordia University in Montreal, Canada similar to that of Hassan et al. (1997). It consisted of a T-shaped pressurized reservoir with controllable air and water inlets to provide the

smooth stratified two-phase environment. The test section used by the authors was also similar in design to that of Hassan et al. (1997) and consisted of a semi-circular cross section with three 6.35 mm diameter branches located at 0°, 45° and 90° from the horizontal axis. They used air and water in their experiments, at operating pressures of 206.8 and 413.7 kPa. The air-water interface, throughout their experimental cases, was always above the top branch. That is, in all cases water was the initial fluid phase in all active branches before onset of gas entrainment occurred. The authors presented results for the onset of gas entrainment under single, dual and triple discharge cases for a wide range of Froude numbers. They demonstrated the effects of vertical separating distance between the branches, and secondary branch flow rates, on the critical height for gas entrainment. The authors also demonstrated that regions exist where the onset of gas entrainment will occur in the branch closest to the air-water interface, in both branches or in the branch furthest away from the interface.

2.5 Current Investigation

The current work is an experimental investigation and will present data pertinent to LOCA in a CANDU header-feeder, and generally speaking, any application that demonstrates single, dual or triple discharges from a stratified two-phase region. To further add to the contribution of Hassan et al. (1997) and Ahmad and Hassan (2005), the present work will provide new information regarding the onset of liquid entrainment under a variety of discharge scenarios from a stratified two phase region. The critical height for the onset of liquid entrainment will be presented for single, dual and triple discharges, and the effects of branch separating distance, branch Froude number, location of the air-water interface relative to the branches will be investigated. Additionally the results for the onset of liquid entrainment will be presented using two methods to record the critical height, the increasing and decreasing liquid level techniques as demonstrated by Hassan et al. (1994).

The second objective of this experimental investigation will be to measure the liquid velocity field at the onset of gas entrainment in a single discharging bottom branch using the particle image velocimetry technique. This will provide new information regarding the onset of gas entrainment phenomena, and is intended as a preliminary study which can be used to guide future investigations. The practical aspect of the velocity field is that it can be used to solve theoretical models that require semi-empirical solutions, and ultimately be used in their validation.

Chapter III

Experimental Investigation

3.1 Facilities and Resources

Recently an experimental test facility was established at Concordia University in Montreal, Canada, by Ahmad and Hassan (2005) and used in the present investigation. The facility incorporated design features as outlined by Hassan et al. (1997), including a similar test section. The present work featured this test facility and test section but also modified the setup to include the PIV measurement technique. To incorporate the PIV system the design of a new test section was required. Below, the two test sections used in this work will be described followed by the experimental facility, including the two-phase reservoir flow loop and PIV system, and finally the experimental procedures used in both experimental runs will be described in detail.

3.2 Test Sections

The test section geometry used to simulate a typical CANDU header-feeder system is shown in Figure 3.1. It has a semi-circular cross section with branches located at 0°, 45° and 90° from the horizontal axis, which are referred to as branches A, B and C respectively throughout this text. A dimensional analysis of the geometry, using relevant physical parameters and neglecting viscous and surface tension effects, provides the following relationship,

$$\frac{H}{d} = f(\frac{L}{d}, Fr_1, Fr_2, Fr_3). \qquad 3.1$$

The parameter H is the critical height at the onset of gas or liquid entrainments, and measured from the branch center to the gas-liquid interface. The branch diameter d, and the center-to-center distance between two branches L are defined. With a circular branch the Froude number, Fr, is defined as,

$$Fr = \frac{4\dot{m}}{\pi\sqrt{(gd^5\rho\ \Delta\rho)}}. \qquad 3.2$$

The mass flow rate of the single phase fluid flowing in the branch is defined by $\dot{m}$, and gravitational acceleration is defined as g. The difference between the heavier and lighter fluid phases, $\Delta\rho$, and the density of the single phase fluid ρ are defined. The convention used throughout this text uses 'primary branch' to denote the branch where onset occurs and is denoted by subscript '1' in Equation 3.1. If additional branches are active then they are denoted as secondary branches and denoted with subscripts '2' and '3' for dual and triple discharges respectively in Equation 3.1. Two test sections were used during experimentation, and it is helpful to point out that for each of the phenomena studied, onset of liquid or gas entrainments, only one test section was used for each study. The OLE experiments were performed using the semi-circular brass test section shown in Figure 3.2, and the OGE experiments were performed with the quarter-circular acrylic test section as shown in Figure 3.3. A further discussion regarding the design features of both will be presented below.

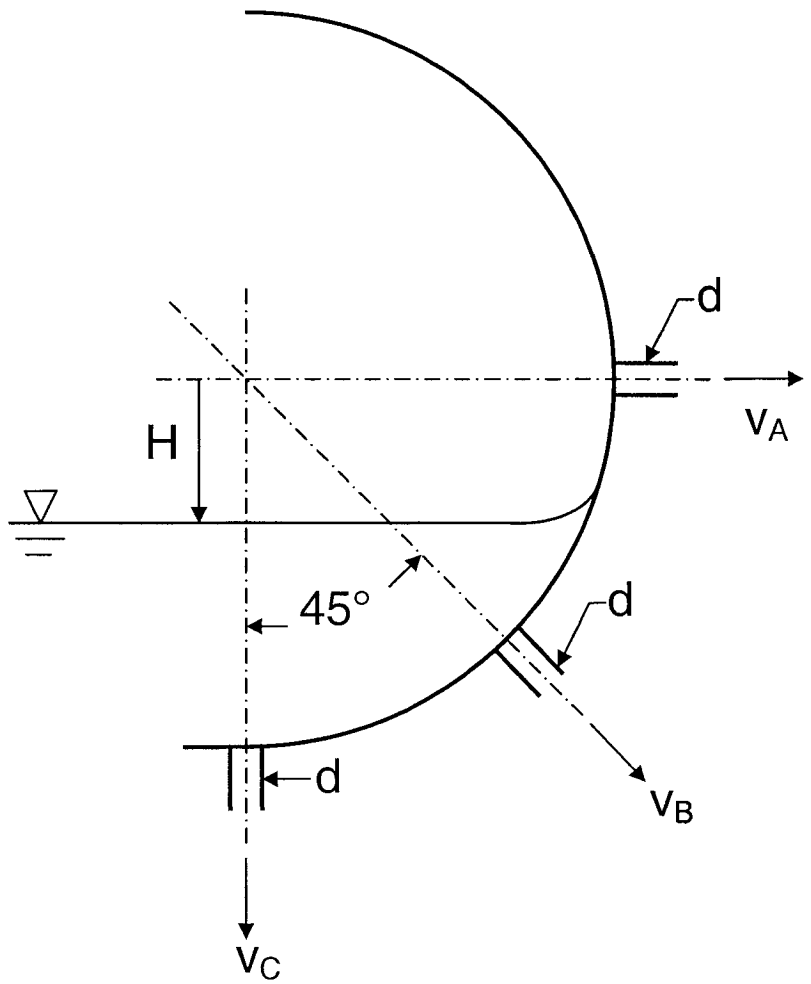

Figure 3.1 Test section geometry simulating a CANDU header-feeder.

3.2.1 OLE Experiments

The brass test section used in the OLE experiments is shown in Figure 3.2, and was manufactured by Ahmad and Hassan (2005). The figure shows the test section mounted in the two-phase reservoir, as will be discussed later. The test section was designed to provide experimental advantages, such as flow visualization conducive to the OLE measurements. Due to it's design, the test section is also exposed to a smooth stratified two-phase region when installed in the test facility. Hassan et al. (1997) concluded that the semi-circular test section design could reasonably simulate a single CANDU header-feeder bank.

The test section was manufactured from a solid brass block, with a diameter of 50.8 mm and a length of 50.8 mm. Three 6.35 mm diameter holes were drilled into the semi-circular surface at 0°, 45° and 90°, and extended until a minimum of four diameters and then enlarged to a diameter of 9.56 mm. The test section represents a 1/8 scale of a typical header-feeder bank section.

3.2.2 OGE Experiments

The test section used in the OGE experiments, with the PIV system, required a modification to enhance optical access. As a result, the test section shown in Figure 3.3 was designed and manufactured. The overall concept of the design was similar to that of Ahmad and Hassan (2005), with the objective to simulate the CANDU header-feeder geometry. Three 6.35 mm diameter holes were drilled into the quarter-circle surface at 0°, 45° and 90° and extended until a minimum of four diameters, and then enlarged to

9.56 mm. The difference with this design is that the top quarter of the semi-circular cross section was replaced by a flat vertical wall. It is expected that this will result in a small difference in the OGE results due to the effect of wall curvature. The advantage of this design is that it allows the velocity fields to be captured in a horizontal plane using the PIV system, previously not possible with the brass test section. Another new feature of the test section was the material from which it was made, cast clear acrylic. After machining the test section, all surfaces were polished using an abrasive technique to maintain the surface quality. An unexpected outcome of this test section, due to the high quality of machining and polishing, was the ability to visualize the flow inside the branches, as was previously not possible with the brass test section. In order to mount copper plumbing to the outlet side of the test section branches it was necessary to design a rugged seal capable of withstanding the operating pressures. To accomplish this three brass blocks were machined with a groove on one face to accept an o-ring, and a larger hole on the opposite face to accept a 12.7 mm I.D. copper pipe. The copper pipe was inserted into the brass block and soldered together. This assembly was mounted onto the outlet side of each branch and fastened using four 10-24 UNC cap screws.

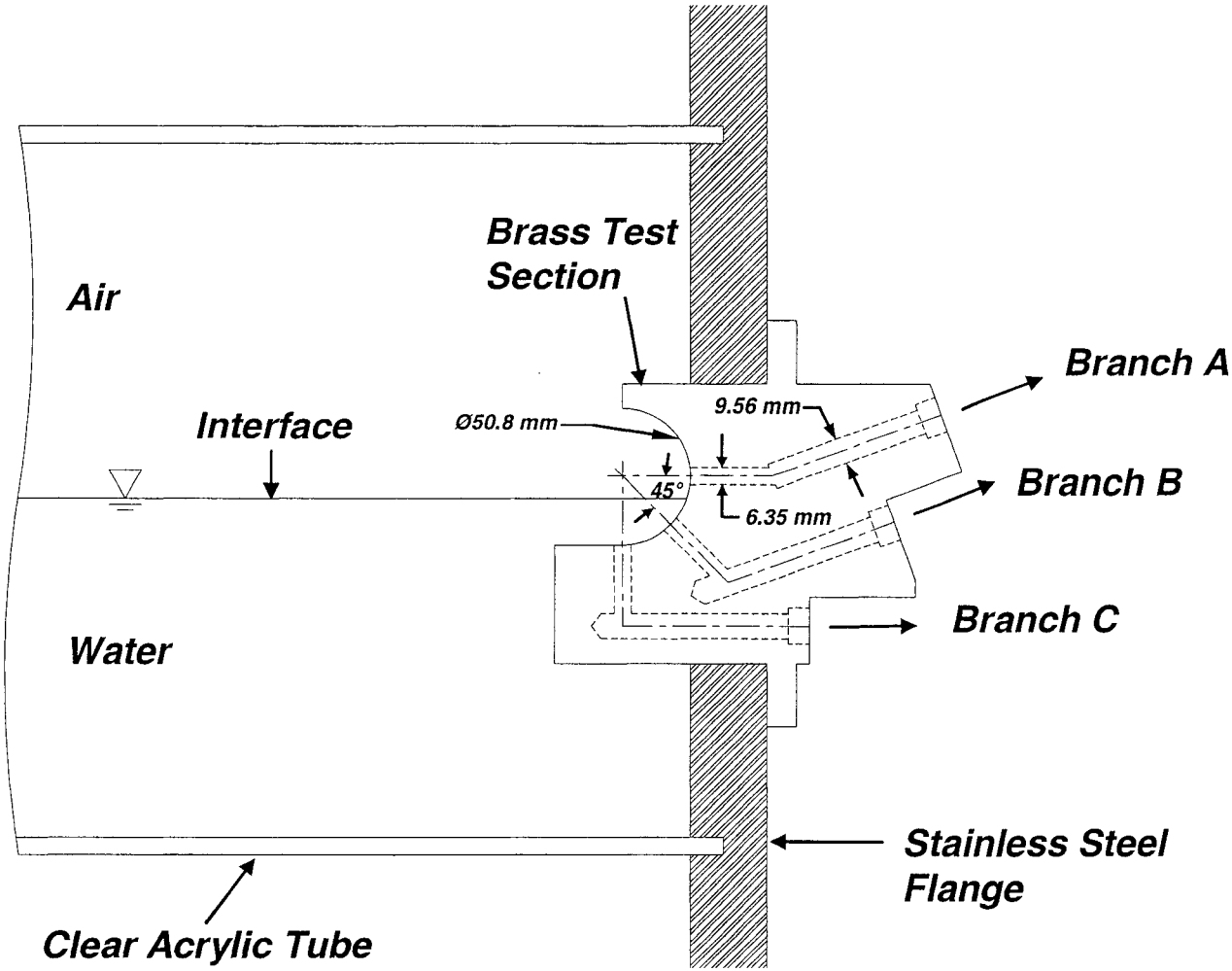

Figure 3.2. Brass test section, shown installed in two-phase test facility.

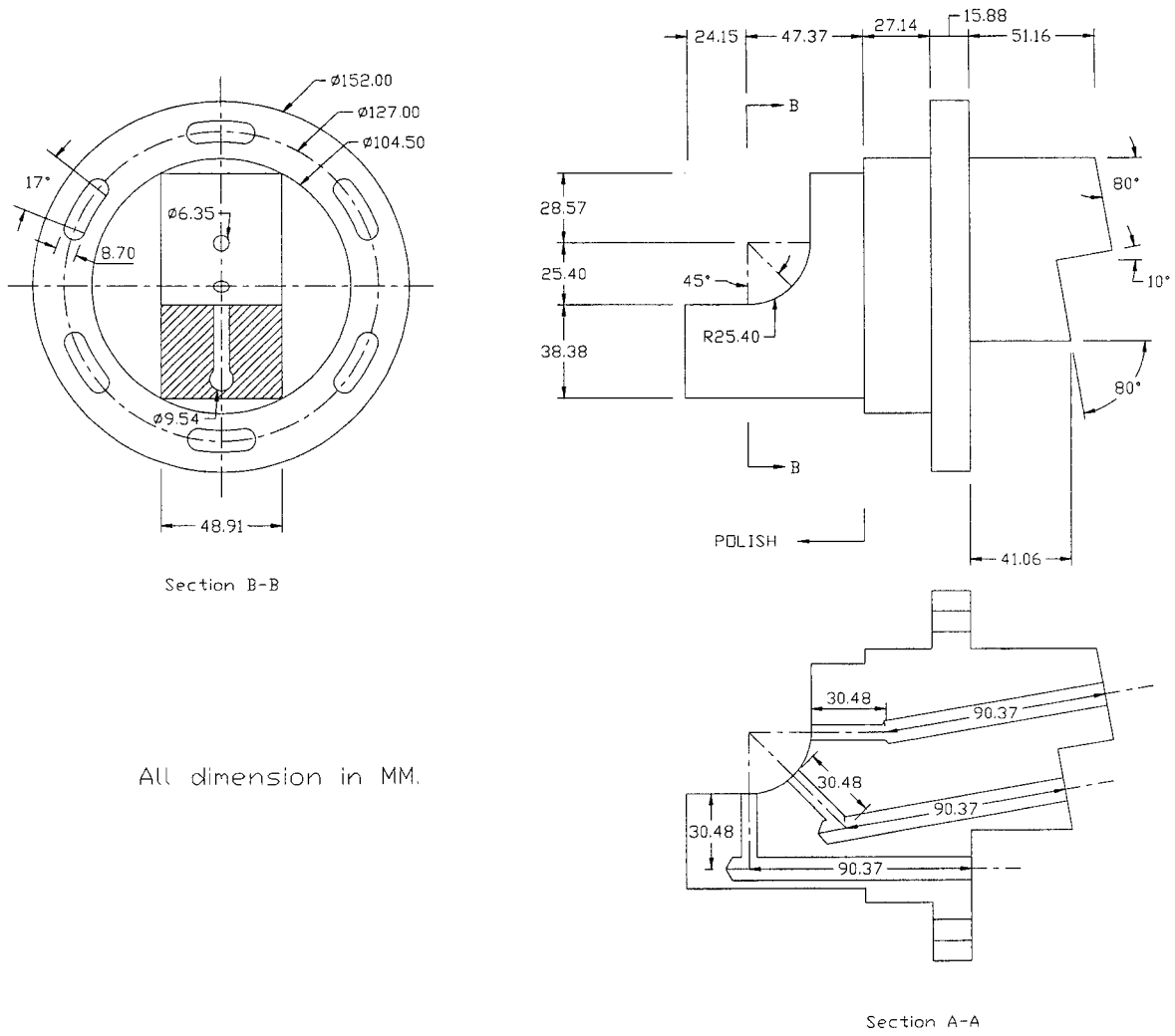

Figure 3.3. Acrylic test section

3.3 Experimental Test Facility

The experimental test facility consists of two main systems, and will presented here as such, the flow distribution and the particle image velocimetry (PIV) systems. The flow distribution consists of the components necessary to establish the two-phase environment and maintain the operating set points, such as pressure and flow rate. The PIV system is a standalone package that can be adapted to a particular fluids experiment.

3.3.1 Flow Distribution

The test facility flow loop is presented in Figure 3.4, of which further details can be found in Ahmad and Hassan (2005). An image of the two-phase reservoir is presented in Figure 3.5. The two-phase reservoir was made from thick walled stainless steel pipe capped at the three ends. At the right, a section of clear acrylic tube is fastened to the two-phase reservoir. The test section is mounted on a flange to the right of the acrylic tube, and sealed with an O-ring. To supply air to the two-phase reservoir, an open loop system is used. To provide a steady controllable source of air a Fisher Pressure Controller was selected to maintain the air pressure at a set-point. As air discharges through the test section branches, from the two-phase reservoir, it enters a distribution block connected to five air flow meters connected in parallel, with overlapping ranges up to 2.83 m^3/min (100 ft^3/min). To monitor the static air pressure in the two-phase reservoir, a Rosemount LCD pressure transducer was used and factory calibration provided a range of 0-830 kPa. To supply water to the two-phase reservoir, a closed loop system was used. Water was stored in a 208 L (55 gallon) tank and was connected to a 3 hp SSV 8-stage vertical pump, which directed the water flow to the inlet of the two-phase

reservoir. As water exits the branch it is directed towards a distribution block connected to four water flow meters connected in parallel, with overlapping flow rates up to 75 L/min. From the water flow meter the flow is directed back to the water tank, completing the loop. To measure the liquid height inside the two-phase reservoir, a Rosemount LCD digital display differential pressure transducer was used, and factory calibration provided a 0-255 mm H_2O range. Connections were established using flexible PVC tubing, maintaining hydraulic resistance throughout, valves provided flow control. A summary of the measurement components are presented in Table 3.1.

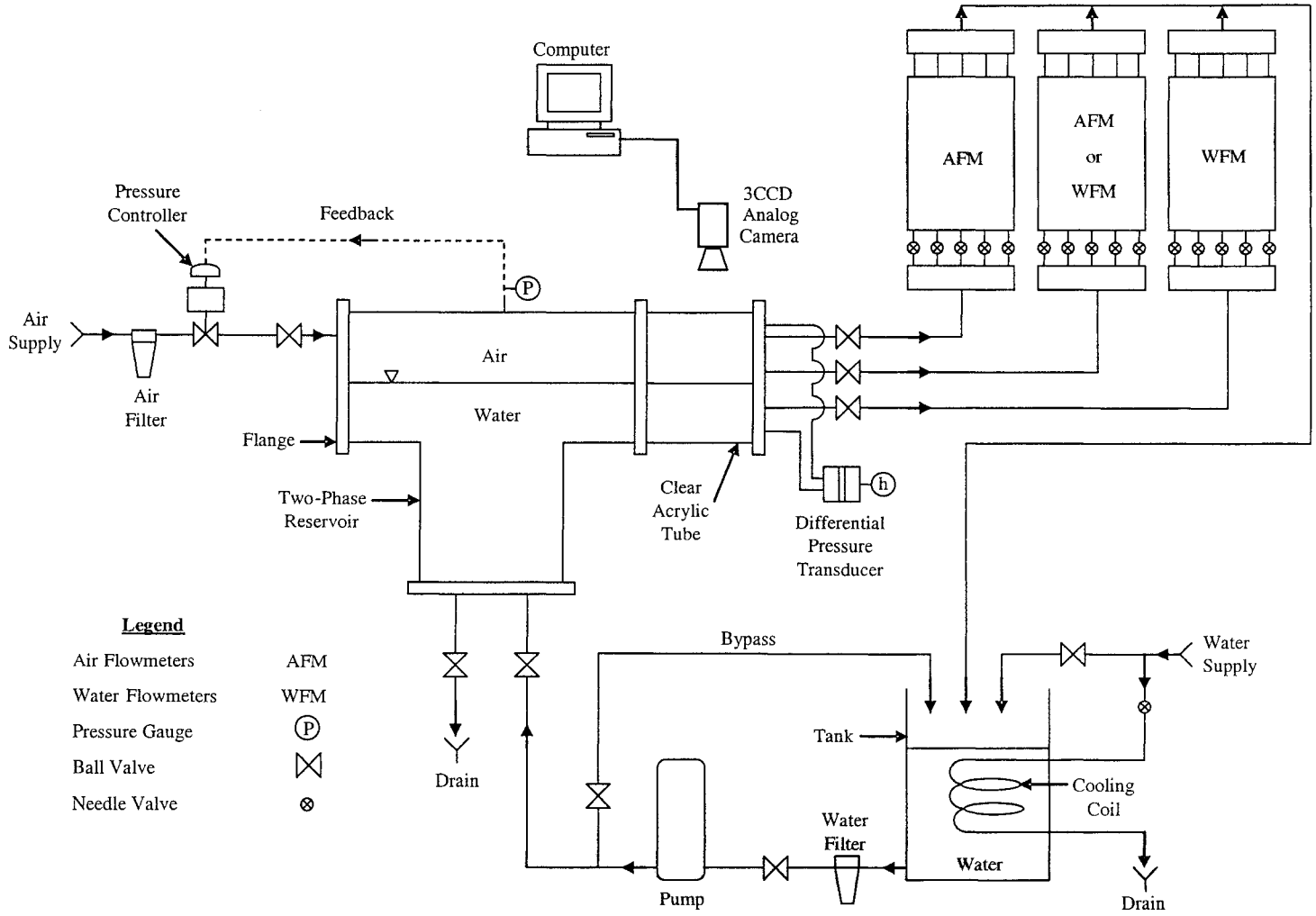

Figure 3.4. Experimental test facility flow loop.

Table 3.1 Measurement components

Device	Model	Range	Accuracy
Air flow meter	FL-1343-G	40 - 400 cm^3/min	±10% Full scale
	FL-1344-S	333.3 - 3333 cm^3/min	±10% Full scale
	FL-2042	3000 - 30000 cm^3/min	±2% Full scale
	FL-1503-A	29590 - 295900 cm^3/min	±2% Full scale
	FL-2093	283168 - 2831680 cm^3/min	±2% Full scale
Water flow meter	FL-3805-G	8.4 - 84 cm^3/min	±2% Full scale
	FL-1448-G	57.3 - 573 cm^3/min	±5% Full scale
	FL-1502-A	548.88 - 5488.84 cm^3/min	±2% Full scale
	FL-2128	5000 - 75000 cm^3/min	±5% Full scale
Static pressure	Rosemount 2088G	0 - 830 kPa	±0.1% Full scale
Differential pressure	Rosemount 3051 CD	0 - 255 mm H2O	±0.15% Full scale

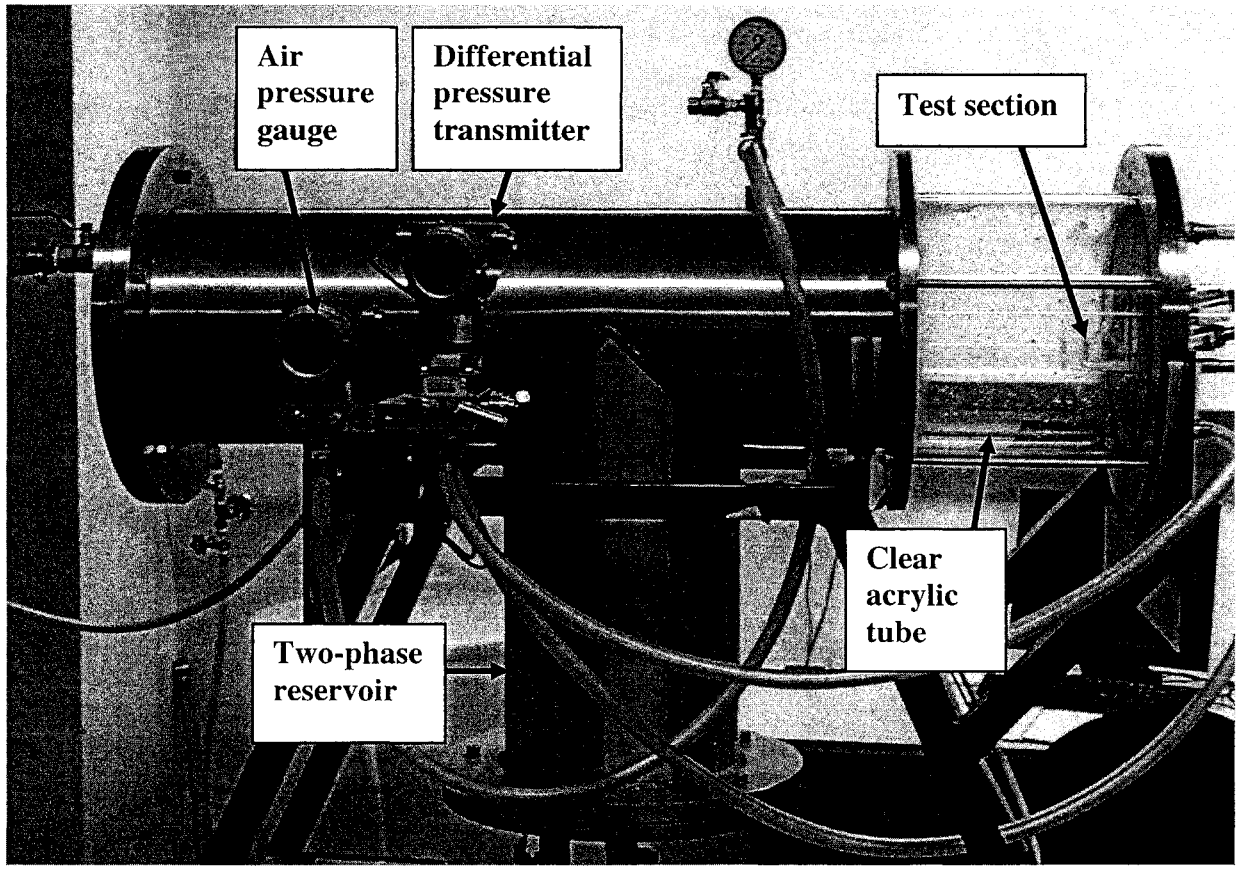

Figure 3.5. Image of the two-phase reservoir.

3.3.2 PIV System

The particle image velocimetry system was obtained from Dantec Dynamics and has both two-dimensional, as well as three-dimensional capabilities. The current study takes advantage of the two-dimensional abilities, and the system will be described as such. An image of the PIV system adapted to the two-phase test facility is presented in Figure 3.6. The particles used to seed the liquid flow were polyamide, PSP-20, having a mean diameter of 20 μm and have the property of being nearly neutrally buoyant in water. A New Wave Research Solo XT 120 Nd:YAG pulsed laser, capable of 120 mJ/pulse at a 532 nm wavelength and a maximum pulse rate of 15 Hz, was used to illuminate the particles. Pre-packaged optics converted the single beam output from the laser head, into a light sheet. To capture the particle displacement a HiSense MkII 12 bit digital output CCD camera with 1344x1024 pixel resolution was used, and in the current setup, allowed for a maximum capture rate for a pair of images at 5.67 Hz. A Nikon objective lens, mounted to the camera, provided focal length and shutter illumination adjustments. To record the images a National Instruments NI-IMAQ PCI-1426 frame grabber card was used in conjunction with the camera. The camera and laser pulses were synchronized using a National Instruments NI-DQQ PCI-6601 timer board. In order to handle the large data processing requirement a Dell Precision Workstation with two 3.60 GHz Intel Xeon processors, 4 GB of RAM, two 250 GB 7200 RPM hard disks, and a 128 MB video card was used. The Flow Manager software, provided by Dantec Dynamics, performed the necessary data processing such as cross-correlation, adaptive-correlation, filtering, and statistical analysis to generate the desired velocity field.

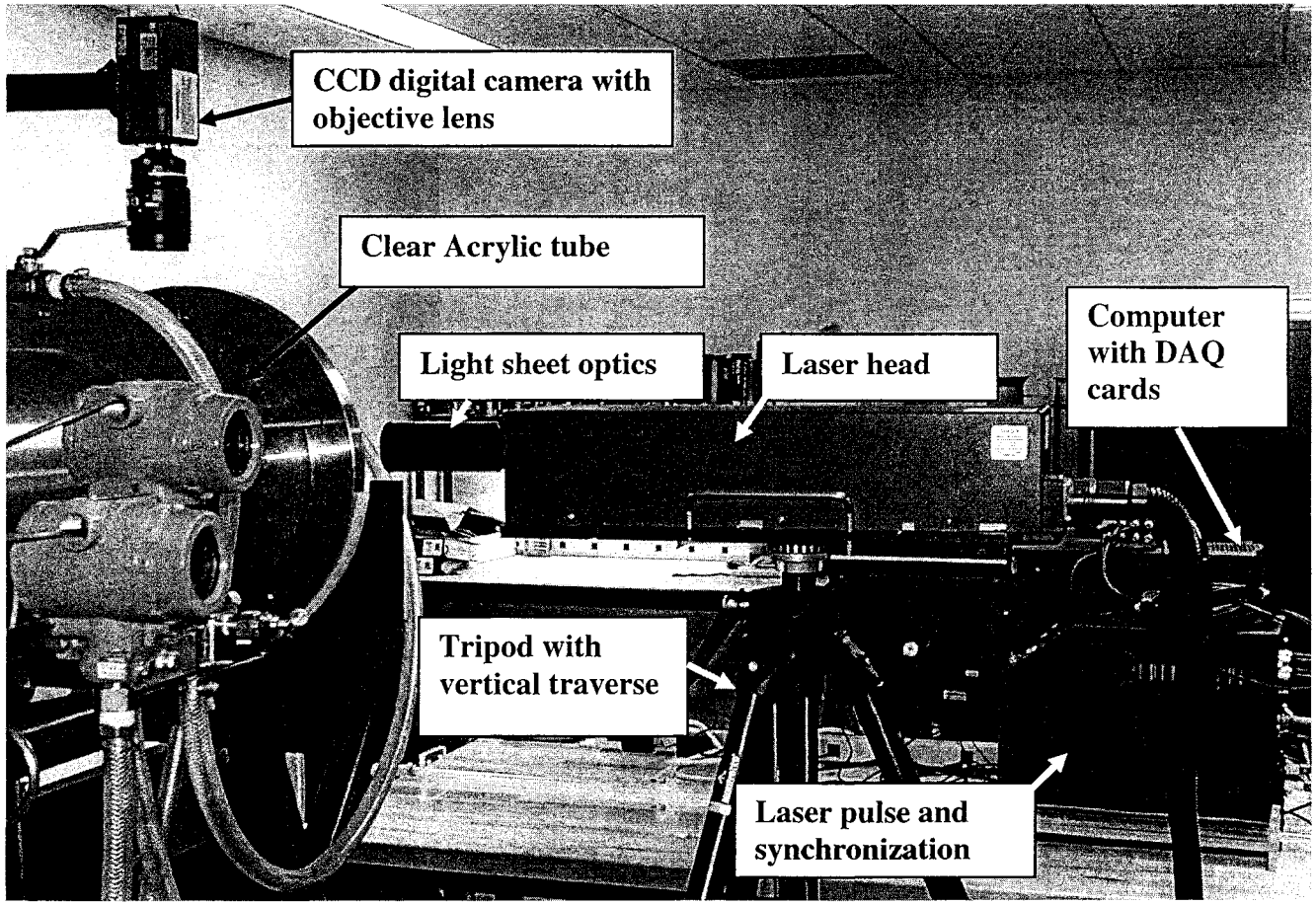

Figure 3.6. Image of PIV system adapted to two-phase test facility.

3.4 OLE Experimental Procedure

The procedure for recording the onset of liquid entrainment is described below. It should be noted that the following procedure yields results for both increasing liquid level (ILL) and decreasing liquid level (DLL). The method to capture OLE is determined based on flow visualization, as will be described below. Routine cleaning of the test section surface was performed to maintain surface integrity.

Water was first added to the two-phase reservoir, keeping the air-water interface well below the primary branch. The two-phase reservoir was then pressurized to the desired set point. The primary branch air flow rate was adjusted to the desired value, as well as, the flow rates of any additional branches. The water level was slowly increased until a stream of water was seen to be pulled into the primary branch, as shown in Figure 3.7. The liquid height was recorded as the onset of liquid entrainment with ILL. It is important to note that at low Froude numbers, with ILL, care must be taken to observe the air-water interface near the inlet of the branch. The water level was then slowly decreased until the stream of water ceased to flow into the primary branch, at which time the liquid height was recorded. This value determined the onset of liquid entrainment with DLL. The brass test section was dried using a high air flow rate and the procedure was repeated for the next primary branch flow rate.

The test matrix of experimental data for the single, dual and triple discharge cases are presented in Table 3.2, Table 3.3 and Table 3.4 respectively. The physical representations of Cases 1 to 9 are presented in Figure 3.8. This figure demonstrates the

location of the air-water interface with respect to the primary branch, prior to OLE. From the tables, and Figure 3.8, it can be seen that branch C is omitted as a primary branch. The reason for this is that branch C is located at the physical lower limit of the test section. At any liquid level above this limit implies that water is present in branch C, so onset of liquid entrainment is not definable for that branch. The heavier fluid used in all experimentation was filtered water and maintained at a constant temperature using the cooling coil. Air was used as the lighter fluid at an absolute pressure of 510.2 kPa and room temperature was taken as the bulk temperature. It is important to note that throughout this investigation the critical height, H, was measured from the center of the primary branch to the water free surface as shown in Figure 3.1. This was selected for consistency between the two methods, ILL and DLL.

Following Maier et al. (2001b), a data reduction method was required to correct the properties at the branch inlet. To determine the air density at the branch inlet, the following method was used. The measurement of air pressure and temperature at the branch inlet was not practical, but the stagnation pressure and temperature are known inside the two-phase reservoir. An energy balance between the stagnation conditions and the inlet to the branch, assuming isentropic conditions and air as an ideal gas produces,

$$T_0 C_p = \frac{V_b^2}{2} + T_b C_p . \qquad 3.3$$

Subscript '0' and 'b' refer to the stagnation properties and branch inlet properties respectively. Also, C_p is defined as the specific heat at constant pressure for air, 1005 J/kgK. The mass flow rate of air, at the onset of liquid entrainment, $\dot{m}_b$ is defined as,

$$\dot{m}_b = \frac{\pi}{4} d^2 \rho_b V_b . \qquad 3.4$$

The density of air, ρ_b, at the inlet of the branch can be found with R′, the ideal gas constant taken as 287 J/kgK for air, and with P_b and T_b defining the pressure and temperature at the inlet of the branch,

$$\rho_b = \frac{P_b}{R' T_b} . \qquad 3.5$$

An isentropic process between the stagnation conditions and the inlet of the branch is used to define the relationship between pressure and temperature as,

$$\frac{T_b}{T_0} = \left(\frac{P_b}{P_0} \right)^{\frac{k-1}{k}} . \qquad 3.6$$

The ratio of specific heats 'k' is defined here as being 1.4 for air. An iterative process was used to solve Equations 3.3 to 3.6 simultaneously for pressure, temperature and velocity at the inlet of the branch. The known quantities are the mass flow rate of air at onset, $\dot{m}_b$, and the stagnation pressure and temperature. An initial guess for density at the branch inlet was determined, and then verified for every iteration, until a satisfactory error was obtained; here 1×10^{-9} error was observed. The Froude number was then determined from Equation 3.2 using the values obtained from above.

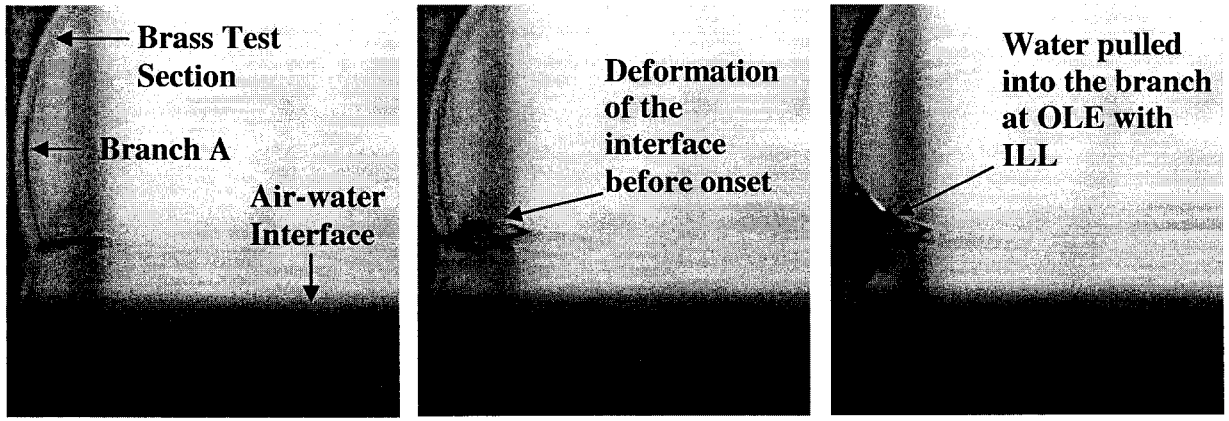

Figure 3.7. OLE using ILL method, single discharge at side branch A.

Table 3.2. OLE single discharge test matrix

Single Discharge			
CASE	**Primary Branch**	**Fr**	**L/d**
1	A	0.004 - 20	-
2	B	0.004 - 20	-

Table 3.3. OLE dual discharge test matrix

Dual Discharge					
CASE	**Primary Branch**	**Fr_A**	**Fr_B**	**Fr_C**	**L/d**
3	A	0.004 – 20	0, 5.10, 15.9, 26.4	-	3.06
4		0.004 – 20	-	0, 5.10, 15.9, 26.4	5.65
5	B	0, 1.15, 6.13, Fr_B	0.004 - 20	-	3.06
6		-	0.004 - 20	0, 0.14, 0.38	3.06

Table 3.4. OLE triple discharge test matrix

Triple Discharge							
					L/d		
CASE	**Primary Branch**	**Fr_A**	**Fr_B**	**Fr_C**	A	B	C
7	A	0.004 - 20	0, 5.10	0, 5.10	-	3.08	5.65
8	B	0, 1.15, 13.8	0.004 - 20	0.38	3.08	-	3.08
9		1.15	0.004 - 20	0, 0.14, 0.38			

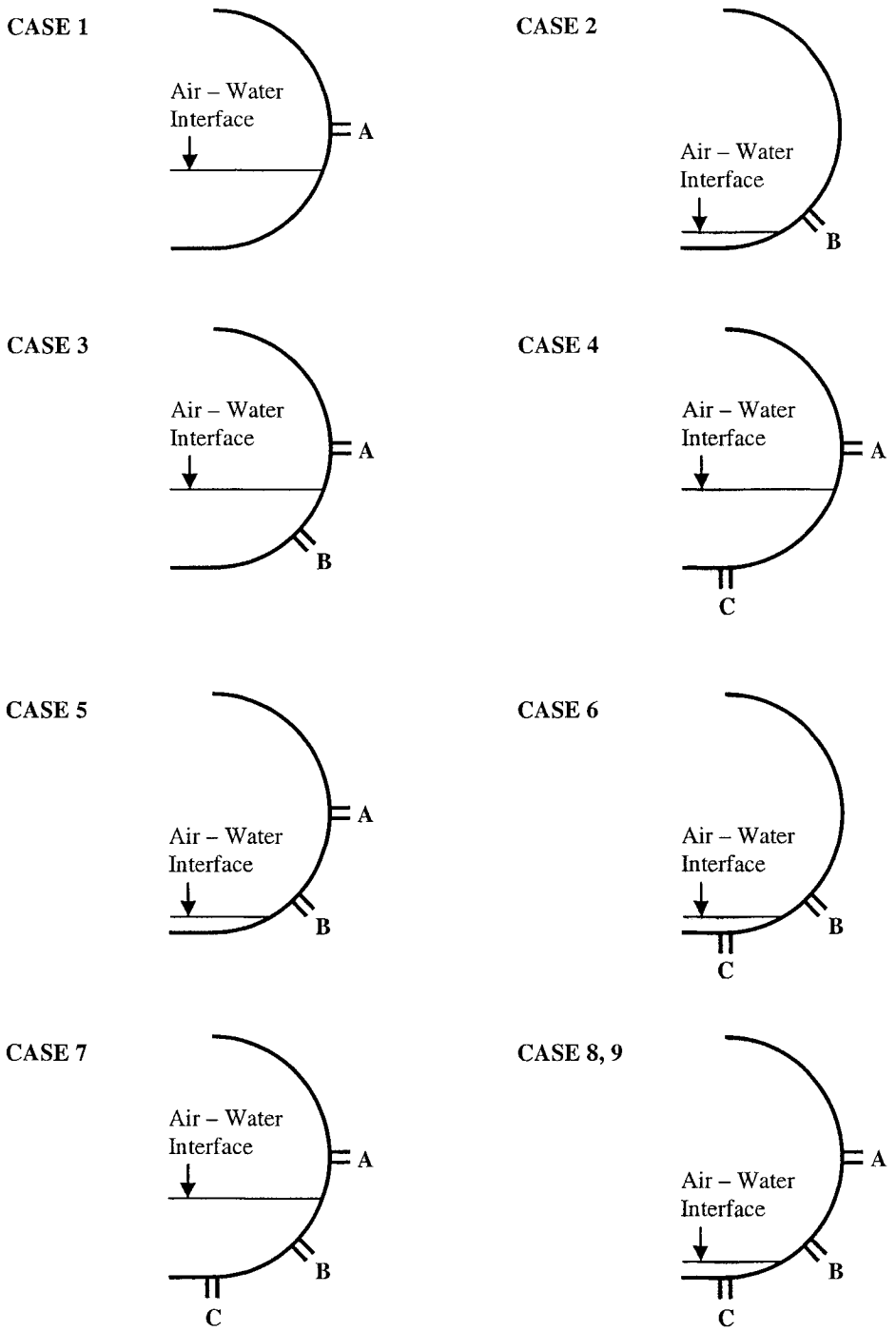

Figure 3.8. Experimental cases demonstrating air-water interface.

3.5 OGE Experimental Procedure using PIV

The procedure used for recording the liquid velocity field at the onset of gas entrainment, in the bottom branch C of the acrylic test section, is described below. It should be noted that the following procedure yields results for decreasing liquid level (DLL) only. Routine cleaning of the test section surface was performed to maintain surface integrity.

The polyamide seeding particles were mixed with the water in the storage tank. Water was then added to the two-phase reservoir until the air-water interface was well above the primary branch, which throughout this study was the bottom branch C. The two-phase reservoir was then pressurized to the desired set point. The primary branch water flow rate was adjusted to the desired value, and the flow rate of water into the reservoir was adjusted such that a steady liquid height was obtained. The liquid height that is desired to be maintained constant is the instance when a steady stream of air can be seen to entrain into the primary branch liquid flow. At this point the onset of gas entrainment due to vortex-free gas pull through is defined, and is presented in Figure 3.9.

The digital CCD camera was positioned such that the desired field of view was obtained and the laser was pulsed at low intensity to make adjustments to the focal length and light shutter until a reasonable particle resolution was obtained. To determine the scaling of the field of view, an image was captured with a known distance in the image. For the scaling factor, the branch diameter was used as the reference. Typically, finding the most suitable particle resolution was on a best effort basis, this technique requires many fine adjustments to the focal length, light shutter and orientation of the camera and laser light

sheet. In some instances, it was possible that the seeding density required adjustment, to resolve this issue more particles could be added until the seeding density was satisfied. Having obtained the best possible particle resolution, the laser is then run with a higher intensity, typically the light shutter needs to be closed slightly at this point, and a sample image is captured. Using the cross-correlation technique, outlined in the Flow Manager software, the timing sequence used to capture the flow appropriately is determined. The timing sequence is defined as the time between the captured image pair. If the validation shows poor correlation then capture time between image 1 and image 2 is adjusted, and a new sample image is captured. This iterative procedure is repeated until a satisfactory validation is obtained. Satisfactory validation occurs when the maximum particle displacement in an interrogation area does not exceed 25% of the interrogation area. With a satisfactory timing sequence established a set of images is captured, typically on the order of 100, at the onset of gas entrainment in the primary branch.

For each primary branch flow rate four camera-laser setups were used to resolve the gas entrainment liquid flow structure in three dimensions. A typical experimental setup, as shown in Figure 3.10, captured the liquid velocity flow field in a vertical plane. The coordinate system to describe the vertical image plane is shown in Figure 3.11. In the vertical image plane it is shown that the origin of the coordinate system is centered at the branch inlet. The velocity vector, V, is resolved into components in the x and z directions respectively as V_x and V_z,. Note here that V_x is taken positive to the right and V_z positive upwards.

The setup shown in Figure 3.12 enabled to capture the velocity field in three horizontal planes by traversing the light sheet vertically. Three horizontal planes were selected, the first at just below the air-water interface, at $z = H_{OGE}$, the second at the mid-plane, where $z = H_{OGE}/2$, and the last just above the branch inlet, where $z = 0$. The coordinate system used to describe the horizontal image plane is shown in Figure 3.13. In the horizontal image plane it is shown that the origin of the coordinate system is centered at the branch inlet. The velocity vector, V, is resolved into components in the radial and tangential directions relative to the branch center as V_r and V_t. Note that V_r is taken positive towards the branch center and V_t is positive counterclockwise.

Using the adaptive correlation technique provided by the Flow Manager software, the data set of raw PIV images were correlated to produce the velocity vectors for each image pair. The validation used an interrogation area of 32x32 pixels, and a relative peak validation of 1.2. Next, each image pair velocity field was filtered using a moving-average filter provided by the Flow Manager software, with a 3x3 neighborhood size. A statistical analysis was performed on the full set of images captured to provide the best estimate of the liquid velocity field at the onset of gas entrainment.

The test matrix of the experimental runs performed for the onset of gas entrainment during single discharge through a bottom branch is presented below in Table 3.5. The two fluids used were again, air and water. The temperature of the water was maintained through the use of a cooling coil, and the absolute air pressure was maintained at 306 kPa and at room temperature. The data reduction method determined the Froude number of

the branch flow rate using Equation 3.2, knowing the properties of air and water and in addition the mass flow rate of the water.

3.5.1 Technical Challenges of Implementing PIV

Although the PIV system used in this investigation is a turn-key product, several technical challenges were met in order to produce results in the two-phase test facility. Due to the necessity for the laser light sheet to be perpendicular to the field of view of the camera, and the fact that many curved surfaces were present, complicated the alignment process. In fact the calibration and alignment process consumed a significant portion of the time to record a single set of data. Originally the cylindrical acrylic viewing section was to be replaced by a square section to reduce distortions. However, it was believed that due to the large radius of curvature of the acrylic viewing section relative to the small field of view, this modification would not be required. The second challenge was the uncertainty of capturing the displacement of the seeding particles given the two-phase nature of the flow field. In fact, it was found that at the inlet of the branch this issue was most noticeable.

To overcome the challenge of providing a vertical light sheet a mirror was used to reflect a horizontal light sheet downward 90 degrees. Using a mirror resulted in an additional loss of laser light sheet intensity and therefore the quality of the images that could be captured. Once the alignment issues were overcome through the acrylic viewing section and the laser light sheet aligned with the area of interest it became evident that the reflections produced distorted the image quality significantly. As a result of the laser

light sheet reflecting on the surface of the branch inlet and air-water interface, large reflections could be observed on the image which resulted in a loss of viewable area. To overcome this obstacle a masking method was used whereby the areas that laser light was reflecting from were masked temporarily until the reflections were minimized. Additionally to improve the contrast within the field of view all surfaces in the background were also masked temporarily. An additional issue that the laser light reflections generated was with respect to safety and when possible all external reflections were minimized through masking.

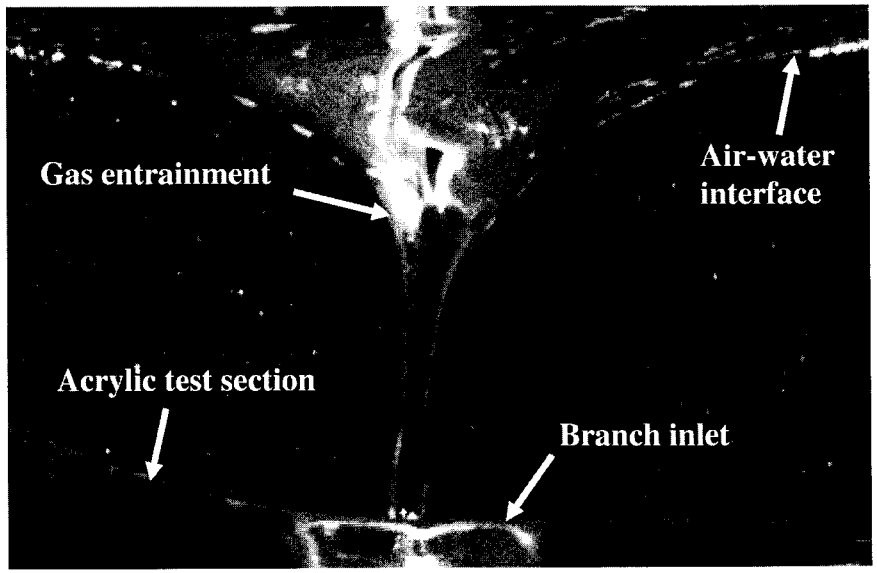

Figure 3.9. OGE due to vortex-free gas pull through in a bottom branch.

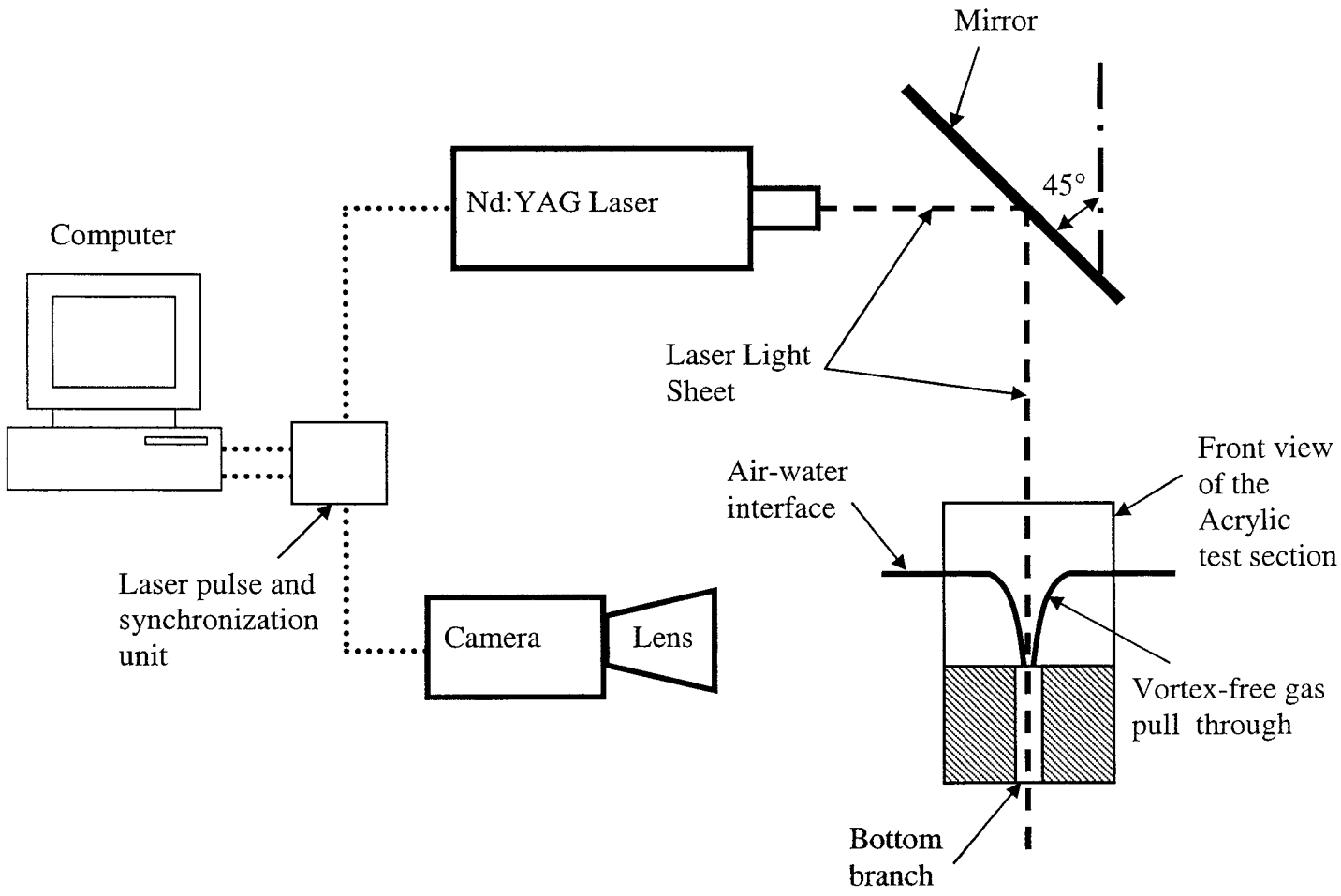

Figure 3.10. Typical vertical plane setup using PIV system.

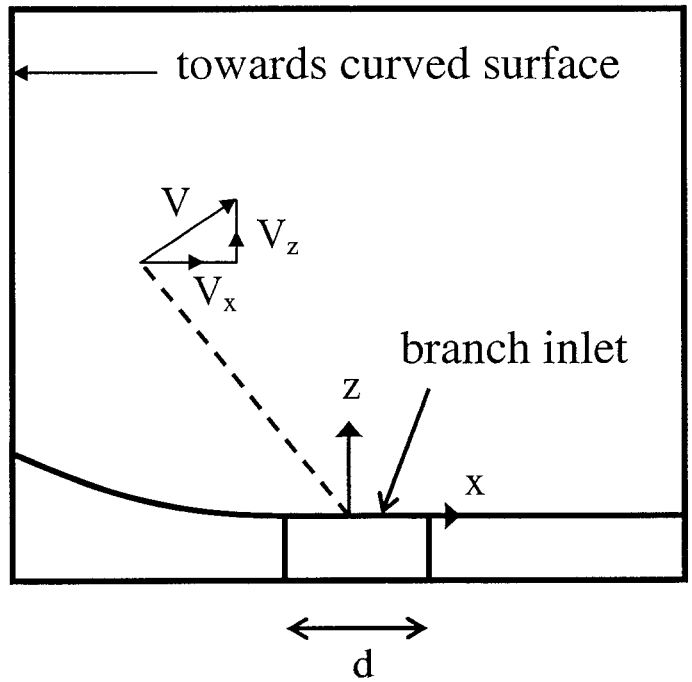

Figure 3.11. Vertical plane co-ordinate system.

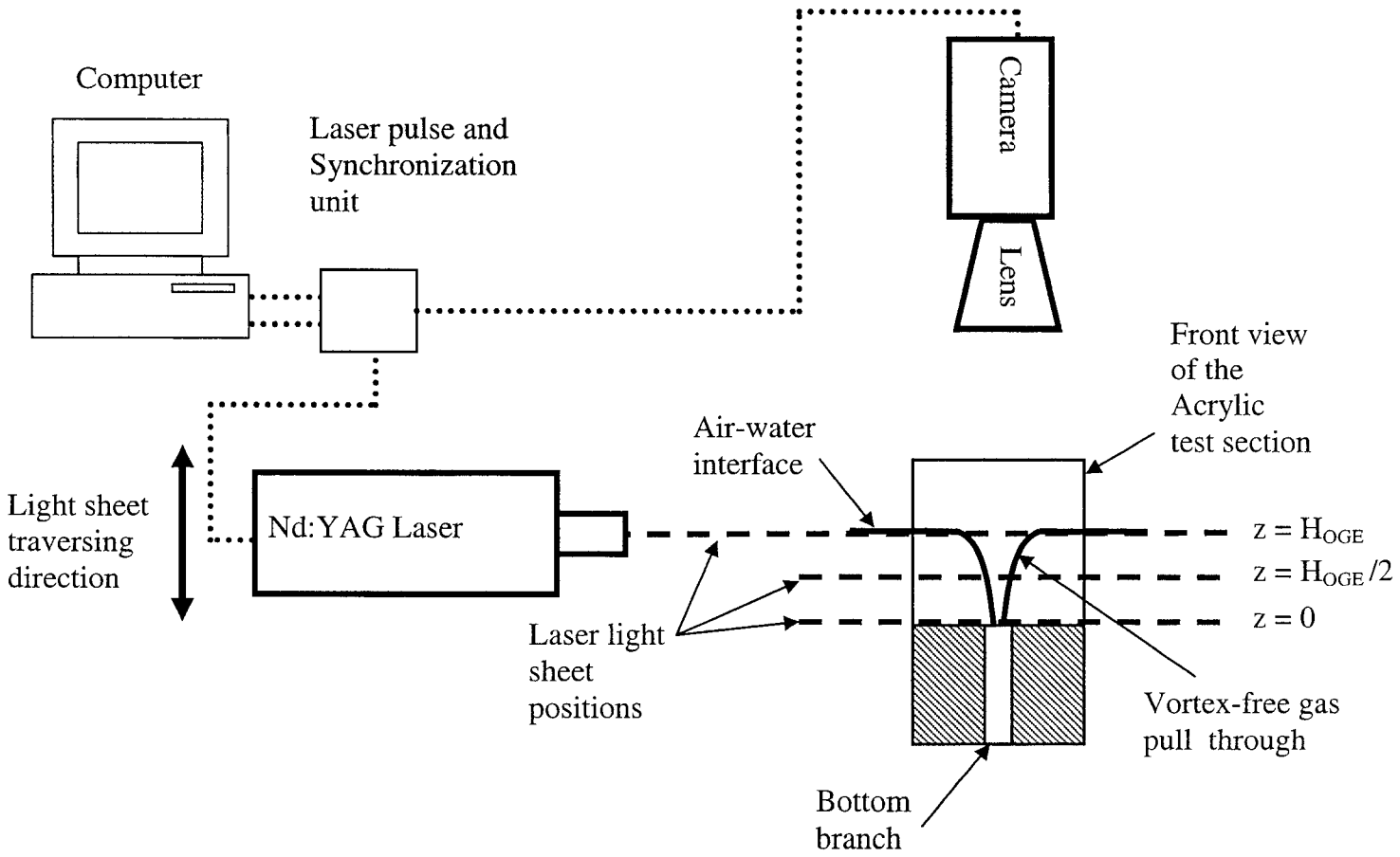

Figure 3.12. Typical horizontal plane setup using PIV system.

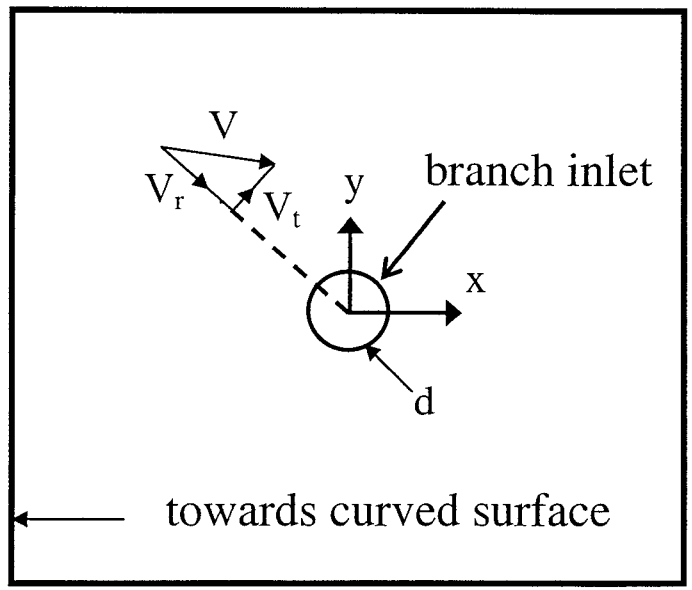

Figure 3.13. Horizontal plane co-ordinate system.

Table 3.5. OGE test matrix using PIV system

Single Discharge			
CASE	**Fr_C**	**Velocity profile plane**	**Plane location**
1	3.47	Vertical	y/d = 0
2		Horizontal	z/d = 0
3		Horizontal	z/d = 0.47
4		Horizontal	z/d = 0.94
5	15.84	Vertical	y/d = 0
6		Horizontal	z/d = 0
7		Horizontal	z/d = 0.91
8		Horizontal	z/d = 1.81
9	36.96	Vertical	y/d = 0
10		Horizontal	z/d = 0
11		Horizontal	z/d = 1.39
12		Horizontal	z/d = 2.79

3.6 Uncertainty Analysis

All measurement devices were calibrated by the manufacturer as per component specifications. The maximum uncertainty in the calculation of the Froude number, where air was the working fluid, was found to be ±11%. The maximum uncertainty in the calculation of the Froude number, where water was the working fluid, was found to be ±5%. The instrument uncertainty in measuring P_0 was ±0.83 kPa, and an acceptable range for this parameter during experimentation was 510.2 ± 6.8 kPa. The instrument uncertainty in measuring the height of water, H, in the reservoir was found to be ± 0.165 mm H_2O. An estimation of the liquid velocity field uncertainty, using the PIV system, could not be determined at the present time.

Chapter IV

Results and Discussion of OLE Experiments

4.1 Results

The results obtained from the experimental onset of liquid entrainment cases will be discussed below. When reviewing Figures 4.1 to 4.11, it is helpful to distinguish between the two methods used to record OLE. The decreasing liquid level (DLL) cases are represented with symbols, and the ILL cases are shown with filled symbols. A trend that exists in all the results, and previously not reported, is an inflection point in the increasing liquid level results near Froude number equal to 1. The DLL method does not predict this inflection point, it is only found using the ILL method. It is due to the air-water interface increasing beyond the center of the primary branch without the presence of liquid entrainment. This means that, as the air-water interface approaches the center of the primary branch the critical height decreases towards zero. As the air-water interface is increased beyond the center of the primary branch the critical height increases again but negatively (Fr < 1 typically). By taking the absolute value of the critical height it is possible to present this on a log-log scale. This new information for the ILL method, however, does not present a danger in the use of the DLL method to predict the onset of liquid entrainment. In fact using the DLL method leads to a more appropriate estimate of OLE, due to the actual physical scenario occurring during LOCA.

To aid with interpretation of Figures 4.1 to 4.11 some general features will be consistent throughout. The horizontal axis represents the Froude number, Fr, of the primary branch, the primary branch is indicated with a subscript being either A or B. The vertical axis represents the critical height ratio, H/d, for OLE at a given Froude number. Two horizontal lines are also shown on each figure at constant H/d. The lower line represents the edges of the primary branch, while the upper line represents the dry-out condition. The branch edges line represents the bottom of the primary branch inlet for the DLL results, and to the right of the inflection point for ILL results. The branch edges line to the left of the inflection point, for ILL results only, represents the top of the primary branch inlet. When the primary branch is A the lower line is 0.5 and the upper line is 4. When the primary branch is B the lower line is 0.3535 and the upper line is 1.1715. The term dry-out refers to the condition that exists when the air-water interface is at the bottom of the test section, and a physical limit is reached. Any further increase in Froude number will result in the same value of H/d.

4.2 Single Discharge

Figure 4.1 demonstrates Case 1 for OLE in branch A with ILL and DLL results. The current results indicate that for all Fr_A values the critical height ratio, H/d, is greater with DLL than for ILL. This trend is also shown for Hassan et al. (1994)'s experimental results, where both ILL and DLL methods were also used. This implies the presence of an additional physical parameter that directly affects OLE. This physical parameter is defined here as the surface wetness between the air-water interface, and the primary branch inlet. The surface wetness contributes to the degree of surface tension between

the air-water interface and the brass surface. The difference between the two ILL and DLL methods describes the effect of surface wetness. This can be explained in that with the ILL method the surface above the interface is dry before OLE, and with the DLL the surface above the interace is wet. As Fr_A is increased, however, the effect of surface wetness is seen to decrease as both ILL and DLL results tend to converge. The ILL results demonstrate an inflection point near Fr_A equal to 1. To the left of the inflection point the values of H/d are lower than the 0.5 limit. This indicates that the air-water interface is between the center and top of branch A. When the ratio H/d increases negatively, to the left of the inflection point, the new physical limit becomes the top of the branch, but from symmetry H/d is also equal to 0.5. It is believed that increasing the primary branch diameter can remove the inflection point. The surface tension is independent of the branch diameter, and will remain constant with increasing branch diameter. A larger branch diameter increases the distance between the center and the bottom of the primary branch, the inflection point is dependant on this distance. Both the ILL and DLL methods tend towards the expected physical upper and lower limits of H/d, 4 and 0.5 respectively. At the upper range (Fr_A>10) the current DLL results have good agreement with Maier et al. (2001)'s and Hassan et al. (1994)'s experimental results for a flat vertical wall. The difference observed below this range is due to the curvature of the wall. In the same Froude range, good agreement between the present DLL and analytical results of Maier et al. (2001), Armstrong et al. (1992), Yonomoto and Tasaka (1988) can be seen. As Fr_A decreases, only Maier et al. (2001) correctly predicts the limiting value for H/d of 0.5. Their correct prediction shows good agreement with the present DLL results but does not predict the ILL results.

Figure 4.2 demonstrates Case 2 for OLE in branch B, with ILL and DLL results. Similar trends, as reported for Case 1, are demonstrated in the figure. Both the ILL and DLL results tend towards convergence with increasing Fr_B. The critical height ratio, H/d, is shown to be higher with DLL than ILL with similar conclusions as presented in Case 1. Both the ILL and DLL methods tend towards the expected physical upper and lower limits of H/d, 1.1715 and 0.3535 respectively. The ILL results demonstrate an inflection point near Fr_B equal to 1. Of interest, it was observed with the ILL method and low Fr_B numbers the water level could surpass the top of the primary branch before OLE occurred. As was discussed in Case 1, a larger branch diameter will reduce the relative effect of surface tension on OLE. The experimental work of Hassan et al. (1997) indicates an agreement with the present data, and the dry-out condition is correctly predicted by both. The theoretical finite-branch model by Hassan et al. (1999) for a side branch on a flat inclined 45° wall demonstrates a reasonable prediction of the DLL results. It is believed that the differences between Hassan et al. (1999)'s results and the present are contributed to by the curvature of the test section. The ILL show a discrepancy with Hassan et al. (1999)'s model due to surface wetness.

4.3 Dual Discharge

Figure 4.3 demonstrates Case 3 for OLE in branch A with ILL and DLL results. This figure demonstrates the effect of Fr_B (0, 5.10, 15.9, 26.4) on OLE at branch A. The critical height ratio, H/d, is shown to be higher with DLL than ILL. The ILL and DLL results tend towards convergence with increasing Fr_A. Both the ILL and DLL methods tend towards the expected physical upper and lower limits of H/d, 4 and 0.5 respectively.

The ILL and DLL results demonstrate that by increasing Fr_B the critical height ratio H/d decreases. This means that the air-water interface is closer to the primary branch as OLE occurs as compared with the single discharge case. The effect of Fr_B, therefore, is to pull the air-water interface in it's direction. Of interest, it was seen that air could be entrained into branch B at some critical height H/d. Reporting the two-phase nature of the flow after the onset of gas entrainment (OGE) occurred, was beyond the scope of this study. On the figure, the last data point symbol to the right (Fr_B = 5.10, 15.9, 26.4) indicates when OGE began and OLE could still be recorded. For both ILL and DLL the critical height ratio is almost the same as at OGE, but Fr_A is seen to vary greatly. The momentum difference between an upward or downward traveling air-water interface is believed to contribute to this difference.

Figure 4.4 demonstrates Case 4 for OLE in branch A with ILL and DLL results. This figure demonstrates the effect of Fr_C (5.10, 15.9, 26.4) on OLE in branch A. The critical height ratio, H/d, is shown to be higher with DLL than ILL. The ILL and DLL results tend towards convergence with increasing Fr_A. Both the ILL and DLL methods tend towards the expected physical upper and lower limits of H/d, 4 and 0.5 respectively. It is seen that Fr_C has little impact on the critical height ratio, H/d. By increasing the ratio L/d to 5.65 (Case 4), from 3.06 (Case 3), the effect of the Froude number of a second branch on H/d is seen to decrease. Of interest, it was seen that air could be entrained into branch C at some critical height H/d, similar to Case 3. On the figure the last data point symbol to the right (Fr_C = 5.10, 15.9, 26.4) indicates when OGE began and OLE could still be

recorded. An image of the instance when OGE began in branch C with OLE in branch A is presented in Figure 4.12.

Figures 4.5, 4.6 and 4.7 demonstrate Case 5 for OLE in branch B with ILL and DLL results. The critical height ratio, H/d, is shown to be higher with DLL than ILL. The ILL and DLL results tend towards convergence with increasing Fr_B. Both the ILL and DLL methods tend towards the expected physical upper and lower limits of H/d, 1.1715 and 0.3535 respectively. The effect of Fr_A (1.15, 6.13) on OLE in branch B is demonstrated in Figure 4.5. It is seen that for both ILL and DLL the critical height increases as Fr_A is increased. This means that the air-water interface is further away from branch B with increasing Fr_A. This implies that, a second branch located above the primary branch will pull the air-water interface in its direction. A comparison of the present results with Hassan et al. (1999) and Armstrong et al. (1992) is presented in Figure 4.6. Hassan et al. (1999)'s experimental results are presented for a flat vertical wall with two branches in the same vertical plane and L/d equal to 3 and top branch Froude number of 5.5. Their theoretical finite branch model is presented for two branches located on a flat 45° inclined wall, with L/d equal to 3, and Froude number of the top branch equal to 5.5. Armstrong et al. (1992)'s point-sink model is presented for two branches located on the side of a flat vertical wall with L/d equal to 3, and top branch Froude number of 5.5. The comparison demonstrates good agreement between Hassan et al. (1999)'s model and the DLL results for moderate Fr_B. Where the dry-out condition is represented at higher Fr_B, both Armstrong et al. (1992)'s and Hassan et al. (1999)'s models do not predict this physical limit but this is believed to be due to the curvature of the wall. The ILL results

are not predicted by either theoretical model. A comparison of the present results with Hassan (1997)'s experimental and Hassan et al. (1999)'s theoretical model are presented in Figure 4.7 for Fr_A equal to Fr_B. Their experimental results are presented for a semi-circular wall with L/d equal to 3.06. Their theoretical finite-branch model is presented for two branches located on a flat 45° inclined wall with L/d equal to 3. The present DLL results demonstrate excellent agreement with both the analytical and experimental results. The ILL results are not accurately represented by the analytical model but show agreement with the experimental data at the dry-out condition.

Figure 4.8 demonstrates Case 6 for OLE in branch B with ILL and DLL results. This figure demonstrates the effect of Fr_C (0.14, 0.38) on OLE in branch B. The critical height ratio, H/d, is shown to be higher with DLL than ILL. The ILL and DLL results tend towards convergence with increasing Fr_B. Both the ILL and DLL methods tend towards the expected physical upper and lower limits of H/d, 1.1715 and 0.3535 respectively. The effect of Fr_C on OLE in branch B is to decrease the critical height ratio H/d. This means that the air-water interface is closer to branch B for OLE to occur, with an increase in Fr_C. The flow in branch C effectively pulls the air-water interface in its direction. Of interest, it was seen that air could be entrained into branch C at some critical height H/d, similar to Case 4. On the figure the last data point symbol to the right (Fr_C = 0.14, 0.38) indicates when OGE began and OLE could still be recorded.

4.4 Triple Discharge

Figure 4.9 demonstrates Case 7 for OLE at branch A with ILL and DLL results. This figure demonstrates the effect of Fr_B (5.10) and Fr_C (5.10) on OLE at branch A. The critical height ratio, H/d, is shown to be higher with DLL than ILL. The ILL and DLL results tend towards convergence with increasing Fr_B. Both the ILL and DLL methods tend towards the expected physical upper and lower limits of H/d, 4 and 0.5 respectively. The effect of having a second branch active below the primary branch is a reduction in the critical height ratio H/d (Case 3). The greatest effect is generated by branches with smaller L/d ratios as discussed in Case 4. Having both branches, B and C, active results in the highest ratio of H/d compared with the dual discharge cases, as shown in the figure, this is opposite of what was expected. It is believed that this is due to flow interaction between branch B and C causes a total reduction in the pull on the air-water interface. It was observed during experimentation that additional traces of air could be seen flowing between branches B and C, an image of this was captured and is presented in Figure 4.13. The image also shows the instance when OLE in branch A can occur simultaneously with OGE in branches B and C. The lowest value of H/d obtained was for Fr_B equal to 0, aside from both equaling 0, and Fr_C equal to 5.10. Of interest, it was seen that air could be entrained into branch B or both branches B and C simultaneously at some critical height. Reporting the two-phase nature of the flow after OGE occurred was beyond the scope of this study. On the figure the last data point symbol to the right (Fr_B = 5.10 and Fr_C = 0, Fr_B = 0 and Fr_C = 5.10, Fr_B = Fr_C = 5.10) indicates when OGE began and OLE could still be recorded.

Figure 4.10 demonstrates Case 8 for OLE in branch B with ILL and DLL results. This figure demonstrates the effect of Fr_A (1.15, 13.8) and Fr_C (0.38) on OLE in branch B. The critical height ratio, H/d, is shown to be higher with DLL than ILL. The ILL and DLL results tend towards convergence with increasing Fr_B. Both the ILL and DLL methods tend towards the expected physical upper and lower limits of H/d, 1.1715 and 0.3535 respectively. The effect of Fr_A on OLE in B is to increase the critical height (Case 5), and Fr_C will decrease the critical height (Case 6). Therefore, the two branches A and C produce a pulling force on the air-water interface in opposing directions. From the figure as Fr_A is increased, maintaining Fr_C constant, the effect is to increase the critical height ratio H/d which was expected from the discussion in Case 5. It was seen that air could be entrained into branch C at some critical height H/d. On the figure the last data point symbol to the right of each data set indicates when OGE began and OLE could still be recorded.

Figure 4.11 demonstrates Case 9 for OLE in branch B with ILL and DLL results. This figure demonstrates the effect of Fr_A (1.15) and Fr_C (0.14, 0.38) on OLE in branch B. The critical height ratio, H/d, is shown to be higher with DLL than ILL. The ILL and DLL results tend towards convergence with increasing Fr_B. Both the ILL and DLL methods tend towards the expected physical upper and lower limits of H/d, 1.1715 and 0.3535 respectively. The effect of Fr_A on OLE in B is to increase the critical height (Case 5), and Fr_C will decrease the critical height (Case 6). Therefore, the two branches A and C produce a pulling force on the air-water interface in opposing directions. The figure demonstrates that increasing Fr_C from 0 to 0.14 results in an increase in critical height

H/d. When Fr_C was increased from 0.14 to 0.38 the critical height H/d is seen to decrease, as expected. From this it can be determined that a second branch located below the primary branch has a higher impact on the critical height H/d than a second branch located above the primary branch.

4.5 Discussion

The simulation of a CANDU header-feeder system under LOCA conditions was presented for the onset of liquid entrainment. The scenarios of single, dual and triple discharge were presented with nine cases where OLE occurred at either branch A or B. In all cases presented the branch above, and closest, to the air-water interface was seen to experience the onset of liquid entrainment. The method for recording the onset of liquid entrainment, the increasing and decreasing liquid level methods, presented unique results towards the understanding of the effects of surface wetness on the onset of liquid entrainment. The increasing liquid level method leads to the discovery of an effect created by surface tension between the air-water interface and the solid surface. The air-water interface was seen to surpass the center of the primary branch without the presence of liquid entrainment. This phenomenon manifested in the results as an inflection point on the log-log plots due to the critical height H/d approaching zero, and then increasing negatively. By increasing the primary branch diameter the inflection point will diminish, and at some critical diameter will cease to exist. By using the increasing liquid level results a safer prediction of OLE is achieved due to an under estimate of the critical height. Future studies will benefit by using only the increasing liquid level method. The presence of a second branch will lead to two results, depending on its location. If the

second branch is located above the primary branch it will increase the critical height. If the second branch is located below the primary branch it will decrease the critical height. The stronger influence on critical height is found with the second branch located below the primary branch. The results predict the phenomena during LOCA conditions with respect to the onset of liquid entrainment in the ongoing effort for safer design standards in the next generation cooling systems.

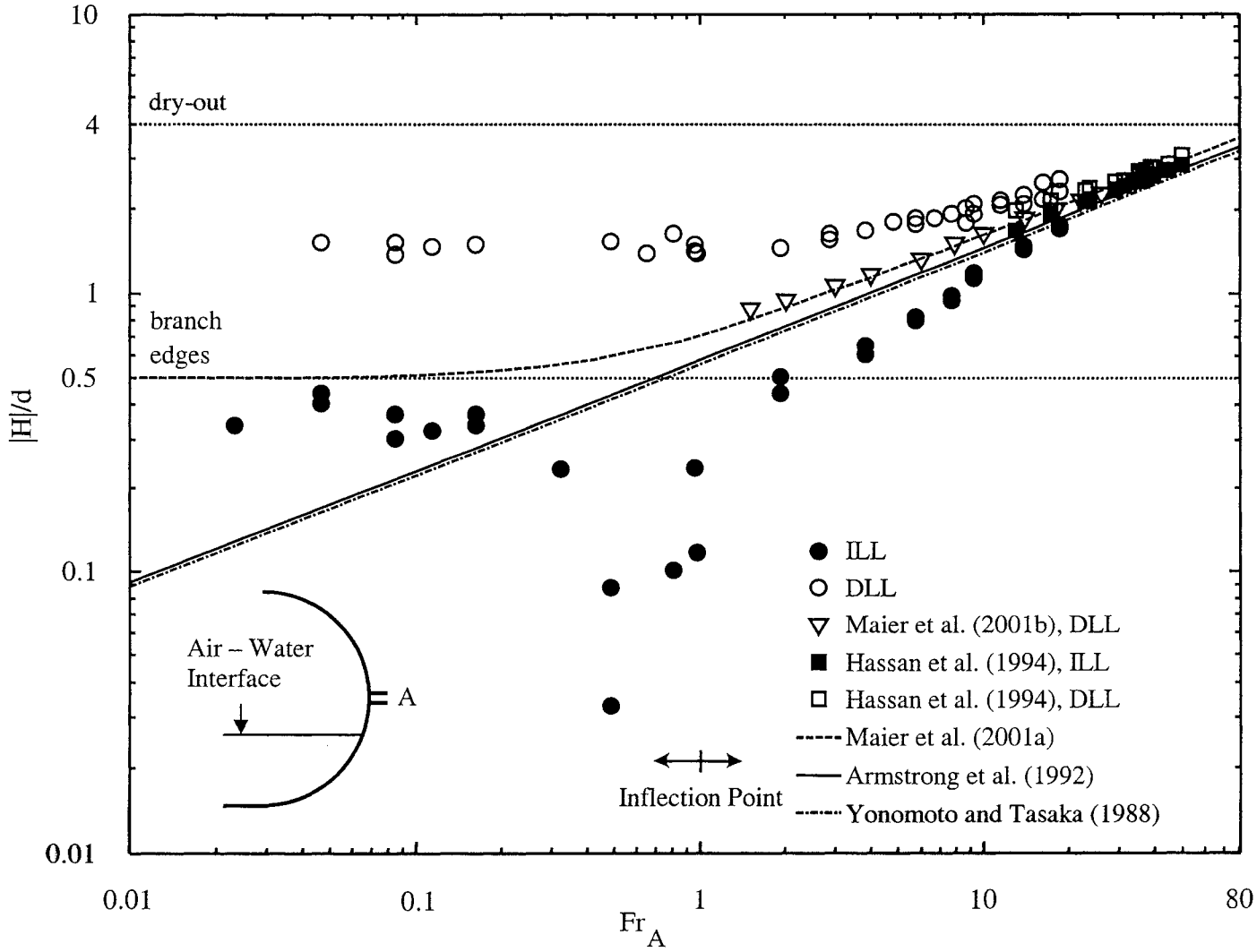

Figure 4.1. OLE in branch A, single discharge, effect of wall curvature – Case 1.

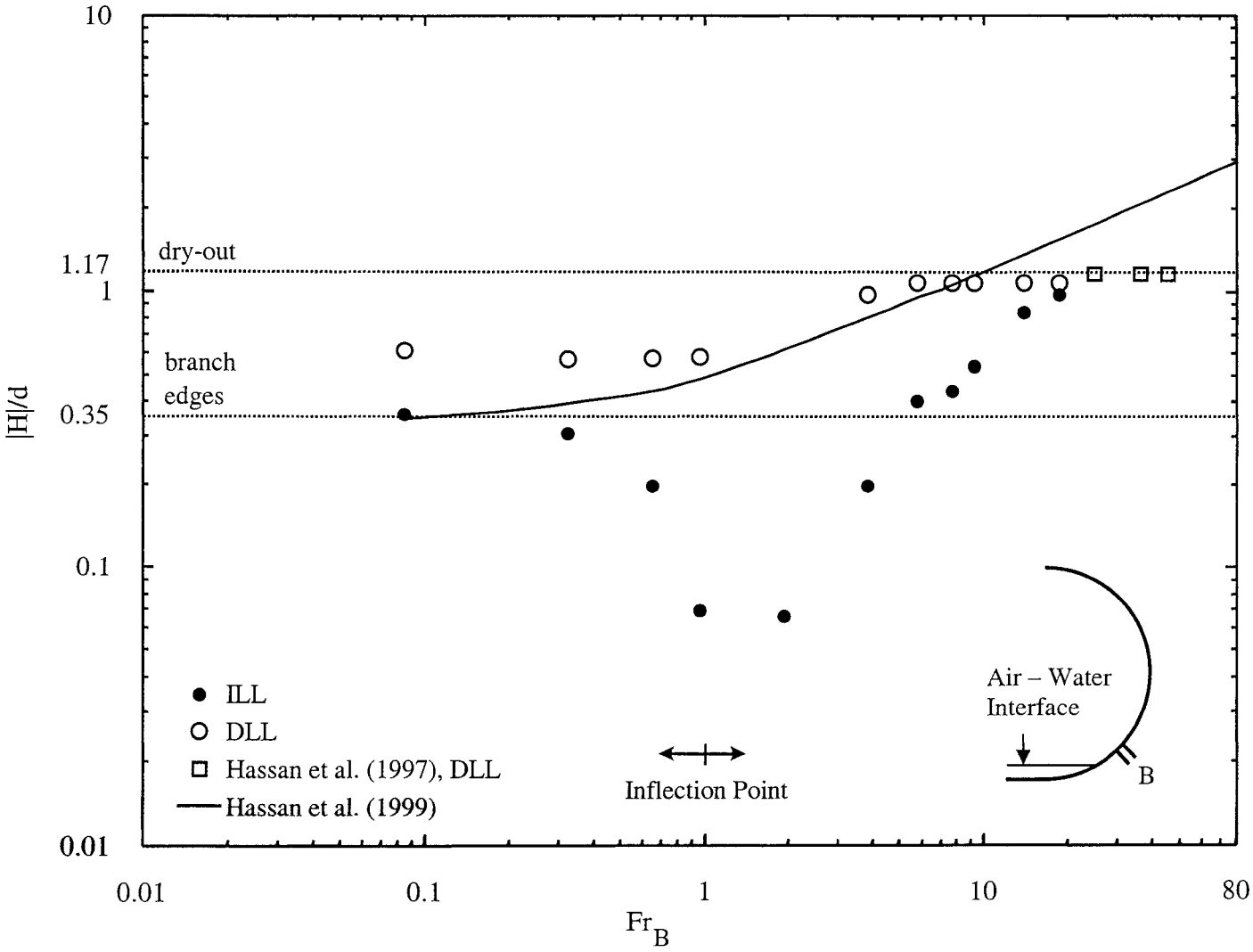

Figure 4.2. OLE in branch B, demonstrating the effect of wall curvature-Case 2.

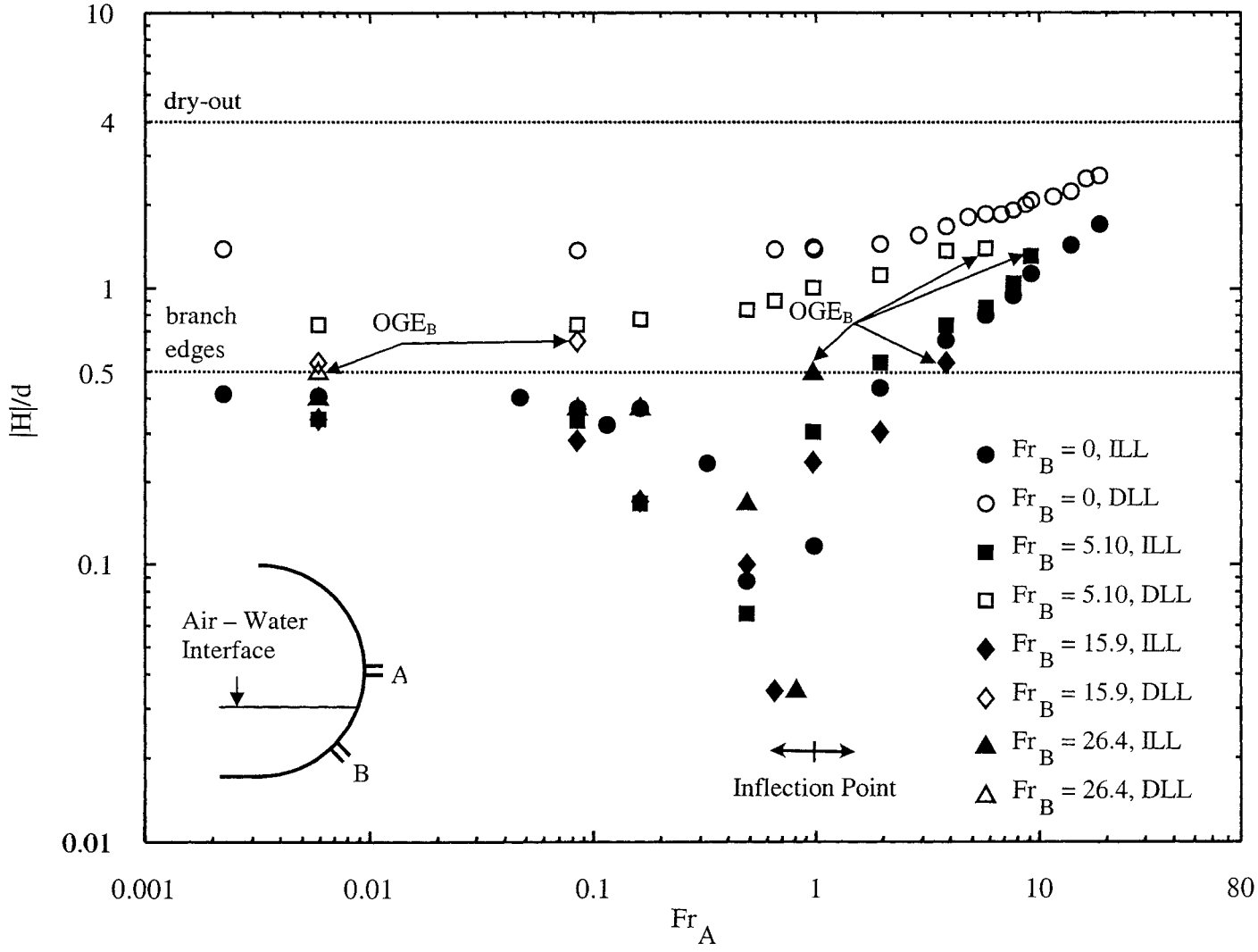

Figure 4.3. OLE in branch A, dual discharge effect of Fr_B-Case 3.

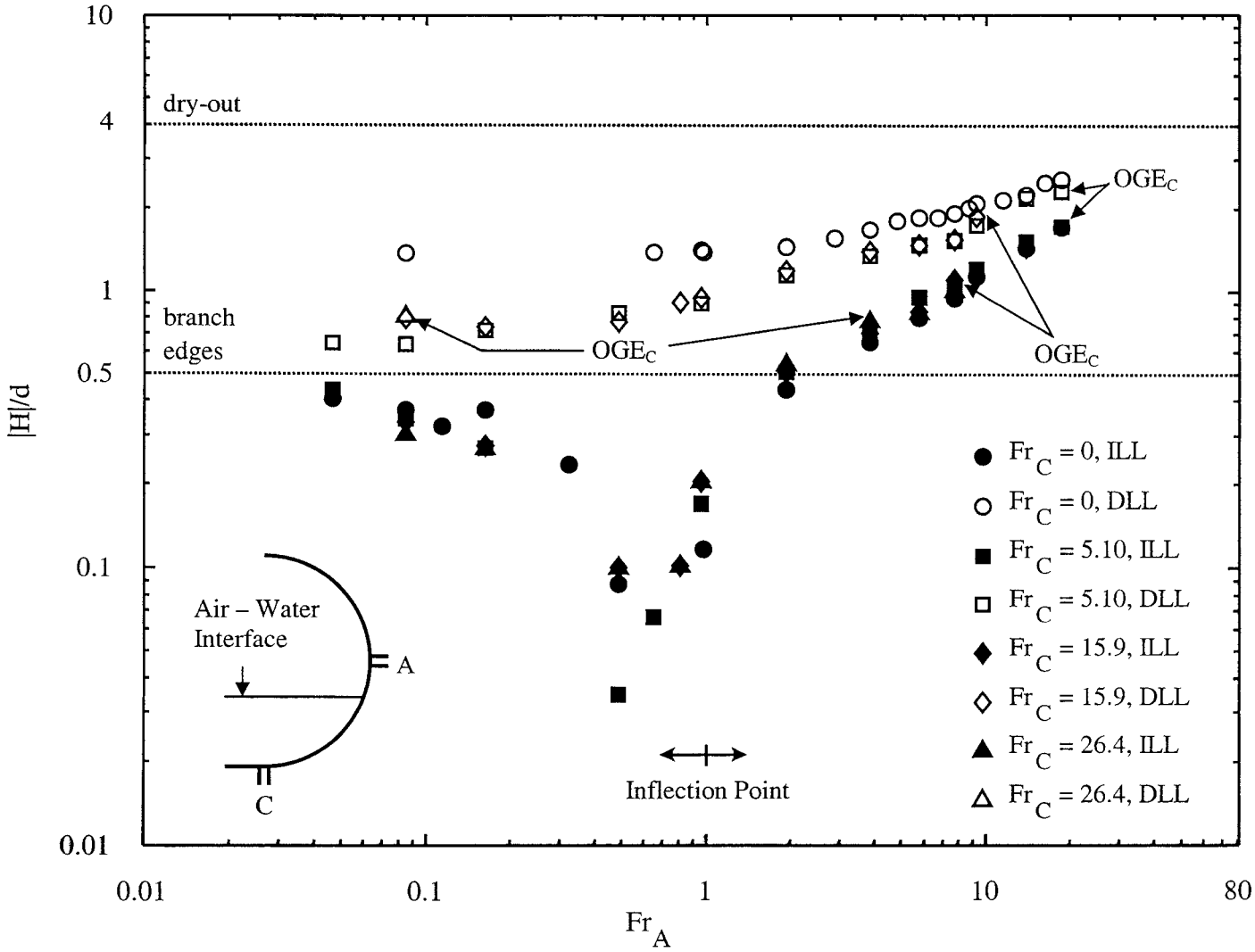

Figure 4.4. OLE in branch A, dual discharge effect of Fr_C-Case 4.

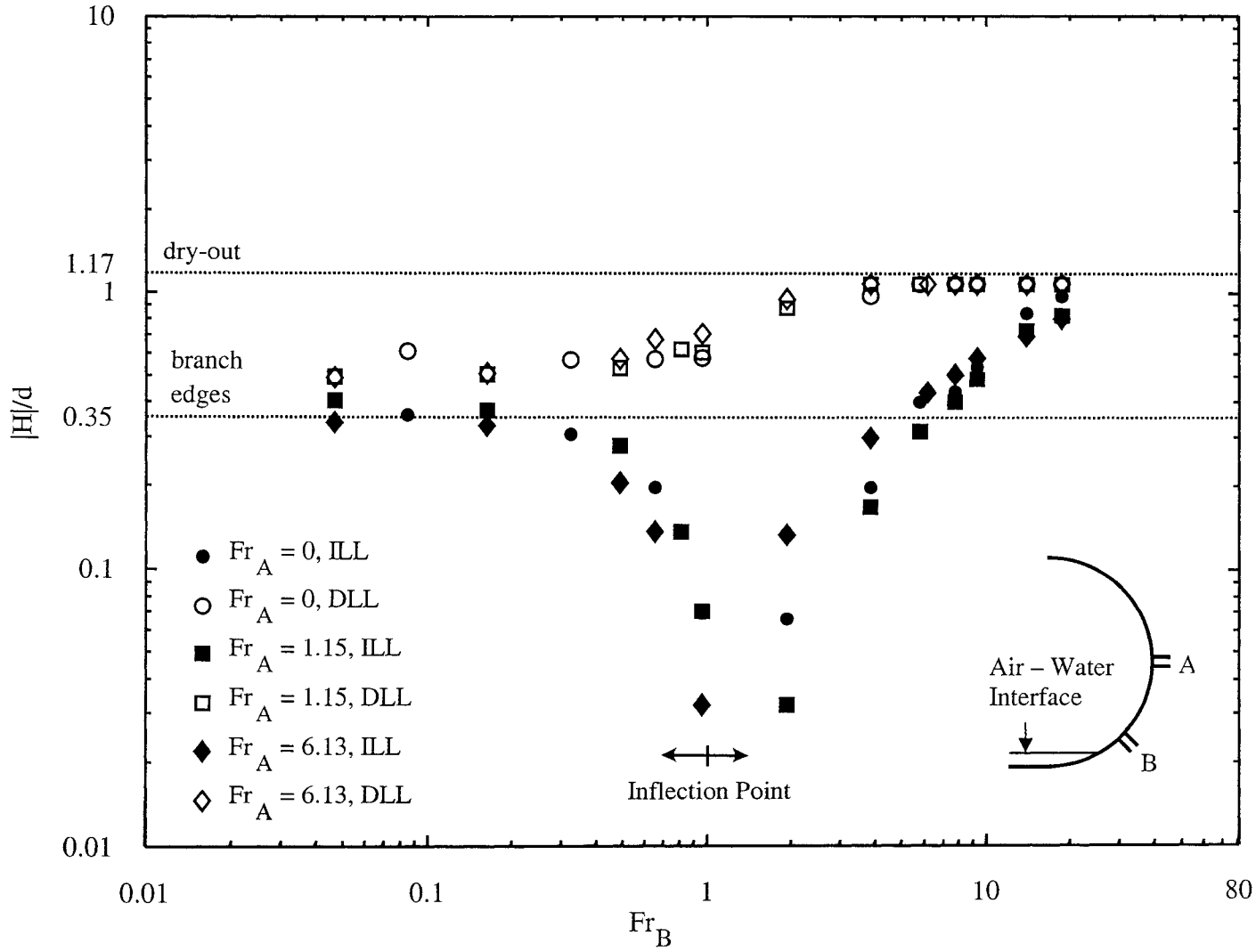

Figure 4.5. OLE in branch B, dual discharge effect of Fr_A-Case 5.

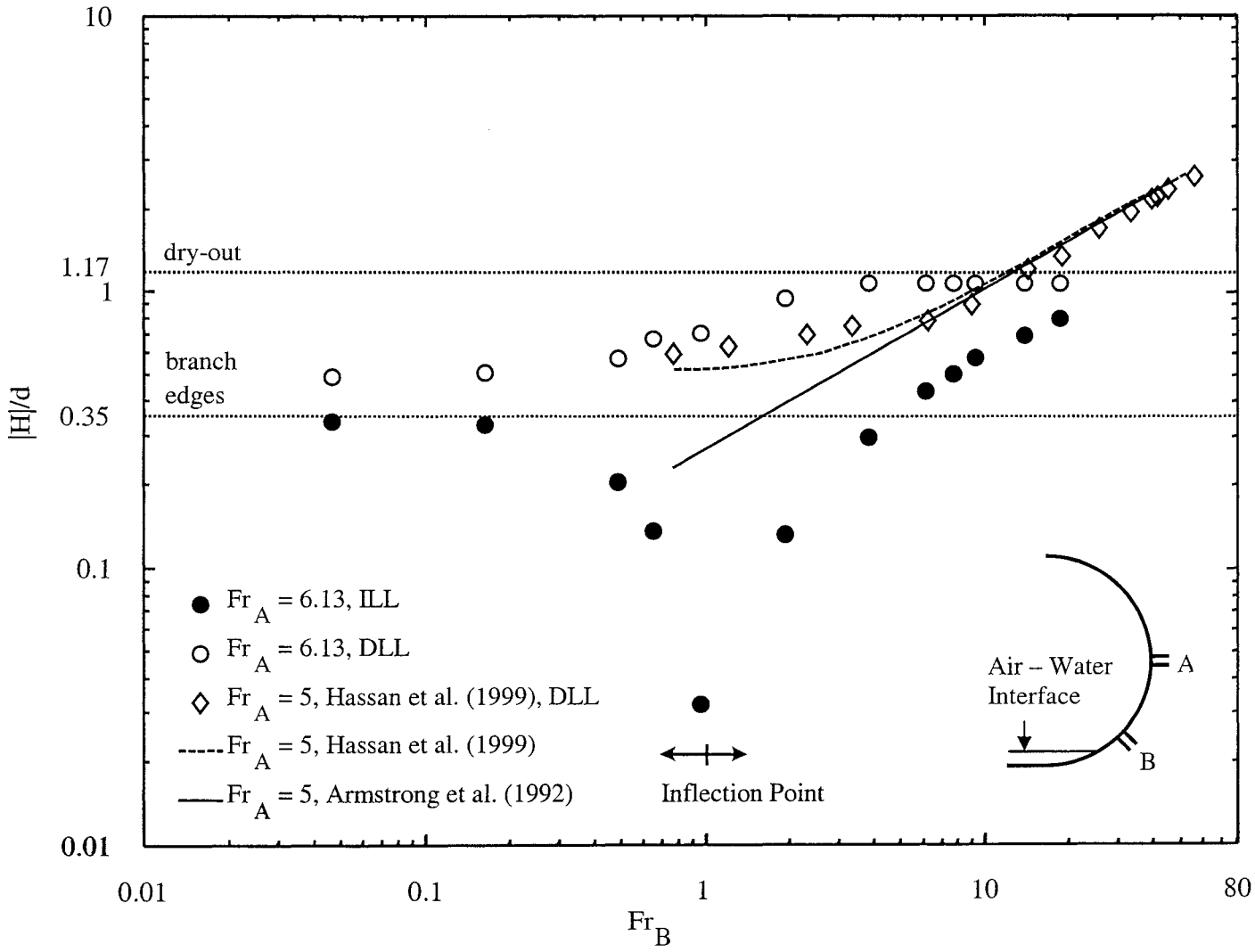

Figure 4.6. OLE in branch B, dual discharge, effect of wall curvature-Case 5.

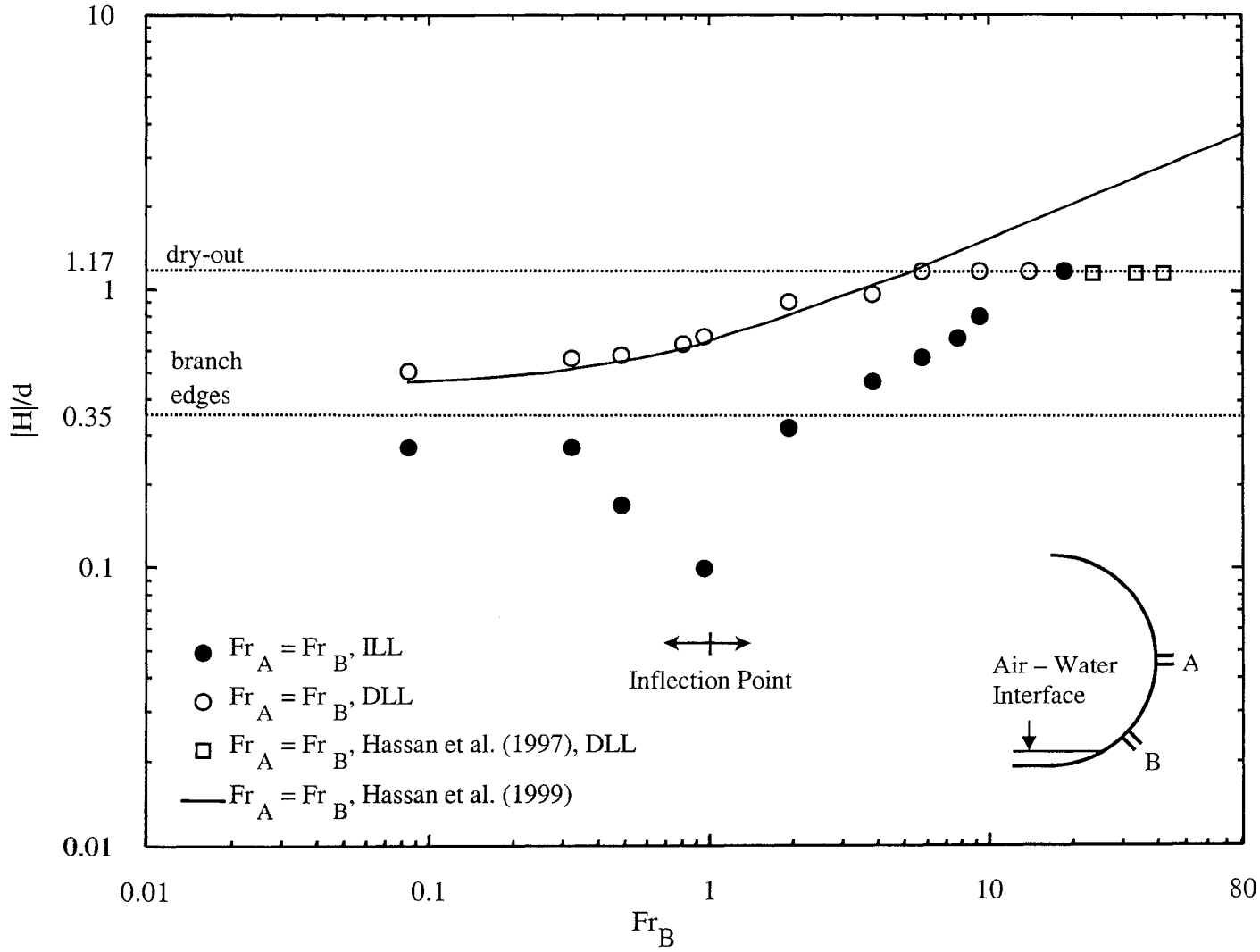

Figure 4.7. OLE in branch B, dual discharge, effect of wall curvature, Fr_A=Fr_B-Case 5.

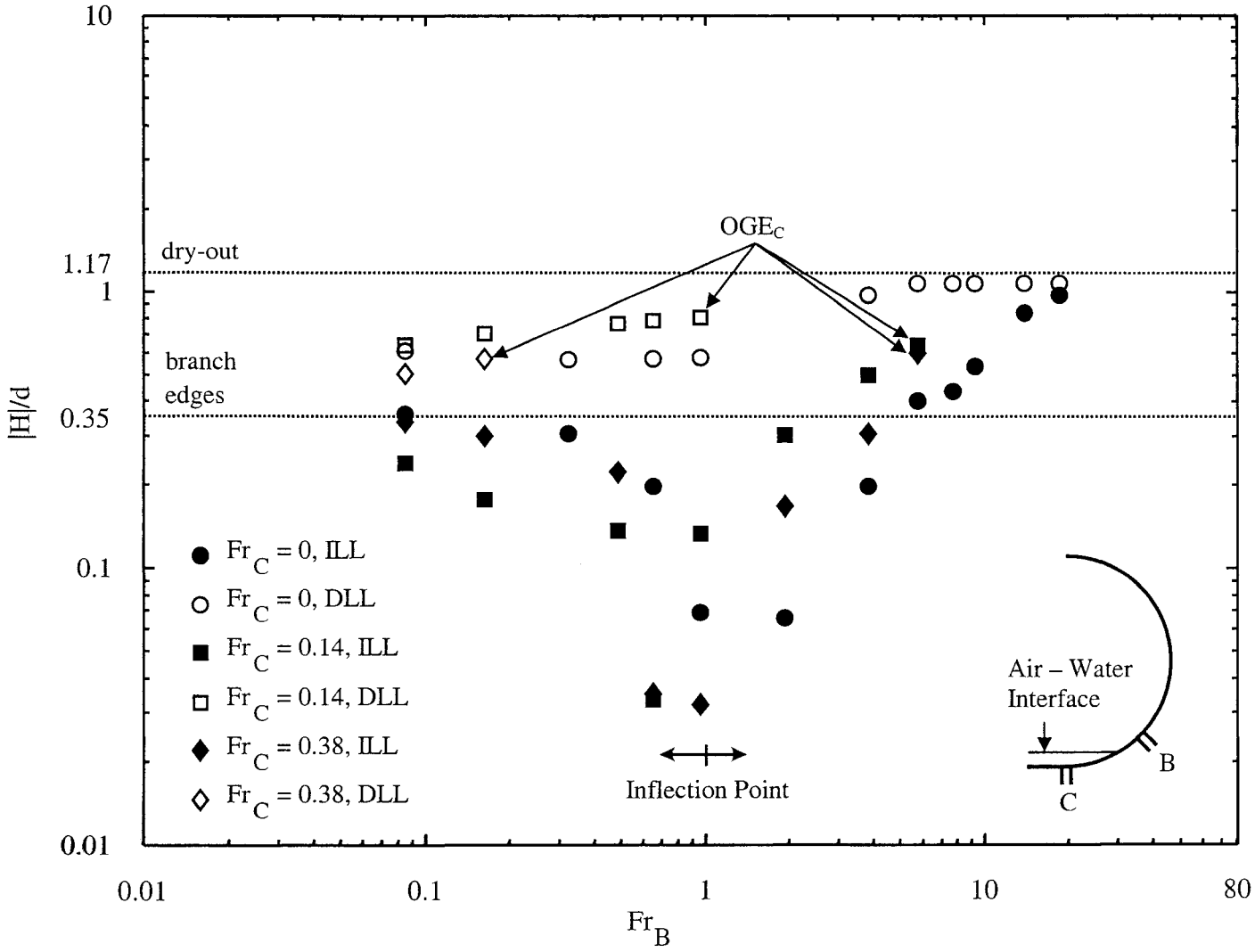

Figure 4.8. OLE in branch B, dual discharge effect of Fr_C-Case 6.

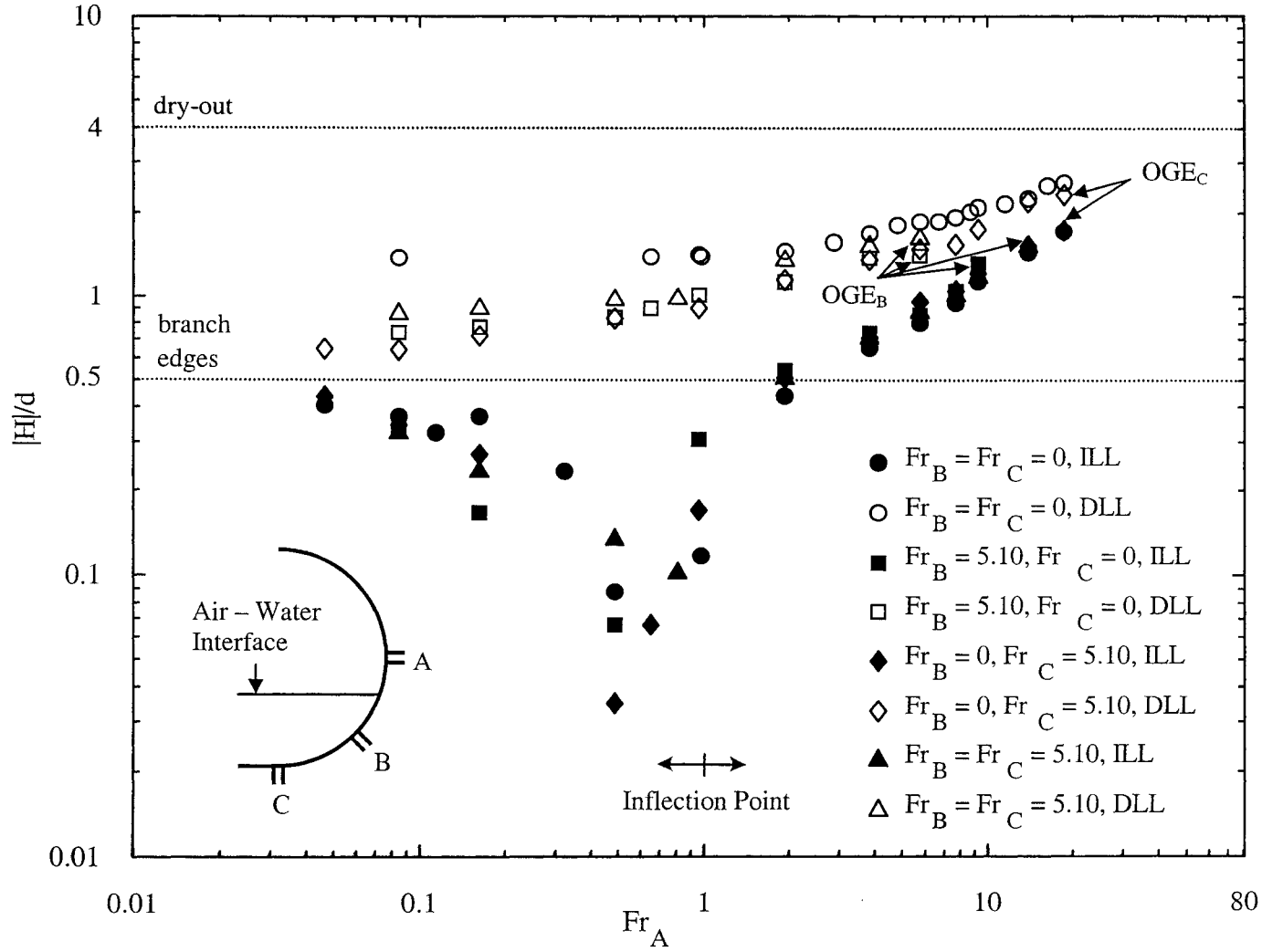

Figure 4.9. OLE in branch A, triple discharge effect of Fr_B and Fr_C-Case 7.

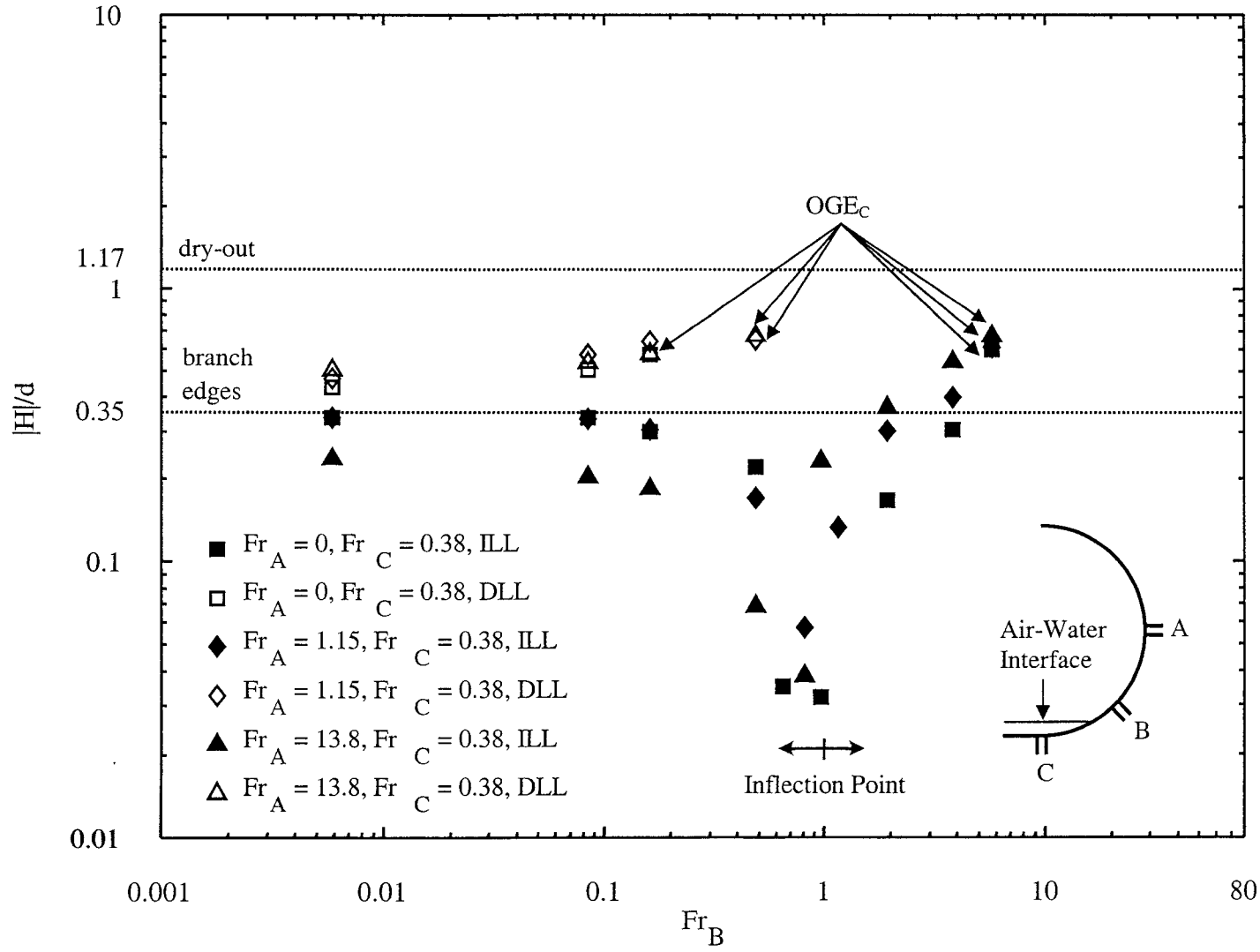

Figure 4.10. OLE in branch B, triple discharge effect of Fr_A and constant Fr_C-Case 8.

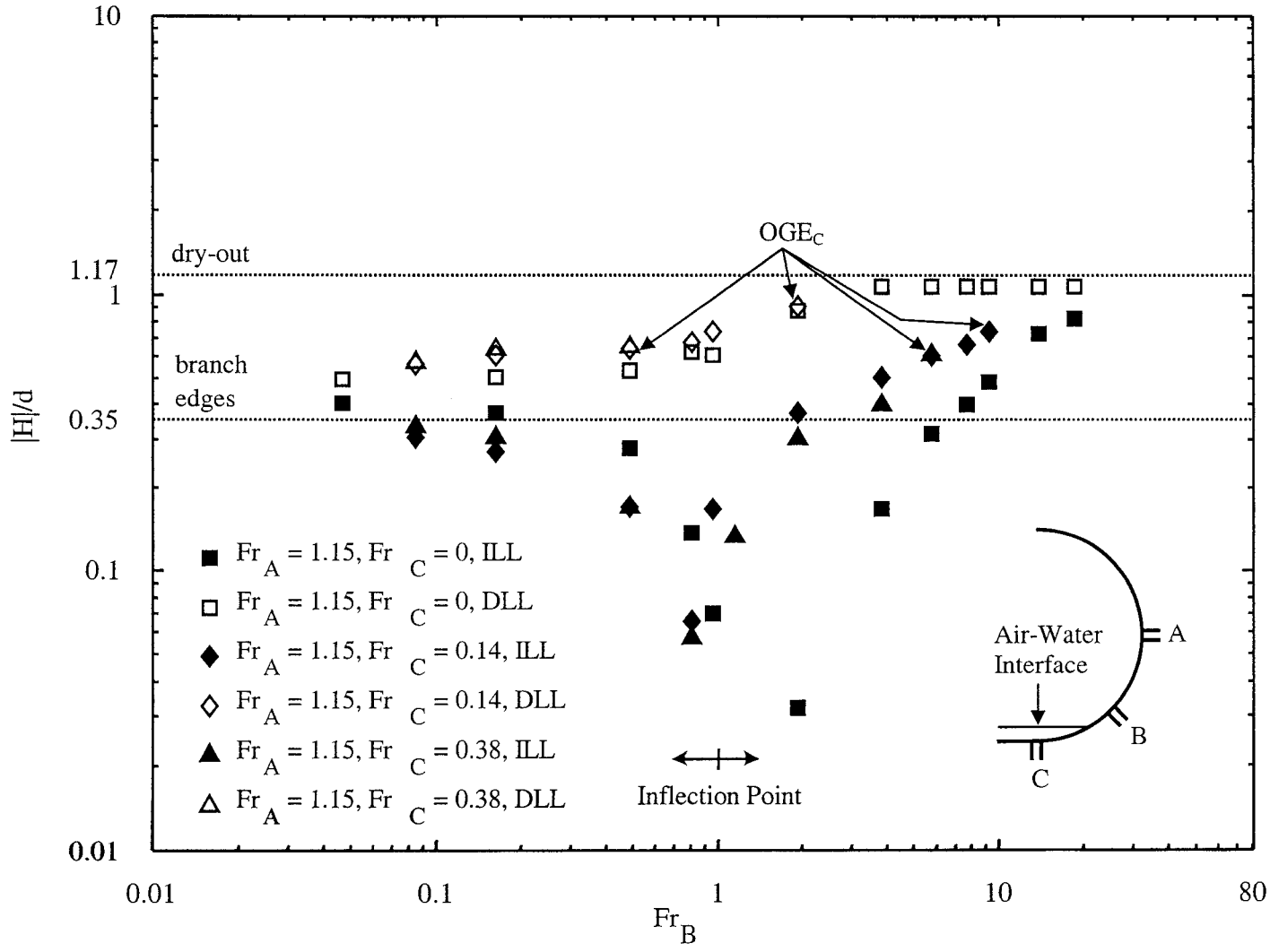

Figure 4.11. OLE in branch B, triple discharge, effect of Fr_C and constant Fr_A-Case 9.

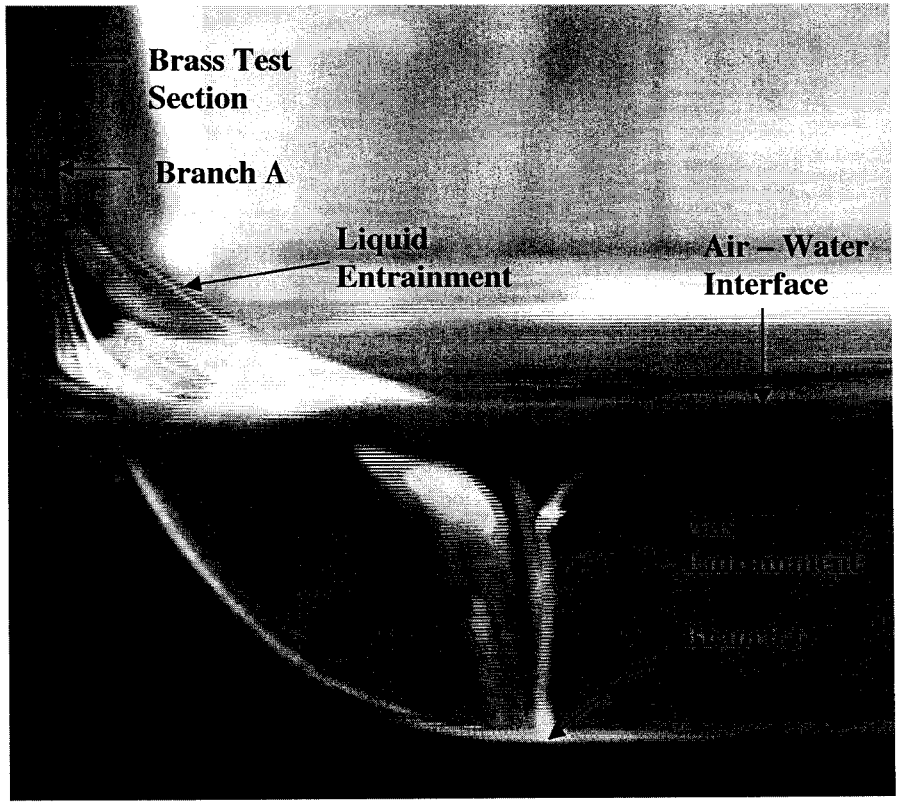

Figure 4.12. OLE in branch A with gas entrainment in branch C.

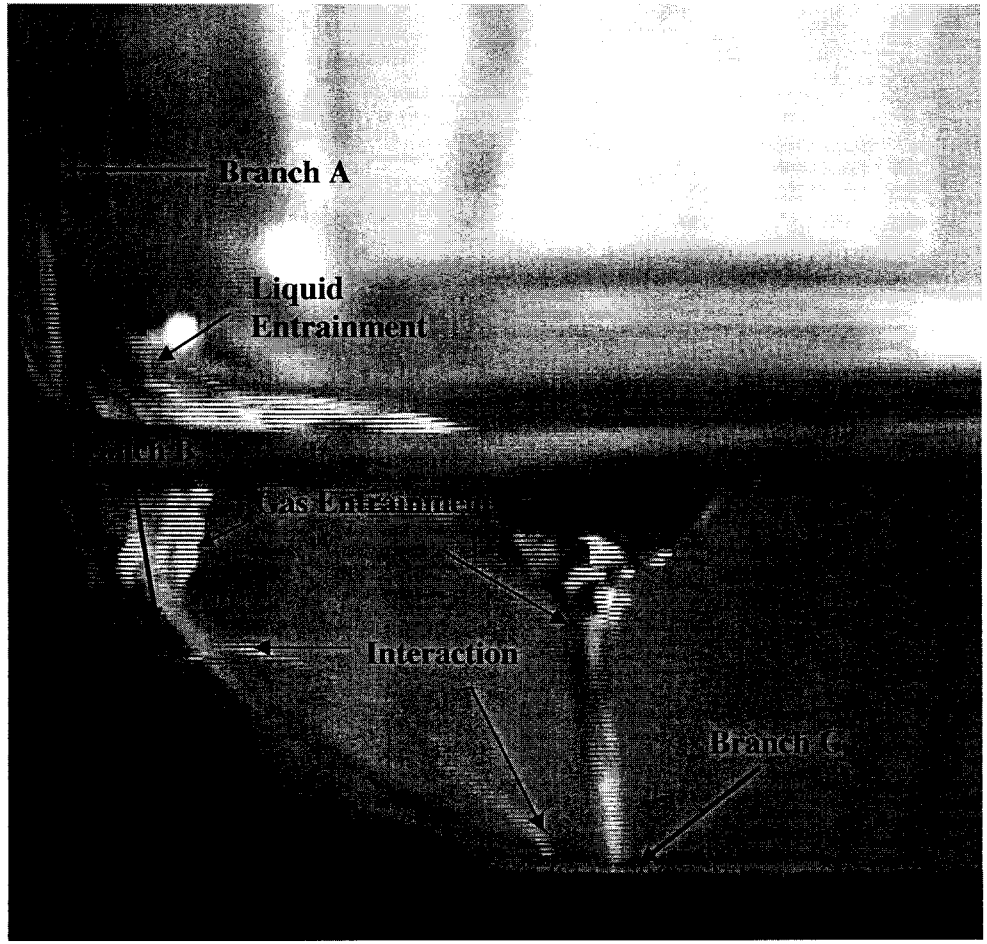

Figure 4.13. Interaction between branches B and C during OLE in branch A.

Table 4.1. OLE in side branch A, single discharge.

CASE 1			
ILL		DLL	
Fr_A	h/d	Fr_A	h/d
18.4612	1.7173	18.4612	2.5594
13.8005	1.4443	16.125	2.4907
9.1794	1.1326	13.8005	2.2562
7.6698	0.9428	11.4859	2.1553
5.7492	0.8002	9.1794	2.0879
3.8313	0.6512	8.6314	2.0173
1.9152	0.4384	7.6698	1.9217
0.8089	0.1009	6.7091	1.8521
0.4853	0.0872	5.7492	1.8521
0.3235	0.2348	4.7899	1.7989
0.1618	0.3706	3.8313	1.6841
0.9706	0.1175	2.8731	1.5584
0.1143	0.3228	1.9152	1.4535
0.0842	0.3706	0.9575	1.4143
0.0465	0.4047	0.6471	1.3808
0.0059	0.4074	0.9706	1.3808
0.0022	0.4167	0.0842	1.38
		0.0022	1.3808

Table 4.2. OLE in branch B, single discharge.

CASE 2			
ILL		DLL	
Fr_B	h/d	Fr_B	h/d
18.4612	0.975	18.4612	1.0761
13.8005	0.8403	13.8005	1.0761
9.1794	0.5372	9.1794	1.0761
7.6698	0.4362	7.6698	1.0761
5.7492	0.4025	5.7492	1.0761
3.8313	0.1967	3.8313	0.975
1.9152	0.0657	0.9575	0.5789
0.9575	0.069	0.6471	0.5712
0.6471	0.1959	0.3235	0.5688
0.3235	0.3047	0.0842	0.6117
0.0842	0.3595	0.0059	0.3858
0.0059	0.3384	0.0022	0.4131
0.0022	0.4057		

Table 4.3. OLE in branch A, dual discharge with branch B.

CASE 3											
$Fr_B = 5.10$				$Fr_B = 15.9$				$Fr_B = 26.4$			
ILL		DLL		ILL		DLL		ILL		DLL	
Fr_A	h/d	Fr_A	h/d	Fr_A	h/d	Fr_A	h/d	Fr_A	h/d	Fr_A	h/d
9.1794	1.309	5.7492	1.3954	3.8313	0.5398	0.0842	0.6433	0.9575	0.4939	0.0059	0.4946
7.6698	1.045	3.8313	1.3759	1.9152	0.3054	0.0059	0.5391	0.8089	0.0346		
5.7492	0.8561	1.9152	1.126	0.9575	0.2367			0.4853	0.1674		
3.8313	0.7419	0.9575	1.0113	0.6471	0.0346			0.1618	0.3694		
1.9152	0.5416	0.6471	0.9046	0.4853	0.1			0.0842	0.3694		
0.9575	0.3041	0.4853	0.8417	0.1618	0.1699			0.0059	0.3998		
0.6471	0.0011	0.1618	0.7756	0.0842	0.2841						
0.4853	0.0663	0.0842	0.7408	0.0059	0.3357						
0.1618	0.1666	0.0059	0.7419								
0.0842	0.3354										
0.0059	0.3357										

Table 4.4. OLE in branch A, dual discharge with branch C.

CASE 4											
Fr_C = 5.10				Fr_C = 15.9				Fr_C = 26.4			
ILL		DLL		ILL		DLL		ILL		DLL	
Fr_A	h/d	Fr_A	h/d	Fr_A	h/d	Fr_A	h/d	Fr_A	h/d	Fr_A	h/d
18.4612	1.7293	18.4612	2.3192	13.8005	1.4509	9.1794	1.8809	7.6698	1.0113	0.0842	0.8082
13.8005	1.5164	13.8005	2.1846	7.6698	1.1009	7.6698	1.5501	5.7492	0.843	0.0059	0.782
9.1794	1.2134	9.1794	1.7343	5.7492	0.8438	5.7492	1.4828	3.8313	0.7795		
7.6698	1.045	7.6698	1.5387	3.8313	0.7082	3.8313	1.3959	1.9152	0.5414		
5.7492	0.9513	5.7492	1.4769	1.9152	0.5069	1.9152	1.1887	0.9575	0.2031		
3.8313	0.7082	3.8313	1.348	0.9575	0.2031	0.9575	0.9439	0.8089	0.102		
1.9152	0.5061	1.9152	1.1449	0.8089	0.102	0.8089	0.9102	0.4853	0.1		
0.9575	0.1694	0.9575	0.9072	0.4853	0.1	0.4853	0.7756	0.1618	0.2683		
0.6471	0.0663	0.4853	0.8328	0.1618	0.2721	0.1618	0.7411	0.0842	0.3011		
0.4853	0.0346	0.1618	0.7183	0.0842	0.3345	0.0842	0.7983	0.0059	0.3357		
0.1618	0.2683	0.0842	0.6395	0.0059	0.3694	0.0059	0.7419				
0.0842	0.3438	0.0465	0.6471								
0.0465	0.4367	0.0059	0.5013								
0.0059	0.509										

Table 4.5. OLE in branch B, dual discharge with branch A.

CASE 5											
Fr_A = 1.15				Fr_A = 6.13				Fr_A = Fr_B			
ILL		DLL		ILL		DLL		ILL		DLL	
Fr_B	h/d	Fr_B	h/d	Fr_B	h/d	Fr_B	h/d	Fr_B	h/d	Fr_B	h/d
18.4612	0.8225	18.4612	1.0761	18.4612	0.8011	18.4612	1.0761	18.4612	1.1797	18.4612	1.1797
13.8005	0.7238	13.8005	1.0761	13.8005	0.6923	13.8005	1.0761	9.1794	0.8066	13.8005	1.1797
9.1794	0.4839	9.1794	1.0761	9.1794	0.5764	9.1794	1.0761	7.6698	0.6718	9.1794	1.1797
7.6698	0.4024	7.6698	1.0761	7.6698	0.5035	7.6698	1.0761	5.7492	0.5709	5.7492	1.1797
5.7492	0.3123	5.7492	1.0761	6.133	0.4362	6.133	1.0761	3.8313	0.4702	3.8313	0.975
3.8313	0.1668	3.8313	1.0761	3.8313	0.2972	3.8313	1.0761	1.9152	0.3189	1.9152	0.9076
1.9152	0.032	1.9152	0.8756	1.9152	0.1331	1.9152	0.9479	0.9575	0.0994	0.9575	0.6794
0.9575	0.0702	0.9575	0.6046	0.9575	0.032	0.9575	0.7055	0.8089	0.0016	0.8089	0.6383
0.8089	0.1364	0.8089	0.6198	0.6471	0.1364	0.6471	0.6718	0.4853	0.1685	0.4853	0.5805
0.4853	0.2789	0.4853	0.5307	0.4853	0.2036	0.4853	0.5709	0.3235	0.271	0.3235	0.569
0.1618	0.3721	0.1618	0.5035	0.1618	0.3266	0.1618	0.5066	0.0842	0.2699	0.0842	0.5074
0.0465	0.4057	0.0465	0.4931	0.0465	0.3384	0.0465	0.4915	0.0059	0.2754	0.0059	0.5006
0.0059	0.3921	0.0059	0.4283	0.0059	0.3384	0.0059	0.4572				
0.0009	0.4394	0.0009	0.3496	0.0009	0.3384	0.0009	0.4346				

Table 4.6. OLE in branch B, dual discharge with branch C.

CASE 6							
Fr_C = 0.14				Fr_C = 0.38			
ILL		DLL		ILL		DLL	
Fr_B	h/d	Fr_B	h/d	Fr_B	h/d	Fr_B	h/d
5.7492	0.6383	0.9575	0.8066	5.7492	0.5973	0.1618	0.5735
3.8313	0.5003	0.6471	0.7863	3.8313	0.306	0.0842	0.5035
1.9152	0.3014	0.4853	0.7688	1.9152	0.1668	0.0059	0.4362
0.9575	0.1331	0.1618	0.7055	0.9575	0.032		
0.6471	0.0335	0.0842	0.6378	0.6471	0.0351		
0.4853	0.1364	0.0059	0.6046	0.4853	0.2214		
0.1618	0.1765			0.1618	0.2989		
0.0842	0.2373			0.0842	0.3384		
0.0059	0.26			0.0059	0.3384		

Table 4.7. OLE in branch A, triple discharge with branches B and C.

CASE 7			
Fr_B= 5.10, Fr_C = 5.10			
ILL		DLL	
Fr_A	h/d	Fr_A	h/d
13.8005	1.5164	5.7492	1.6129
9.1794	1.1797	3.8313	1.5159
7.6698	1.0052	1.9152	1.3444
5.7492	0.8765	0.8089	0.9811
3.8313	0.7082	0.4853	0.9691
1.9152	0.5063	0.1618	0.8994
0.8089	0.102	0.0842	0.8646
0.4853	0.1337	0.0059	0.7243
0.1618	0.2346		
0.0842	0.3225		
0.0059	0.3694		

Table 4.8. OLE in branch B, triple discharge with branches A and C.

CASE 8			
$Fr_A = 13.8$, $Fr_C = 0.38$			
ILL		DLL	
Fr_B	h/d	Fr_B	h/d
5.7492	0.6718	0.4853	0.6718
3.8313	0.5398	0.1618	0.5789
1.9152	0.3696	0.0842	0.5372
0.9575	0.2342	0.0059	0.5035
0.8089	0.0384		
0.4853	0.069		
0.1618	0.1854		
0.0842	0.2036		
0.0059	0.2373		

Table 4.9. OLE in branch B, triple discharge with branches A and C.

CASE 9							
Fr_A = 1.15							
Fr_C=0.14				Fr_C=0.38			
ILL		DLL		ILL		DLL	
Fr_B	h/d	Fr_B	h/d	Fr_B	h/d	Fr_B	h/d
9.1794	0.74	1.9152	0.9076	5.7492	0.608	0.4853	0.6474
7.6698	0.6638	0.9575	0.7392	3.8313	0.4025	0.1618	0.6373
5.7492	0.6046	0.8089	0.6718	1.9152	0.3014	0.0842	0.5709
3.8313	0.5035	0.4853	0.6383	1.1491	0.1331	0.0059	0.4698
1.9152	0.372	0.1618	0.6046	0.8089	0.0572		
0.9575	0.1668	0.0842	0.5638	0.4853	0.1701		
0.8089	0.0657	0.0059	0.5638	0.1618	0.3047		
0.4853	0.1701			0.0842	0.335		
0.1618	0.271			0.0059	0.3384		
0.0842	0.3047						
0.0059	0.3047						

Chapter V

Results and Discussion of OGE using PIV

5.1 Results

The results for the onset of gas entrainment, in the bottom branch, using the particle image velocimetry system will be presented here. The results will demonstrate the velocity fields in the water side of the two-phase environment during vortex-free gas pull through in branch C. The complex flow structure occurring in the water side of the two-phase environment, at the onset of gas entrainment, was divided into four two-dimensional planes. The four planes consist of a single vertical plane through the center of the branch, and three horizontal planes located just below the interface, just above the branch inlet and mid-way between the two. Throughout the text the three horizontal planes will be referred to their vertical coordinate, z, relative to the water height at the onset of gas entrainment H_{OGE}. As such the horizontal plane just below the interface will be denoted by $z/d = H_{OGE}/d$, just above the branch inlet as $z/d = 0$, and at the midway plane as $z/d = H_{OGE}/2d$ where both parameters are non-dimensionalized using the branch diameter, d. The term H_{OGE} refers to the critical height at the onset of gas entrainment. In addition, the values of z/d are only estimates of the actual vertical height of the horizontal plane; this is due in part to the thickness of the laser light sheet and the technical challenges associated with the refraction of the laser light sheet as it passes through the various mediums. It should also be noted here that the results are presented for non-simultaneous measurements of the individual planes, and as such, the out of plane

motions between the three horizontal planes are only estimated by the vertical plane results.

The presentation of the velocity field for each case will be described in four separate plots, in a single figure. First, the velocity vector field will be presented as obtained from the PIV system, followed by a contour plot describing the magnitude of the velocity field. The next two figures will describe the components of the velocity field in terms of V_x and V_y for the vertical planes and V_r and V_t for the horizontal planes. The choice of demonstrating the horizontal plane velocity fields in terms of the radial and tangential components, V_r and V_t respectively, relative to the center of the branch are conducive to the actual flow. This information can be further used to determine additional parameters such as the circulation, and as such, will present more appropriate results than if the vector field were resolved in rectangular components, V_x and V_y. In all the velocity fields presented, both vertical and horizontal, the curved wall is in the negative x-direction, and the open end of the test section in the positive x-direction.

5.2 Test Section Validation

The values for the critical height, H_{OGE}, at the onset of gas entrainment first needed to be determined with the acrylic test section. It was also instructive to determine what the effects were of having the test section made from acrylic as opposed to brass. In addition, the effects of having a quarter-circular cross section instead of a semi-circular one. To demonstrate these two points the results for both the brass and acrylic test sections are presented in Figure 5.1. The figure demonstrates that both the brass and

acrylic test section results are in excellent agreement. As was expected, the results did show some small deviation at the lower Froude ranges and this is understood to be the effect of the difference in material.

5.3 OGE Liquid Velocity Fields

This section will present the liquid velocity fields obtained from the nine cases presented in Table 3.5. First, to demonstrate the raw images captured with the PIV system, during experimentation, two sample images are presented in Figure 5.2 for the vertical and horizontal planes. The images show the illuminated particles that were captured with the PIV system, and were used to generate the liquid velocity fields.

In order to aid the reader with the large amount of information that is presented in the figures, a few key features can be noted that are consistent in the results. For the velocity fields in the vertical planes, presented in Figures 5.3, 5.7 and 5.11 for Fr_C equal to 3.47, 15.84 and 36.96 respectively, a similarity in the flow structure approaching the branch inlet exists at x/d = 0. The similarity, although not entirely symmetric, is represented by two separate regions, as can be seen in the velocity field magnitude contour plots, on either side of x/d = 0. The remaining Figures 5.4 to 5.6, 5.8 to 5.10 and 5.12 to 5.14 demonstrate the results of the velocity fields in the horizontal planes, for Fr_C equal to 3.47, 15.84 and 36.96 respectively. Throughout these figures a noticeable similarity is present between the velocity field magnitude and radial velocity component, V_r, contour plots. As the flow approaches the branch center, located at x/d = y/d = 0, the radial velocity component tends towards zero, in fact this is due to the transition from a radial

velocity component to a vertically downward component, in the z/d direction. What this demonstrates is the presence of a strong dependence of the flow field on the radial component, as would be expected for vortex-free flow. However, it should be pointed out that for vortex-free gas entrainment in the discharging branch to be present, the tangential velocity component should be zero. In fact this is not the case, as will be seen, and the results presented here demonstrate new information for the onset of gas entrainment phenomenon. A problem now arises in the interpretation of the horizontal and vertical velocity fields presented, due to the fact that the actual velocity vector is inherently three-dimensional. As a result the velocity fields presented are only in plane projections of three dimensional velocity vectors. Nevertheless, the results presented here represent the first steps towards resolving the flow structure in three-dimensions.

Presented in Figures 5.3, 5.4, 5.5 and 5.6 are the velocity fields obtained in the vertical, and three horizontal planes with z/d = 0, z/d = 0.47 and z/d = 0.94 respectively for Fr_C equal to 3.47. As stated earlier, the individual figures represent results captured at separate instants in time, yet due to the relatively stable nature of the vortex-free gas entrainment phenomena, they yield a fair approximation of what could be expected from simultaneous measurements. The vertical velocity profile shown in Figure 5.3 demonstrates a similarity of the flow structure about x/d = 0. It can be seen from Figure 5.3 (c) that as the flow approaches x/d, from either side, the magnitude of V_x also increases. In a similar fashion, V_y also increases as it approaches the branch center, at x/d = 0. The velocity field in a horizontal plane, closest to the branch inlet at z/d = 0, is presented in Figure 5.4. The relative magnitudes of the radial and tangential components

suggest that the flow field is strongly related to the radial component. A stronger velocity field magnitude is demonstrated to the right of x/d = 0, as opposed to the left, where the influence of the wall is present. In fact the influence of the wall is exhibited by the larger tangential velocity component, at the left of the branch center x/d = 0. Similar features are demonstrated at the mid horizontal plane, located at z/d = 0.47, in Figure 5.5. In fact this figure demonstrates a slight shift in the tangential velocity component towards the curved wall, in the negative x-direction, from the plane located at z/d = 0. One possible reason for this trend is the fact that with the increase in z/d of the horizontal plane, the horizontal distance between the curved wall and x/d = 0 also increased, thus shifting the influence of the wall to the left of x/d = 0. In Figure 5.6 the shift in tangential velocity component towards the wall is also evident. In comparison of the three horizontal velocity field figures, it is interesting to note that the more significant differences in the velocity field occur about the branch center, at x/d = 0. On the left of the branch center the influence of the curved vertical wall is demonstrated, while on the right no wall effects are felt on the flow field. In addition to this, the complex flow field does not demonstrate exact symmetry about the branch center, at x/d = 0 or at y/d = 0, which raises the question of the effects of having a curved vertical wall also to the right of the branch center.

Presented in Figures 5.7, 5.8, 5.9 and 5.10 are the liquid velocity fields obtained in the vertical, and three horizontal planes with z/d = 0, z/d = 0.91 and z/d = 1.81 respectively, for Fr_C equal to 15.84. As was the case with the Fr_C = 3.47 results presented above, the vertical velocity field results in Figure 5.7 demonstrate some similarity about the branch

center at x/d = 0. Interesting to note in the velocity field magnitude plot in (b), is that the structure of the liquid velocity field also seems to demonstrate the shape of the air side flow, above z/d = 1 and about x/d = 0. The horizontal velocity fields presented in Figures 5.8, 5.9 and 5.10 demonstrate, again, a strong dependence on the radial velocity component, however, the presence of the tangential component is also observed throughout. As the flow approaches the branch center, the radial velocity component tends towards zero as it transitions in the negative z/d direction. The shift in the tangential velocity component to the left of x/d = 0, towards the curved wall, is also seen in these figures. Similar to the results for Fr_C = 3.47, this demonstrates the effect of the relative horizontal distance between the wall and the branch center, at x/d = 0. Note that of particular interest in Figure 5.10, a discrepancy in the results is observed below y/d = 0 and near x/d = 0, as compared with the previous results obtained. It is believed that this is due to perhaps poor correlation from the PIV data obtained, or perhaps due to reflections produced as the light sheet passes through the acrylic test section. If the light sheet refracted sufficiently as it passed through the acrylic viewing section, part of the flow field could also potentially be out of focus, resulting in poor correlation. One important outcome of this is the need to refine the experimental technique, by either replacing the curved surface through which the laser light sheet passes or by using a refractive index matching method to reduce the distortions on the light sheet.

Presented in Figures 5.11, 5.12, 5.13 and 5.14 are the velocity fields obtained in the vertical, and three horizontal planes with z/d = 0, z/d = 0.91 and z/d = 1.81 respectively, for Fr_C equal to 36.96. A difference in the velocity field magnitude contour plot is

evident, from the previous two cases of Fr_C = 3.47 and 15.84, in that although a similarity exists about x/d = 0 the two regions that were previously seen on either side are not present. They are present, however, in the contour plot of V_x, similar to the previous two cases. One possible reason for this is that as the Froude number is increased, the critical height also increases. With the increased distance that the gas must travel to entrain into the branch, comes a thinning of the gas cone structure from the interface to the branch inlet. In fact, the gas cone structure near the gas-liquid interface can be observed in Figure 5.11 (c) near z/d = 2 and x/d = 0. The horizontal plane velocity fields, in Figures 5.12, 5.13 and 5.14, demonstrate a similar dependence of the flow field on the radial velocity component. Interesting to note, in the horizontal velocity field contour plots, for the radial velocity component, is that as z/d increases the influence of the curved vertical wall seems to become more apparent to the left of x/d = 0. The tangential velocity field contour plots demonstrate a similar relationship that, as z/d increases, the tangential velocity component shifts to the left of x/d = 0 and closer to the curved vertical wall.

5.3.1 Effects of Froude Number on Velocity

The contour plots presented to demonstrate the velocity fields obtained, while instructive, present a challenge when trying to compare effects of the branch discharge strength. As such presented here will be comparisons of the vertical and horizontal velocity profiles at selected planes.

For comparisons of the vertical velocity fields, Figures 5.15 and 5.16 are presented for selected planes. Figure 5.15 demonstrates the vertical velocity field results to the left of

the branch center, at x/d = -0.5 in the direction of the curved wall, for both V_x and V_z velocity components. In Figure 5.15 (a) the effect of Froude number is a certain increase in the peak value of V_x. In a similar fashion, Figure 5.15 (b) demonstrates a similar relationship with the Froude number. As expected, as the flow approaches the bottom wall, along z/d = 0, the velocity magnitude tends toward zero. Another feature, that is apparent from this plot, is the height of the gas-liquid interface by the maximum value of z/d for each profile. Figure 5.16 presents the development of the velocity field with Fr_C, on either side of the branch centerline in a vertical plane, for a height above the branch of $z/d = H_{OGE}/2d$. What can be seen from Figure 5.16 (a) is that, with increasing Froude number, the magnitude of the vertical component tends to increase towards the branch center, at x/d = 0. Figure 5.16 (b) shows that V_z also increases towards x/d = 0, with increasing Fr_C.

For comparisons of the horizontal velocity fields, Figures 5.17, 5.18 and 5.19 are presented for the three horizontal planes investigated, for each Froude number. Figure 5.17 presents the effects of Fr_C on the radial and tangential velocity components, in a horizontal plane closest to the branch inlet, recall z/d = 0 and at y/d = 0. The evidence is inconclusive regarding the effect of the Froude number at this height above the branch, and this is in part due to the results for Fr_C = 15.84. If the results for Fr_C = 15.84 are disregarded, then it could be said for the other two that an increase in Froude number results in an increase in the magnitude of both the radial, and tangential components. Comparing the other two horizontal plane results, in Figures 5.18 and 5.19, a similar

discussion regarding the effect of Fr_C on the radial, and tangential, components can be found.

5.3.2 Effect of Height above Branch Inlet on Velocity

To demonstrate the effect of height above the branch inlet, on the velocity components in the three horizontal planes, for each of the Froude numbers investigated, Figures 5.20, 5.21 and 5.22 are presented. Figure 5.20 is presented for $Fr_C = 3.47$, along $y/d = 0$ of the horizontal planes at $z/d = 0$, $z/d = 0.46$ and $z/d = 0.94$. The results here demonstrate that at the highest horizontal plane, at $z/d = 0.94$, the highest values of the radial and tangential velocities occur, which is just below the gas-liquid interface. Comparing this with the Figures 5.21 and 5.22, the highest values tend to be closest to the branch inlet, at $z/d = 0$. Recall, it was found from the vertical plane results the highest velocities were found in regions near $z/d = 0.5$, so the fact that Figures 5.21 and 5.22 demonstrate this inconsistency with Figure 5.19, is not altogether incorrect.

5.4 Discussion

Results obtained for the liquid velocity field, at the onset of gas entrainment in a bottom branch, is presented for three discharge flow rates using the PIV measurement technique. To resolve the complex three-dimensional velocity field, using a two-dimensional PIV technique, four non-simultaneous planes were considered. A vertical plane passing through the center of the branch, and extending outward into the flow from the curved vertical wall; along with three horizontal planes just below the gas-liquid interface, z/d =

H_{OGE}/d, just above the branch inlet, $z/d = 0$, and midway between the two, $z/d = H_{OGE}/2d$, were presented. To demonstrate the velocity fields, contour plots of the vertical and horizontal planes were presented. Consistent to the velocity fields, in the vertical planes, was a similarity about the branch center at $x/d = 0$, although not symmetric. In addition, consistent with the horizontal velocity fields was a strong relationship between the velocity field, and the radial component. Also demonstrated was the effect of the curved vertical wall, on both the tangential and radial velocity components. Several comparisons were made to demonstrate the effect of the Froude number, and vertical position above the branch inlet, on the velocity fields. In fact, many inconsistencies were found, and are believed to be in part due to the inherently three-dimensional complex flow being resolved in two-dimensional velocity components. As a result, the two-dimensional velocity fields represent in plane projections of the three-dimensional flow rather than the fully resolved velocity vector. With this being said, the results presented do however demonstrate the first steps towards accurately predicting the liquid velocity field in three-dimensions during the onset of gas entrainment in a bottom branch.

To complete the discussion of the complex, three-dimensional, liquid velocity field using the particle image velocimetry technique, a few improvements can be made to the current experimental setup. First, due to the three-dimensional nature of the flow field a PIV system capable of simultaneous three-dimensional measurements should be incorporated. Secondly, the viewable section of the test facility should be modified to adjust for the laser light sheet refraction. This can be achieved by replacing the cylindrical acrylic viewing section by a section with a square cross section, therefore reducing the refraction

due to the curvature of the section. In order to get a better representation of the complex flow field a new test section could be designed whereby a curved wall extends vertically on both sides of the bottom branch.

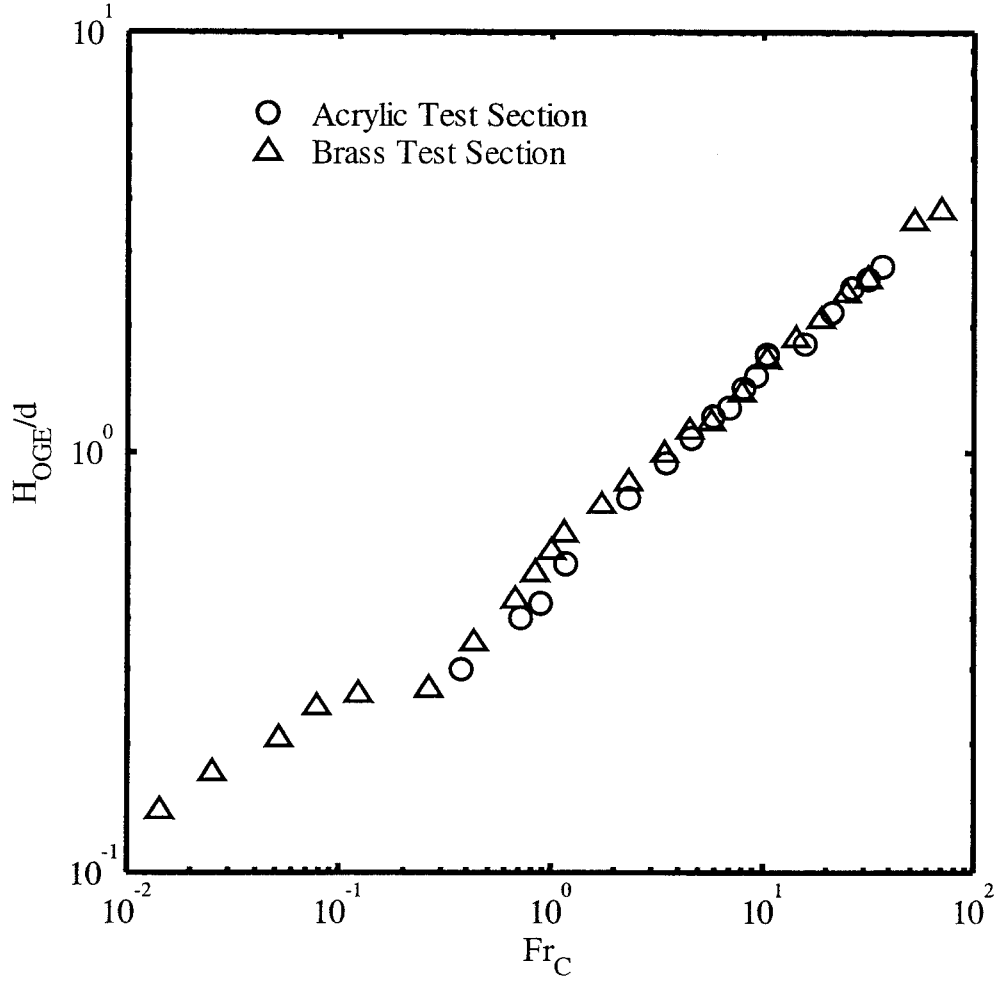

Figure 5.1. Acrylic test section validation.

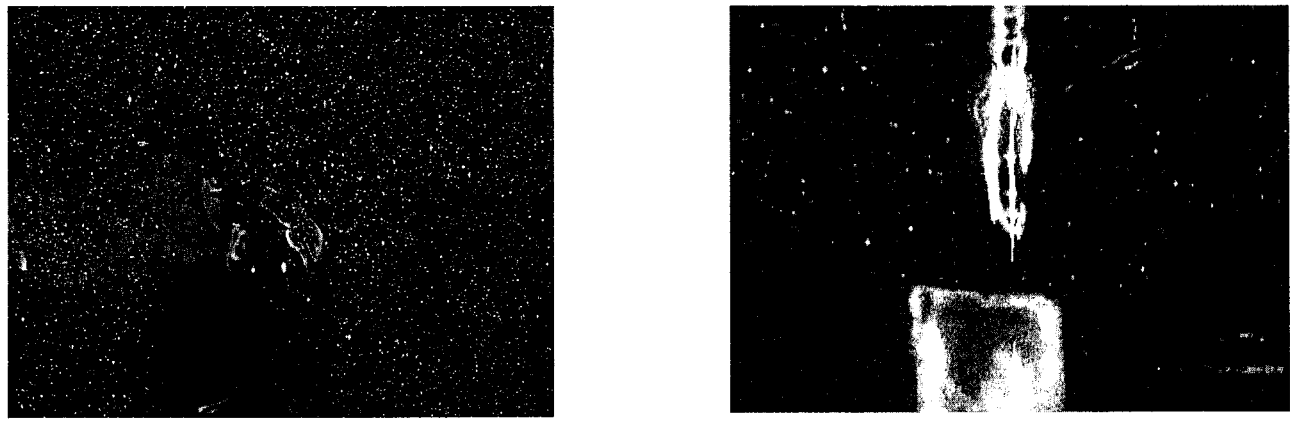

(a) (b)

Figure5.2. Raw PIV images in (a) horizontal and (b) vertical planes.

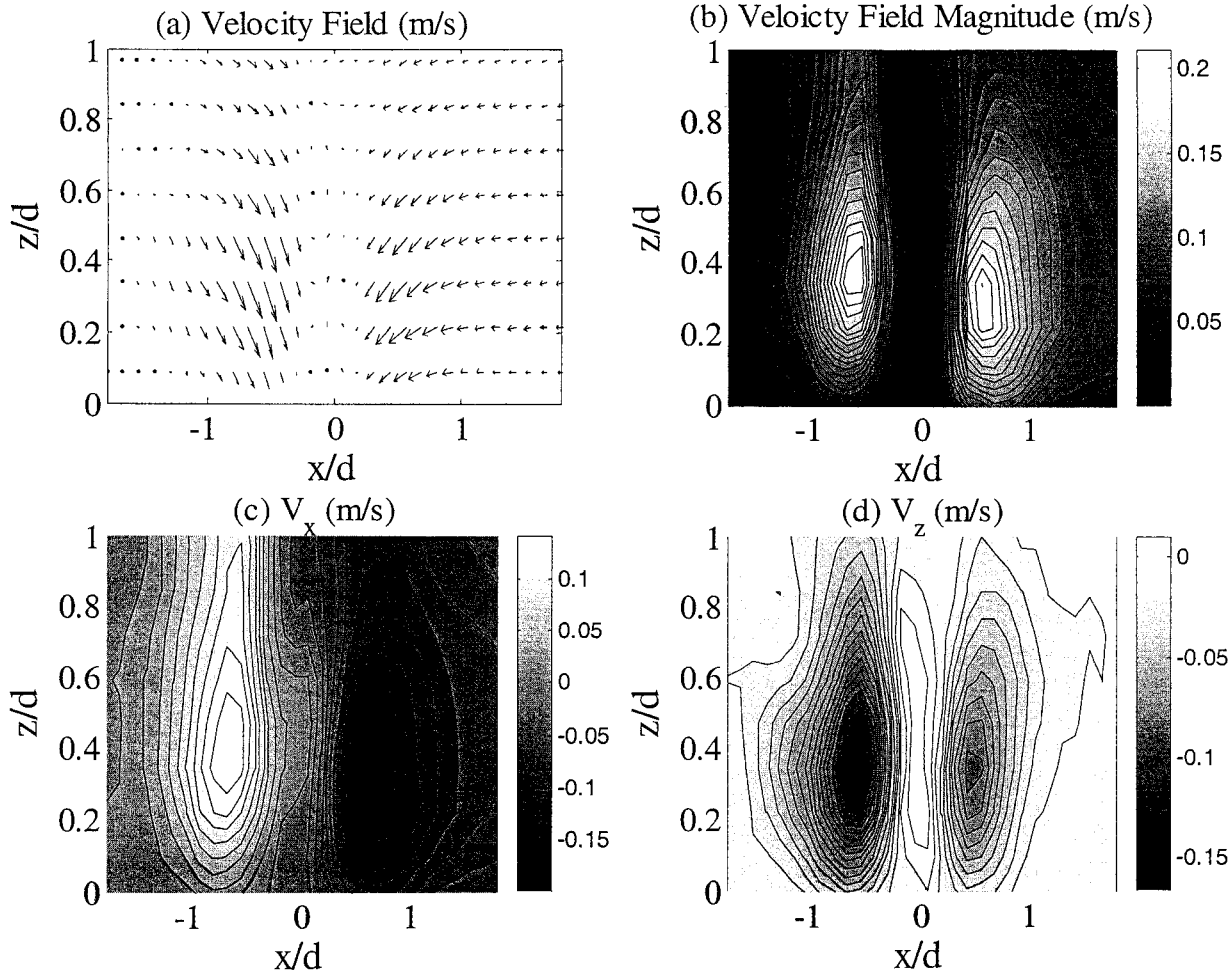

Figure 5.3. Velocity field in a vertical plane at y/d = 0, Fr_C = 3.47-Case 1.

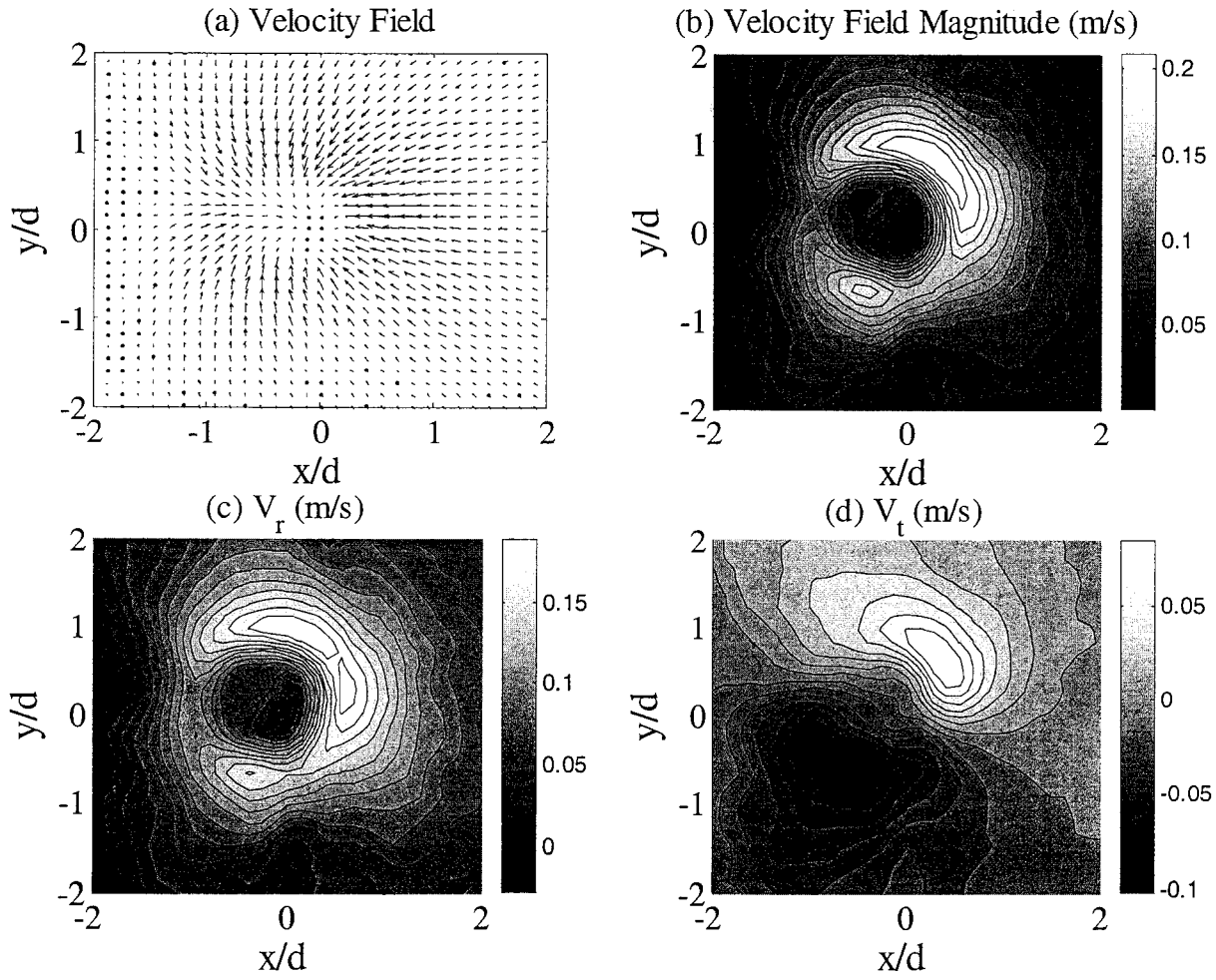

Figure 5.4. Velocity field in a horizontal plane at z/d = 0, Fr_C = 3.47-Case 2.

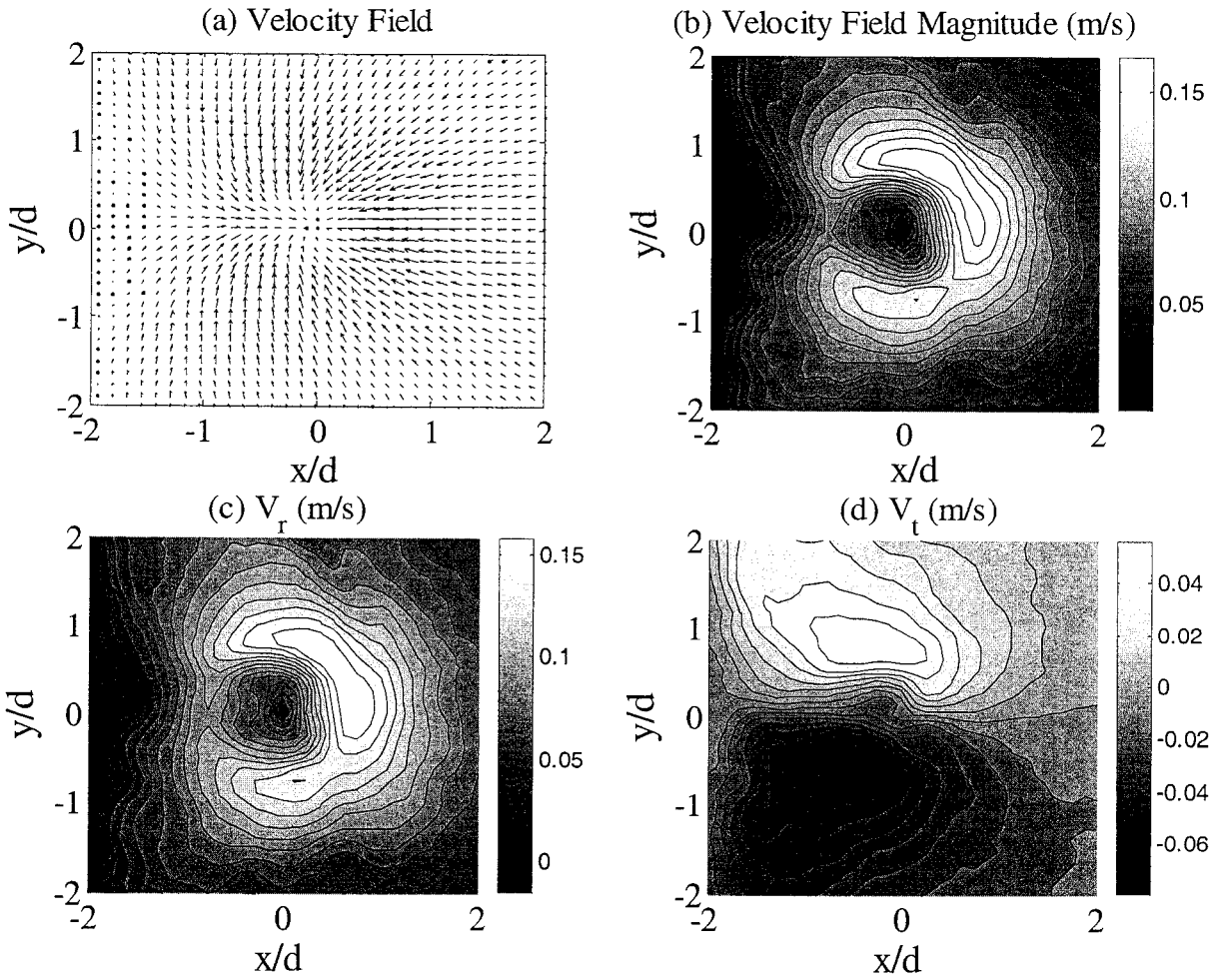

Figure 5.5. Velocity field in a horizontal plane at z/d = 0.47, Fr_C = 3.47-Case 3.

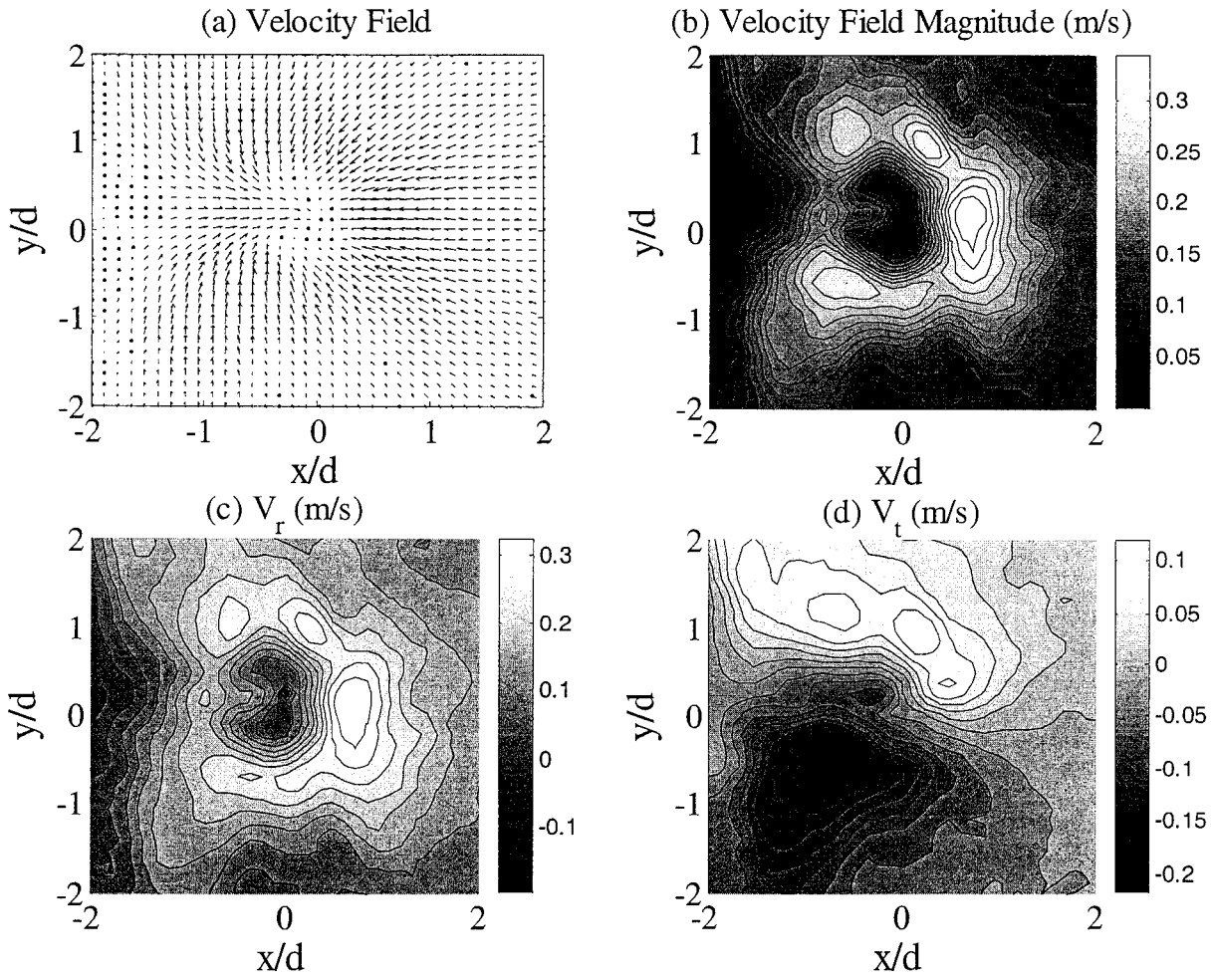

Figure 5.6. Velocity field in a horizontal plane at z/d = 0.94, Fr_C = 3.47-Case 4.

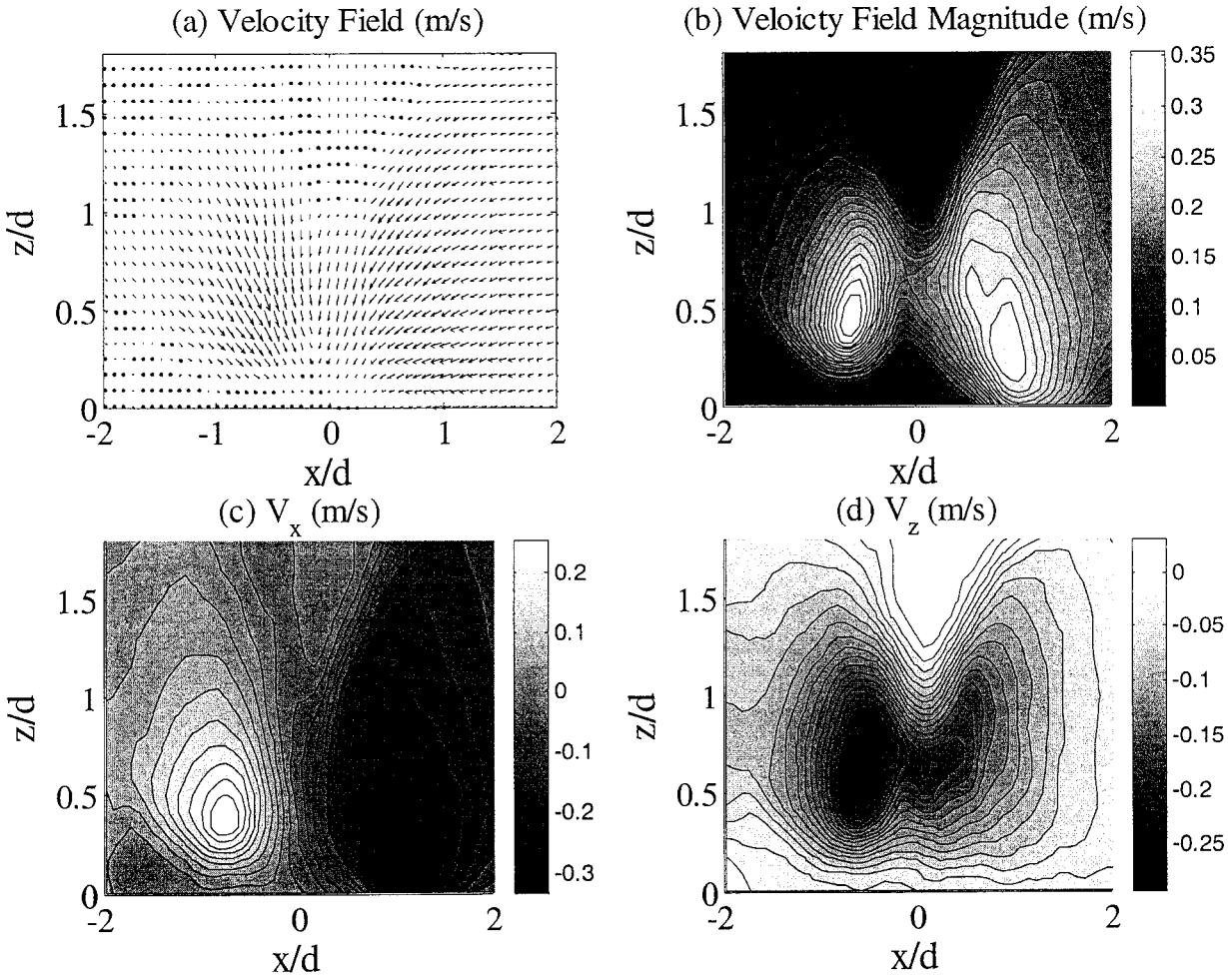

Figure 5.7. Velocity field in a vertical plane at y/d = 0, Fr_C = 15.84-Case 5.

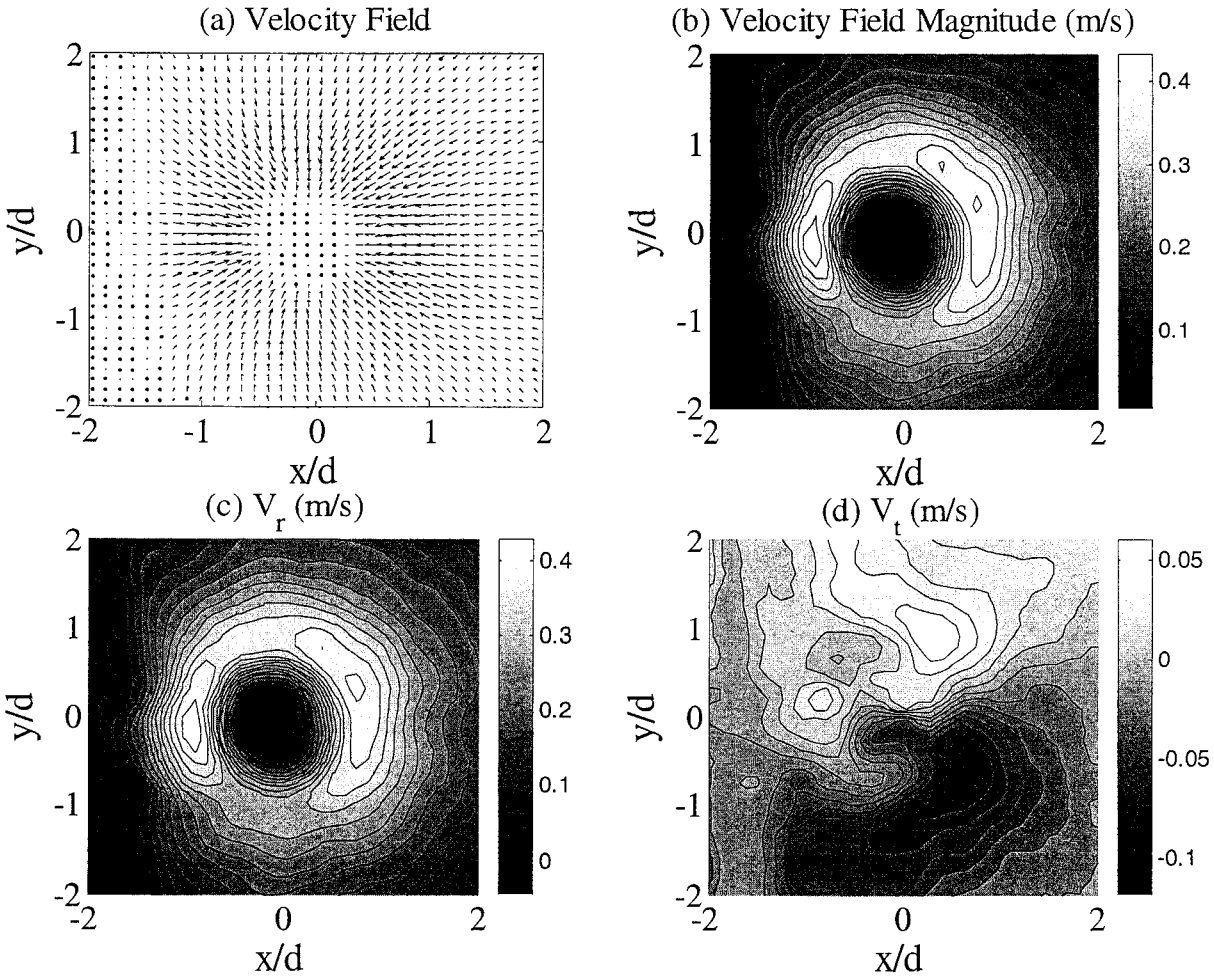

Figure 5.8. Velocity field in a horizontal plane at z/d = 0, Fr_C = 15.84-Case 6.

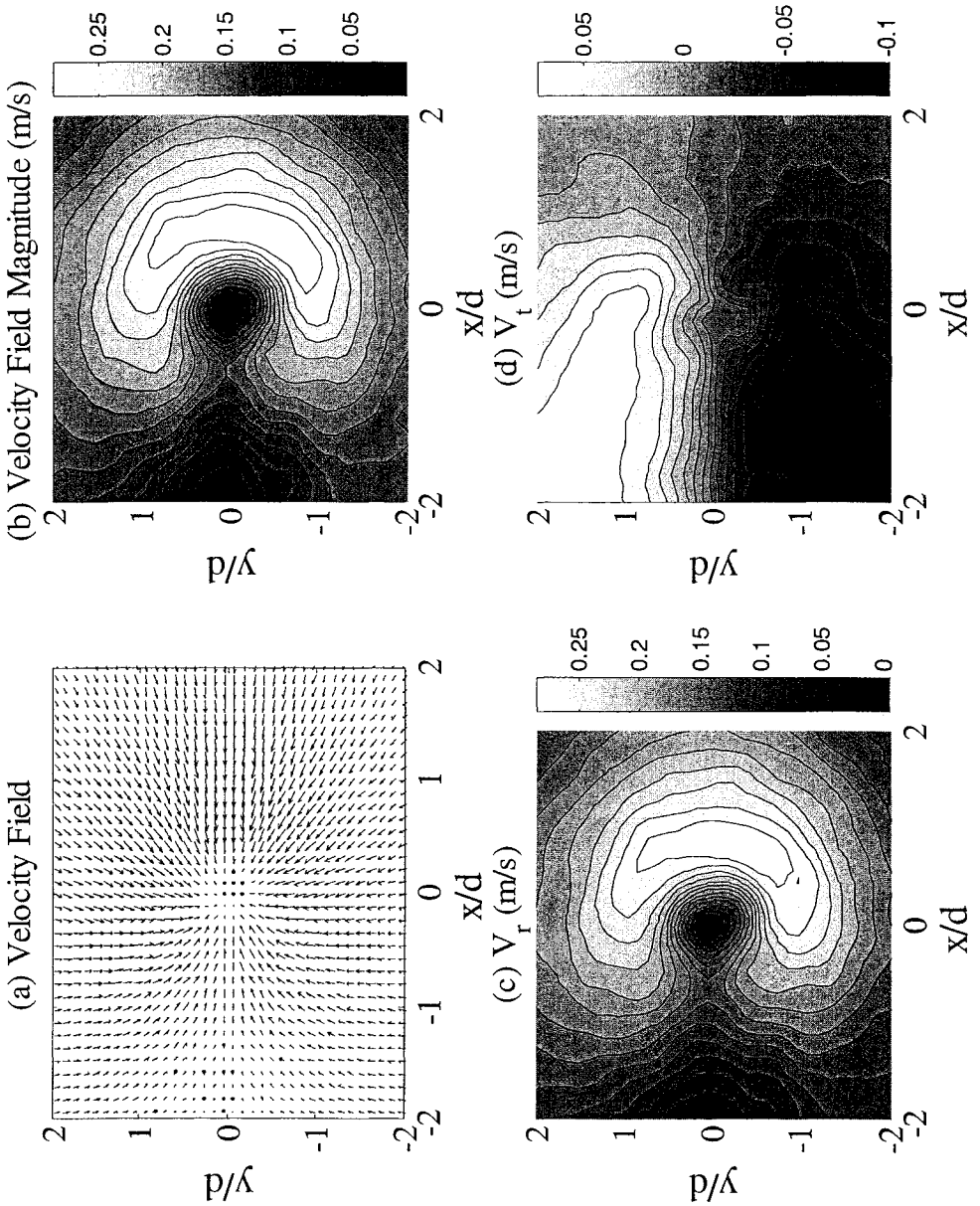

Figure 5.9. Velocity field in a horizontal plane at z/d = 0.91, Fr_C = 15.84-Case 7.

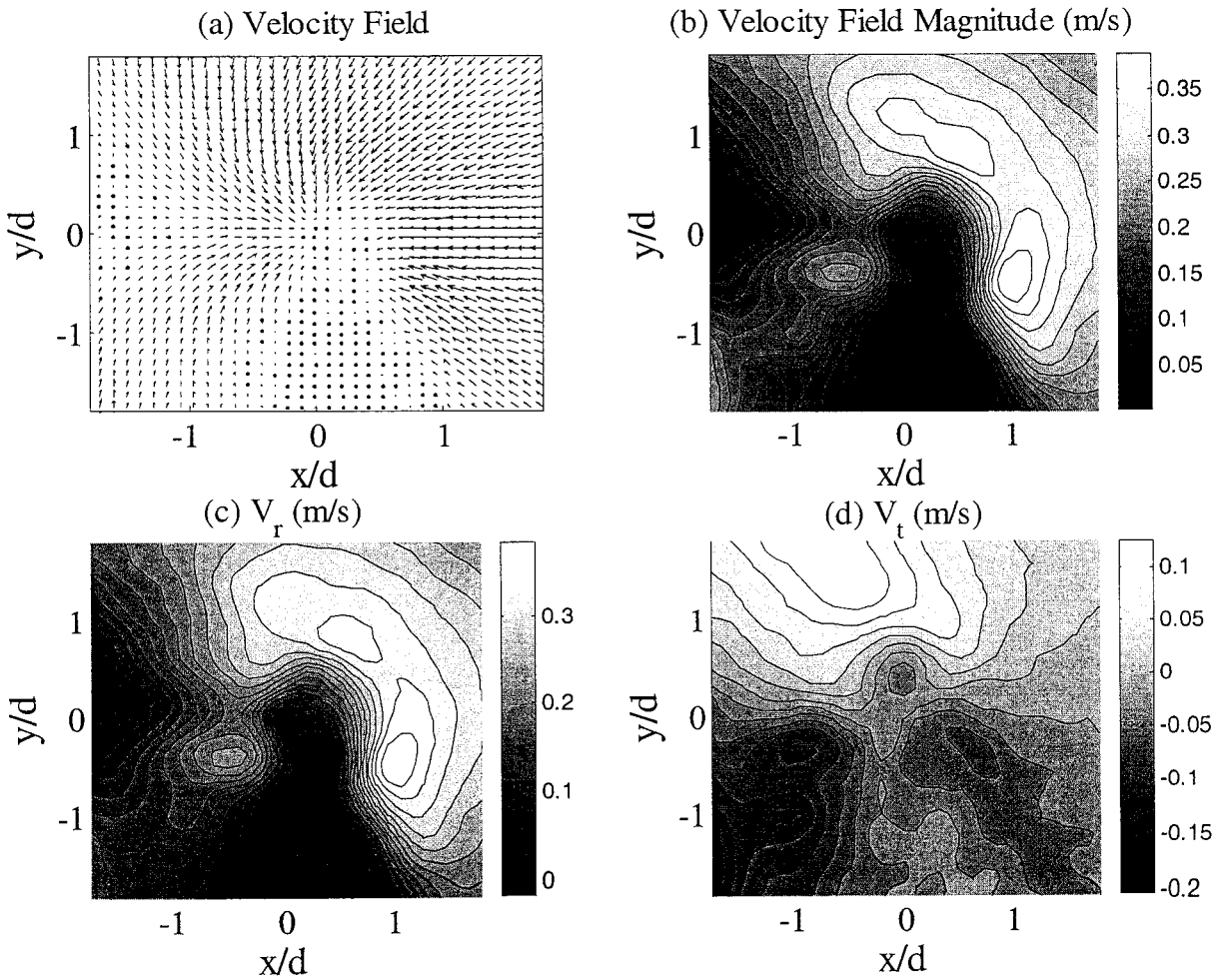

Figure 5.10. Velocity field in a horizontal plane at z/d = 1.81, Fr_C = 15.84-Case 8.

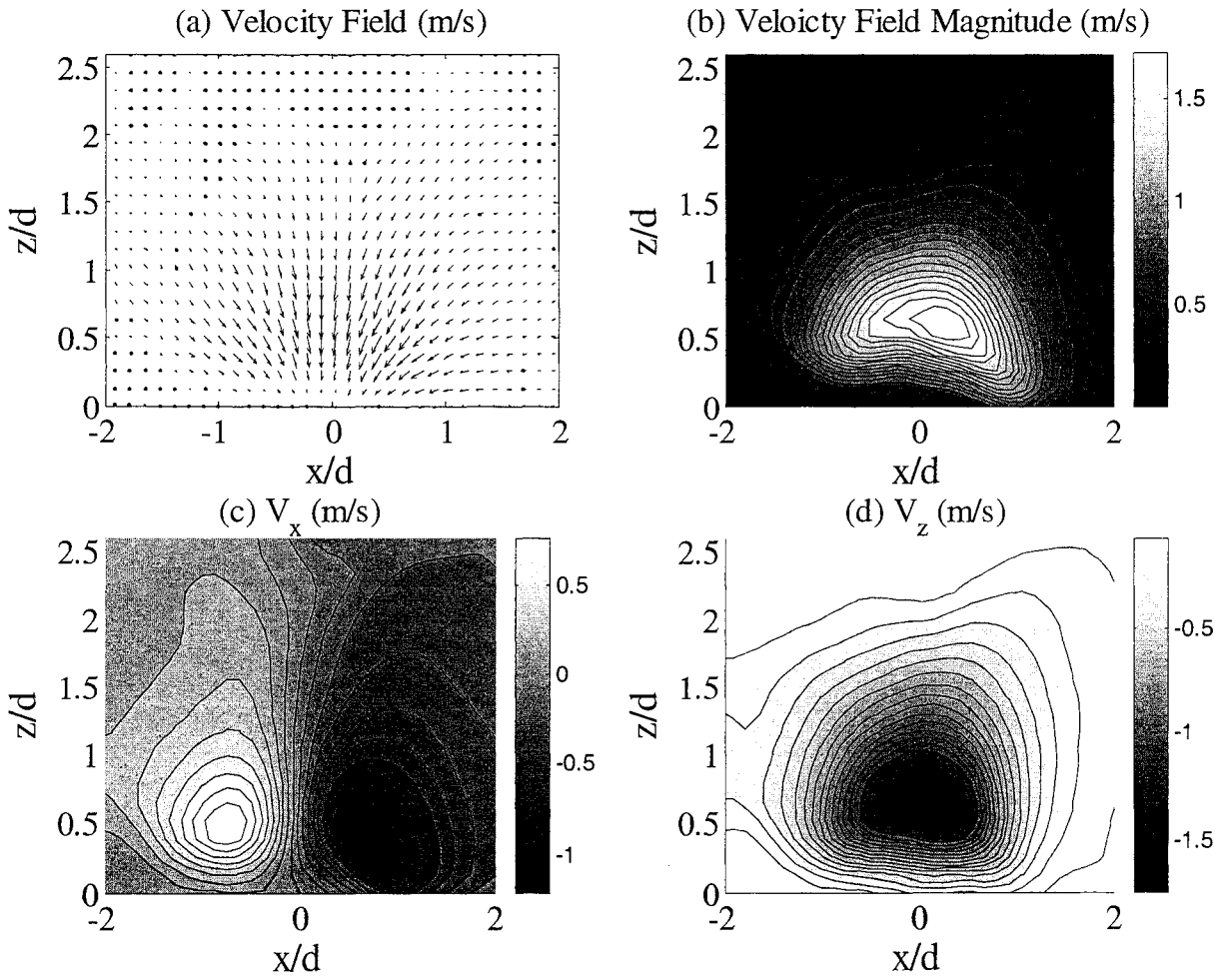

Figure 5.11. Velocity field in a vertical plane at y/d = 0, Fr_C = 36.96-Case 9.

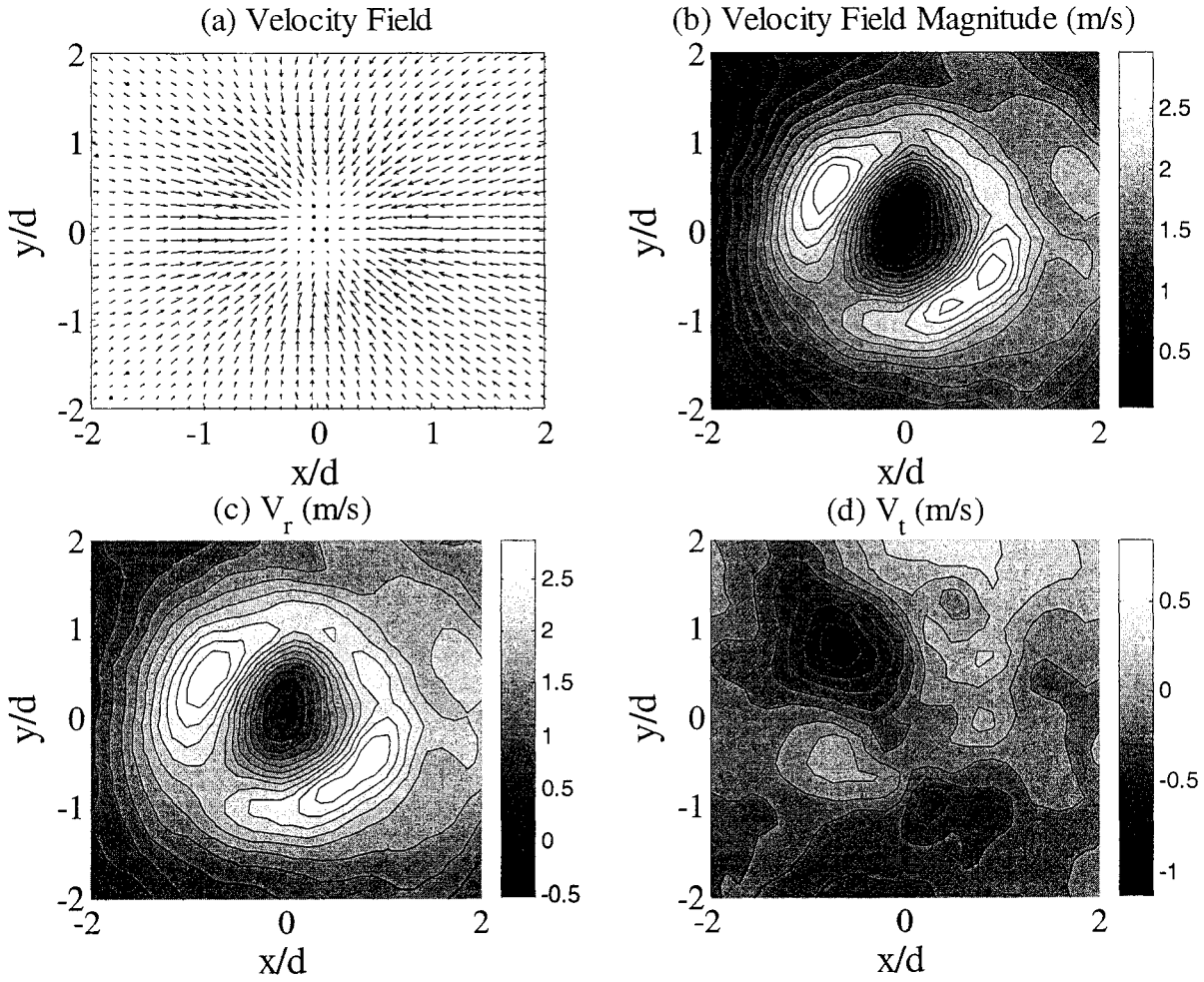

Figure 5.12. Velocity field in a horizontal plane at z/d = 0, Fr_C = 36.96-Case 10.

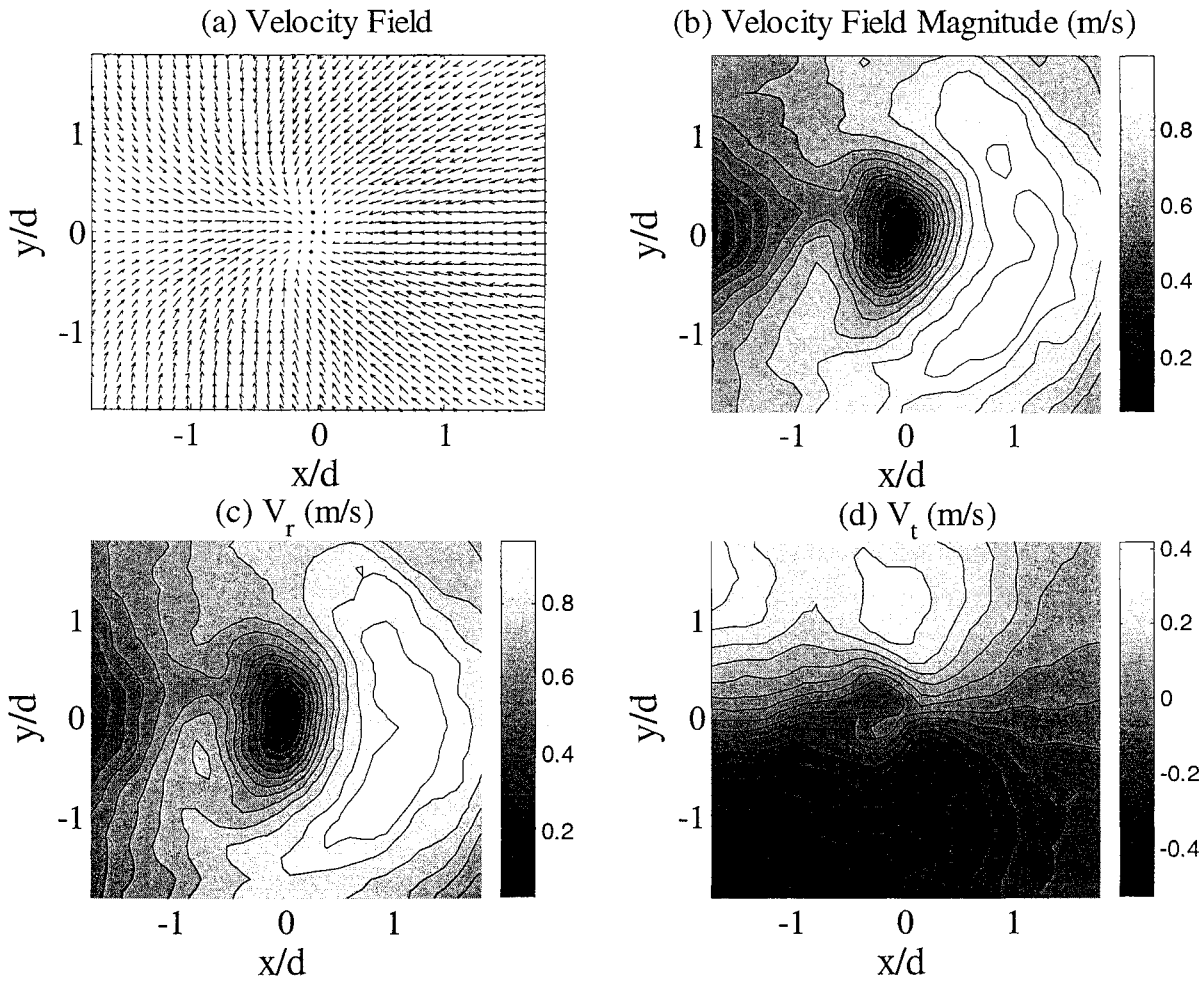

Figure 5.13. Velocity field in a horizontal plane at z/d = 1.39, Fr_C = 36.96-Case 11.

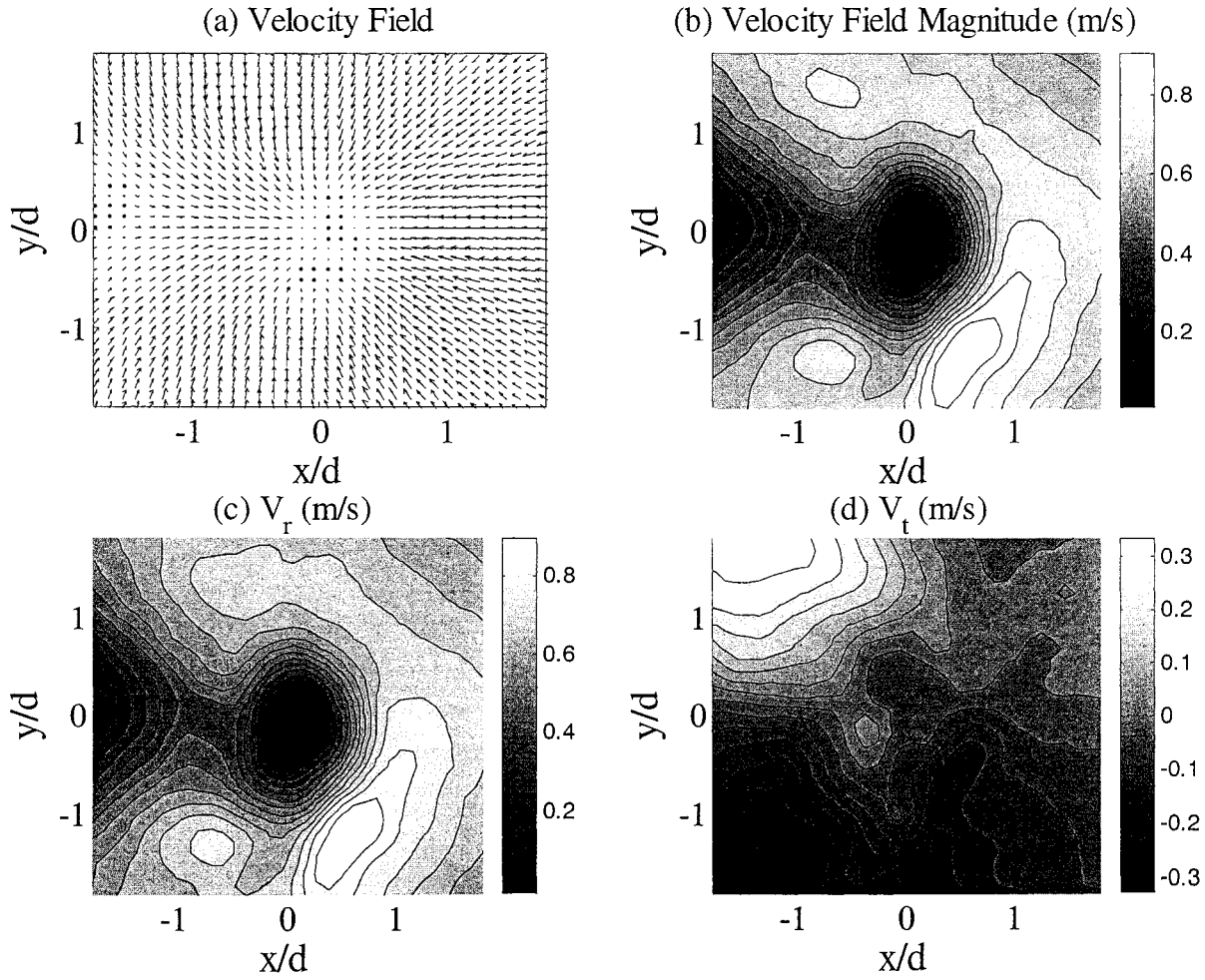

Figure 5.14. Velocity field in a horizontal plane at z/d = 2.79, Fr_C = 36.96-Case 12.

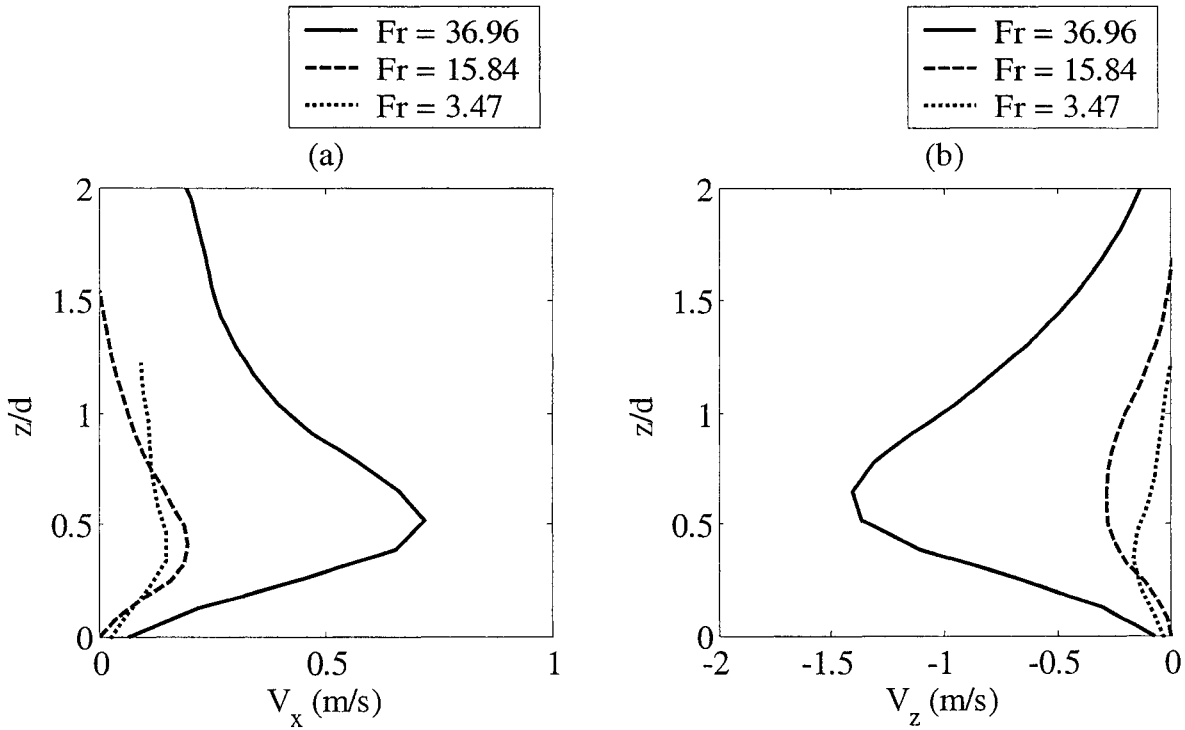

Figure 5.15. Effect of Fr_C on velocity in a vertical plane at x/d = -0.5 and y/d = 0.

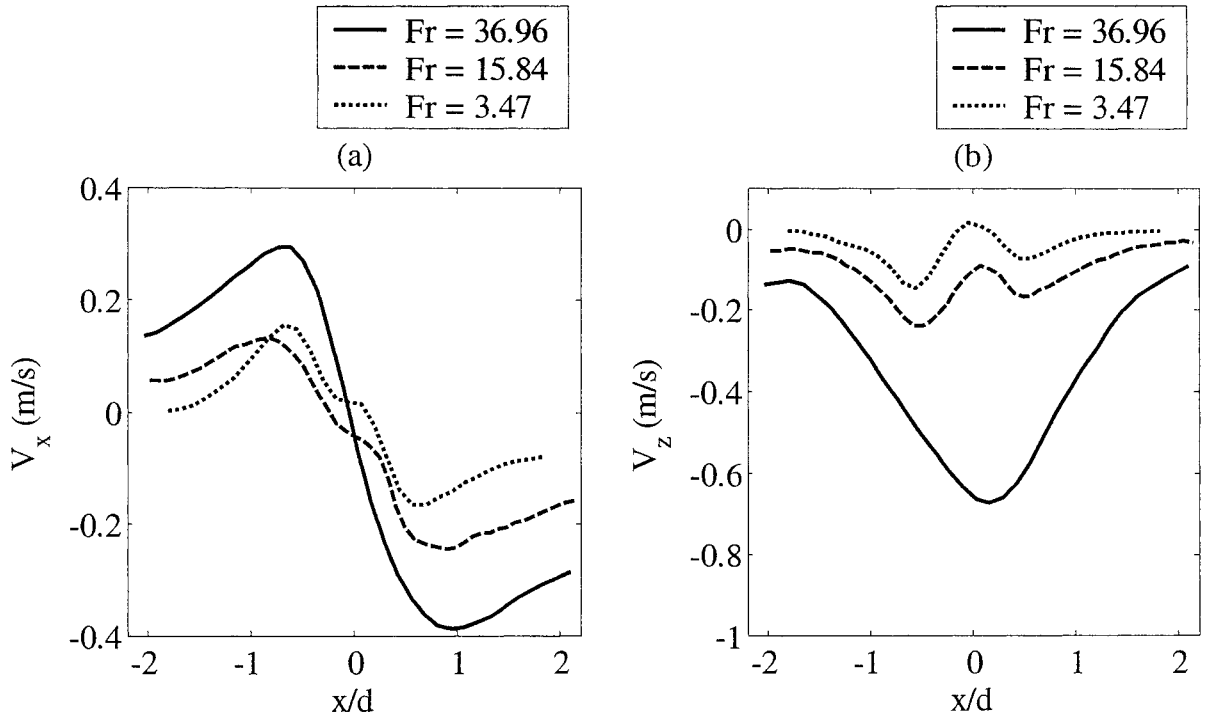

Figure 5.16. Effect of Fr_C on velocity in a vertical plane at $z/d = H_{OGE}/2d$, $y/d = 0$.

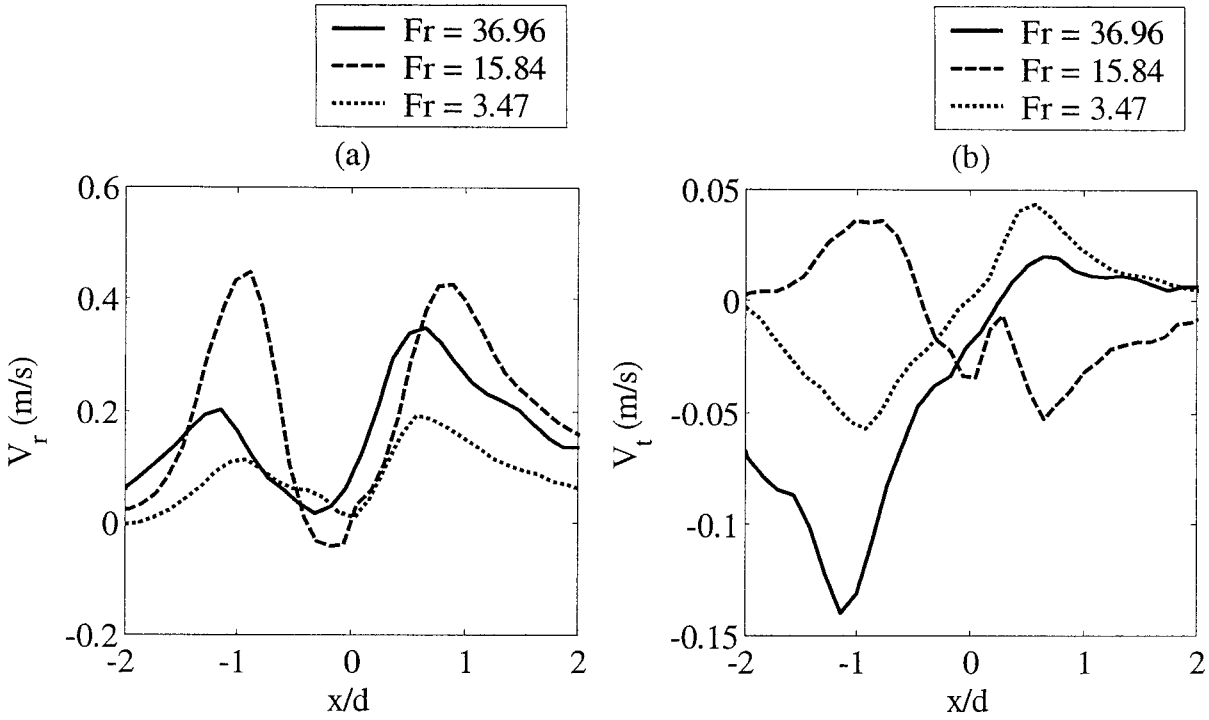

Figure 5.17. Effect of Fr_C on velocity in a horizontal plane at z/d = 0, y/d = 0.

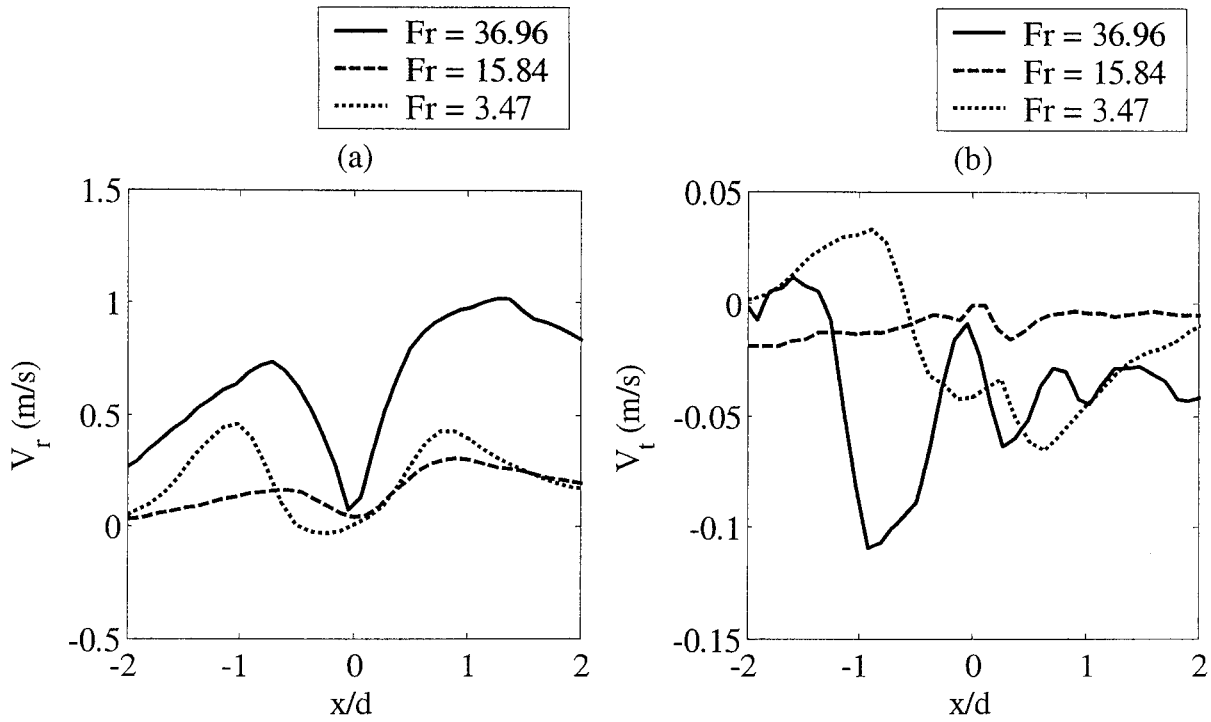

Figure 5.18. Effect of Fr_C on velocity in a horizontal plane at $z/d = H_{OGE}/2d$, $y/d = 0$.

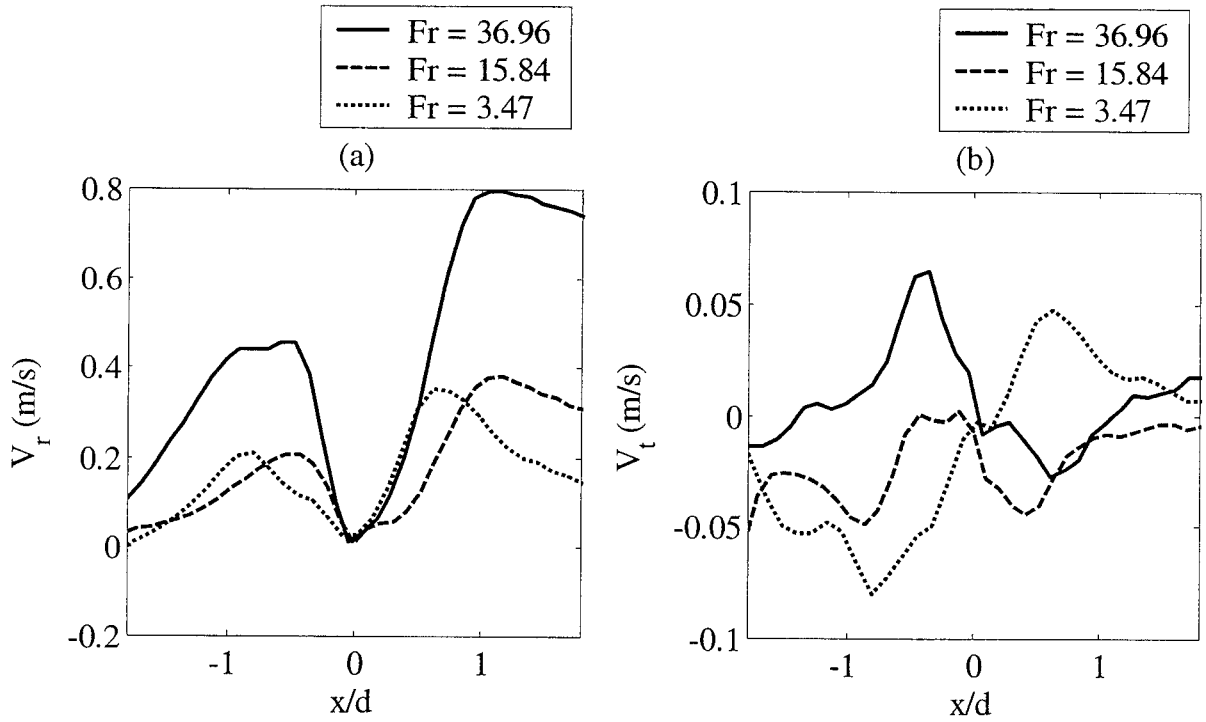

Figure 5.19. Effect of Fr_C on velocity in a horizontal plane at $z/d = H_{OGE}/d$, $y/d = 0$.

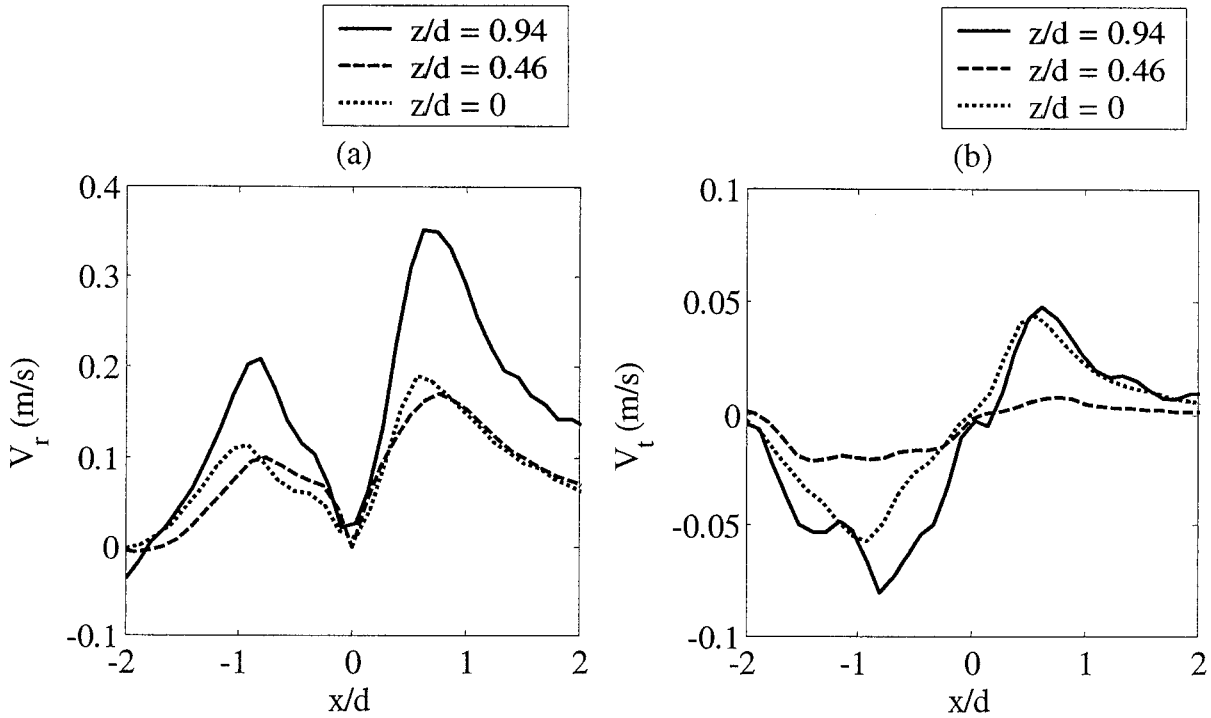

Figure 5.20. Velocity in horizontal planes at y/d = 0 and Fr_C = 3.47, effect z/d.

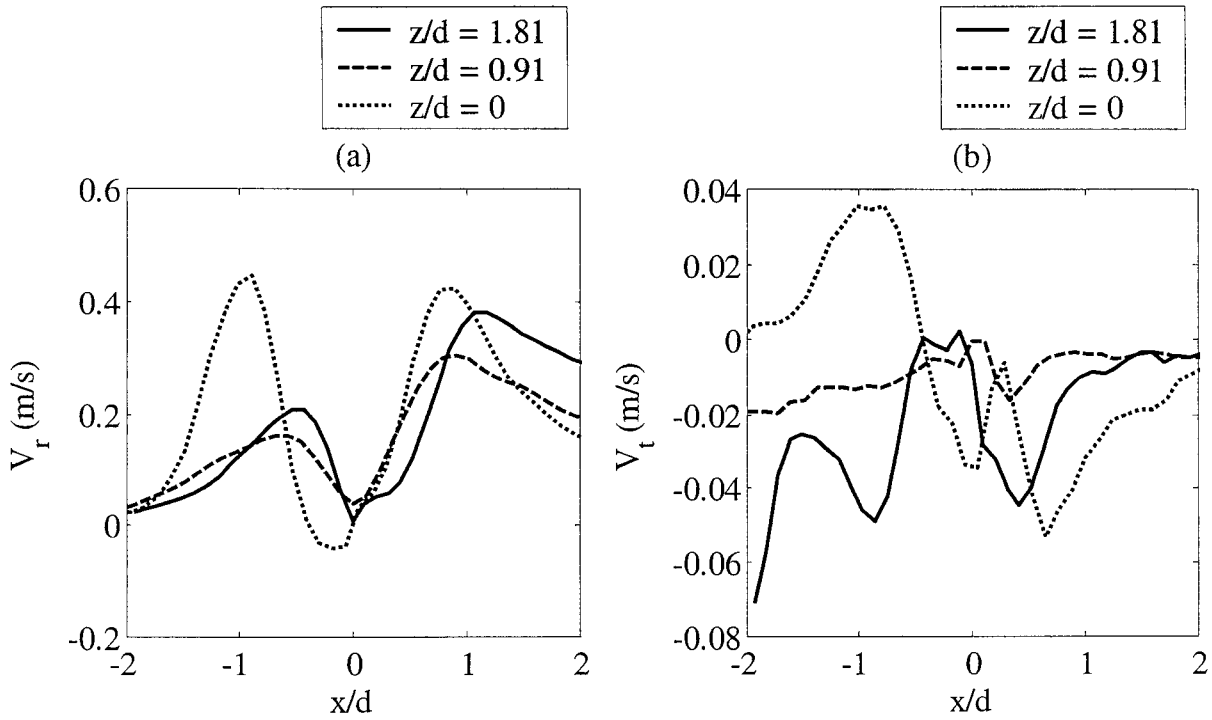

Figure 5.21. Velocity in horizontal planes at y/d = 0 and Fr_C = 15.85, effect of z/d.

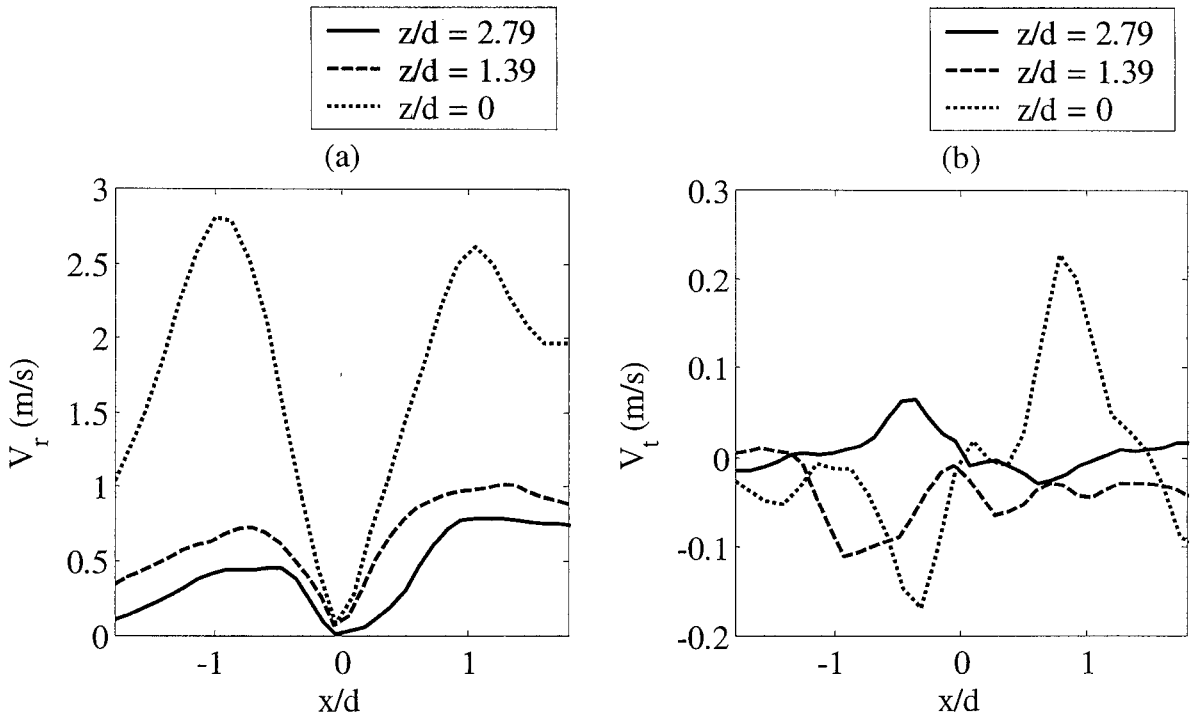

Figure 5.22. Velocity in horizontal planes at y/d = 0 and Fr_C = 36.9, effect of z/d.

Chapter VI

Conclusions and Future Directions

6.1 Conclusions

The importance of predicting the incipience of two-phase flow, from stratified gas-liquid regions, in channels has strong implications in industries where safe operation is of primary concern. This is particularly true in the nuclear industry where two-phase flow occurring in the reactor cooling channels has been responsible for loss-of-coolant accidents (LOCA). It was Zuber (1980), who pointed out that the two-phase flow in cooling channels could be predicted by two phenomena occurring from a stratified two-phase region. It was stated that if the gas-liquid interface was above the discharging branch it was possible for the gas to entrain into the liquid flow. The mechanism by which the onset of gas entrainment occurred was said to be due to either vortex formation, or by vortex-free gas pull through. In a similar fashion, if the gas-liquid interface was below the discharging branch, liquid could be entrained into the gas flow. In both instances, the point at which the onset of entrainment occurs is characterized by the distance of the gas-liquid interface relative to the discharging branch, termed the critical height.

The current two part experimental work presented new information regarding the onset of liquid entrainment, in multiple discharge scenarios, as well as, the liquid velocity field at the onset of gas entrainment. The study presented the results using a scaled cross section

of a typical CANDU header-feeder, using the experimental facility developed by Ahmad and Hassan (2005). In addition a state-of-the-art particle image velocimetry system was adapted to the experimental facility to produce the liquid velocity fields. In fact, the current study is not limited by this single application, and can be applied to similar geometries in industrial applications where a stratified two-phase region is present.

The experiments performed to record the critical height at the onset of liquid entrainment demonstrated new evidence in single, dual and triple discharge cases. It was found that the effect of a second or third discharging branch, on the critical height, could be characterized by two factors. The first is related to the discharge strength of the additional branch, and the second by its relative position to the primary branch and gas-liquid interface. For example, a branch located above the primary branch would increase the critical height, the amount of which is determined by the flow Froude number of that branch. Conversely, a branch located below the primary branch, and therefore the gas-liquid interface, would decrease the critical height, the amount of which is dependant on the flow Froude number. In addition to this, the study demonstrated, through the use of two experimental methods, the effect of surface wetness on the critical height. The two methods used were the increasing liquid level and decreasing liquid level techniques. Comparison of the results from both methods demonstrated that the dry surface will always exhibit a lower critical height than a wet surface, particularly at low branch discharge flow rates. In addition to this, a safer estimate of the onset of liquid entrainment results is demonstrated by using the increasing liquid level method. Of special interest, new information at very low Froude numbers demonstrated the effect of surface tension characterized by an increase of the gas-liquid interface beyond the bottom

of the primary branch. Prior to this study researchers considered that when the gas-liquid interface reached the bottom of the primary branch onset of liquid entrainment was said to occur. In fact, the results presented in the current study demonstrate that the gas-liquid interface can surpass the bottom, and even the center, of the primary branch without the onset of liquid entrainment. It was also described that this effect, while present in the current geometry studied, would diminish with an increase in branch diameter.

The experiments performed to record the liquid velocity field at the onset of gas entrainment due to the vortex-free mechanism in a bottom discharging branch presented novel information of the flow structure at four discrete planes. The motivation for pursuing this study was based on assisting in the validation of analytical models that will try to predict the flow field at the onset of gas entrainment. A particle image velocimetry system developed by Dantec Dynamics capable of recording the velocity field in a two-dimensional plane was used. The planes studied were a single vertical plane passing through the center of the branch, and three horizontal planes at selected liquid heights. The heights selected were just above the branch inlet, just below the branch interface, and midway between the two. The results demonstrated that the flow structure in the horizontal planes were highly dependant on the radial velocity component relative to the branch center. In addition, the tangential velocity component indicated that flow circulation was present and was demonstrated in regions closest to the curved vertical wall. Comparisons in terms of the branch discharge strength and plane location were provided. The results of which demonstrated that due to the complex three-dimensional nature of the flow field, and the two-dimensional measurement technique some

improvements to the system should be made. It was observed that each plane recorded could only demonstrate the projection of the velocity in that plane, and therefore did not present accurately the true velocity field. The results presented, however, do represent the first steps necessary towards fully mapping the liquid velocity field at the onset of gas entrainment in a bottom branch.

6.2 Future Directions

A continuation of the current study could include some of the following improvements, and additions regarding both the experimental setup and methodology. It is expected that these suggestions for improvements could yield additional information regarding the onset behavior.

First, with respect to the current experimental facility at Concordia University, improvements can be made to adapt the particle image velocimetry system more readily to the two-phase reservoir. This can be achieved by modifying the viewable section to minimize the laser refraction caused by the curved acrylic surface. The cylindrical clear acrylic viewing section can be replaced by a section of the same material with a square cross section. An alternative solution would be to attempt a refractive index matching by building an enclosure around the existing viewing section and filling it with a liquid to correct the light sheet refraction.

Second, with respect to the particle image velocimetry technique, it is suggested that due to the complex three dimensional nature of the flow field to use the three-dimensional

capability of the PIV system. Although many more technical challenges will be faced by implementing the 3-dimensional system, the outcome will be improved prediction of the velocity field. This will be achieved through simultaneous measurement of all three velocity components in a particular plane.

Thirdly, the test matrix can be expanded to include the effects of multiple discharges on the liquid flow structure in a similar fashion that the OLE experiments were conducted. The PIV measurement technique could also be extended to include measurements of the gas side velocity field during two-phase flow. Of particular interest the test matrix could also be extended beyond the onset domain to include simultaneous two-phase, quality and velocity field measurements. This information could map, for example, the liquid velocity field as the fluid in the branch goes through the transition from single phase liquid, two-phase gas-liquid, to single phase gas. The results of which could yield a more precise definition of the incipience of the two-phase mechanism from a stratified two-phase region in discharging branches.

Lastly, to approach the real scenario in a header-feeder under LOCA conditions, and in general to expand the applicability of the current work, two additional parameters can be included. The first is the addition of the cross-flow parameter, which would require modifications to the test facility, of which measurements of the flow structure could be obtained with the PIV technique. The second is the inclusion of a stratified wavy surface as apposed to a stratified smooth interface. Such a study would be relevant to a jet

impinging on the gas-liquid interface, and practically speaking, a header-feeder under LOCA will have a jet impinging on the surface from the turrets.

References

Ahmad, T., Hassan, I., "Experimental Study on the Onset of Gas Entrainment from a CANDU Reactor Channel under LOCA Conditions", Accepted at the Journal of Fluids Engineering, ASME (in press), 2005.

Armstrong, K.F., Parrott, S.D., Sims, G.E., Soliman, H.M., Krishnan, V.S., "Theoretical and Experimental Study of the Onset of Liquid Entrainment During Dual Discharge from Large Reservoirs", Int. J. Multiphase Flow , Vol.18, 1992, 217-227.

Craya, A., "Theoretical Research on the Flow of Nonhomogeneous Fluids", La Houille Blanche, Vol. 4, 1949, 44-55.

Daggett, L. L. and Keulegan, G. H., "Similitude in Free-Surface Vortex Formations" Journal of the Hydraulics Division, Proceedings of the ASCE, Vol. 100, No. HY8, 1974.

Gariel, P., "Experimental Research on the Flow of Nonhomogeneous Fluids", La Houille Blanche, Vol. 4, 1949, 56-64.

Hassan, I.G., Soliman, H.M., Sims, G.E., Kowalski, J.E., "Two-phase Flow from a Large Reservoir Through a Small Side Orifice", Experimental and Computational Aspects of Validation of Multiphase Flow CFD Codes, ASME FED, Vol. 180, 1994, 47-58.

Hassan, I.G., Soliman, H.M., Sims, G.E., Kowalski, J.E., "Experimental Investigation of the Two-phase Discharge from a Stratified Region Through Two Side Branches Oriented Vertically", Experimental Thermal Fluid Sci. 13, 1996a, 117-128.

Hassan, I.G., Soliman, H.M., Sims, G.E., Kowalski, J.E., "Discharge from a Smooth Stratified Two-phase Region through two Horizontal Side Branches Located in the Same Vertical Plane", Int. J. Multiphase Flow., Vol. 22, 1996b, 1123-1142.

Hassan, I.G., Soliman, H.M., Sims, G.E. Kowalski, J.E., "Single and Multiple Discharge from a Stratified Ttwo-phase Region Through Small Branches", Nuclear Engineering and Design, Vol.176, 1997, 233-245.

Hassan, I.G., Soliman, H.M., Sims, G.E., Kowalski, J.E., "The Onset of Liquid Entrainment During Discharge from Two Branches on an Inclined Wall", The Canadian Journal of Chemical Engineering, Vol. 77, 1999, 433-438.

Kowalski, J.E. and Krishnan, V.S., "Two-phase Flow Distribution in a Large Manifold", AIChE Annual Meeting, New York, 1987.

Lubin, B. T. and Hurwitz, M., "Vapor Pull-Through at a Tank Drain – with and without Dielectrophoretic Baffling" Proc. Conf. Long Term Cryo-Propellant Storage in Space, NASA Marshall Space Center, Huntsville, Ala., 1966, 173.

Maier, M.R., Soliman, H.M., Sims, G.E., "Onsets of Entrainment During Dual Discharge from a Stratified Two-phase Region Through Horizontal Branches with Centerlines Falling in an Inclined Plane: Part 1 – Analysis of liquid entrainment", Int. J. Multiphase Flow, Vol. 27, 2001a, 1011-1028.

Maier, M.R., Soliman, H.M., Sims, G.E., "Onsets of Entrainment During Dual Discharge from a Stratified Two-phase Region Through Horizontal Branches with Centerlines Falling in an Inclined Plane: Part 2 – Experiments on Gas and Liquid Entrainment", Int. J. Multiphase Flow, Vol. 27, 2001b, 1029-1049.

Micaelli, J.C., Memponteil, A., "Two-phase Flow Behavior in a Tee-junction: The CATHARE Model", In Proceedings of the Fourth International Topical Meeting on Nuclear Reactor Thermal-hydraulics, Vol. 2, Karlsruhe, Germany, 1989, 1024-1030.

Parrott, S. D., Soliman, H. M., Sims, G. E., and Krishnan, V.S., "Experiments on the Onset of Gas Pull-Through During Dual Discharge from a Reservoir", Int. Journal of Multiphase Flow, Vol. 17, 1991, 119-129.

Reimann, J. and Khan, M., "Flow Through a Small Break at the Bottom of a Large Pipe with Stratified Flow", Nuclear Science and Engineering, Vol. 88, 1984, 297-310.

Schrock, V.E., Revankar, S.T., Mannheimer, R., Wang, C.H., Jia, D., "Steam-water Critical Flow Through Small Pipes from Stratified Upstream Regions", In Proceedings of the Eighth International Heat Transfer Conference, Vol. 5, San Francisco, CA, 1986, 2307-2311.

Smoglie, C., Reimann, J., "Two-phase Flow Through Small Branches in a Horizontal Pipe with Stratified Flow", Int. J. Multiphase Flow, Vol. 12, 1986, 609-625.

Soliman, H.M. and Sims, G.E., "Theoretical Analysis of the Onset of Liquid Entrainment for Orifices of Finite Diameter", Int. J. Multiphase Flow, Vol. 18, 1992, 229-235.

Yonomoto, T., Tasaka, K., "New Theoretical Model for Two-phase Flow Discharged from Stratified Two-phase Region Through Small Break", J. Nucl. Sci. Technol., Vol. 25, 1988, 441-455.

Zuber, N., "Problems in Modeling of Small Break LOCA", Nuclear Regulatory Commission Report, NUREG-0724, 1980.